

REMOTE SENSING ASSESSMENT OF SEMI-ARID FOREST STRUCTURE CHANGES
AND ECOHYDROLOGICAL RESPONSES TO THINNING-BASED RESTORATION
PRACTICES

by Adam Jackson Belmonte

A Dissertation
Submitted in Partial Fulfillment
of the Requirements for the Degree of
Doctor of Philosophy
in Informatics and Computing

Northern Arizona University
April 2021

Approved:
Temuulen Sankey, Ph.D., Chair
Joel Biederman, Ph.D.
John Bradford, Ph.D.
Scott Goetz, Ph.D.
Thomas Kolb, Ph.D.

ABSTRACT

REMOTE SENSING ASSESSMENT OF SEMI-ARID FOREST STRUCTURE CHANGES AND ECOHYDROLOGICAL RESPONSES TO THINNING-BASED RESTORATION PRACTICES

ADAM JACKSON BELMONTE

The expansive ponderosa pine forests across the southwestern U.S. have grown significantly denser over the last century, altering the historical ecological functioning, health, and resilience of the entire ecosystem. Coupled with the ongoing threats posed from climate change, namely hotter and drier regional weather conditions, these forests are increasingly vulnerable to drought-related stress and mortality. To help combat these and other deleterious effects, landscape-scale (400+ ha) forest restoration thinning has been used to promote vegetation health and help stabilize regional ecohydrological systems. Assessing restoration-based forest structure changes and the effects of altered forest structure on surface water resources are key to improving management practices. Remote sensing methodologies and datasets offer accurate, cost-effective, and timely ways to quantify aspects of both forest structure and ecohydrological conditions across multiple spatial scales. In this dissertation, I use high-resolution remote sensing to develop and test novel methodologies for quantifying forest structure, snow cover, and soil moisture conditions in response to a restoration thinning treatment. First, I used unmanned aerial vehicle (UAV) image-derived Structure-from-Motion (SfM) models and high-resolution multispectral orthoimagery to quantify vertical and horizontal forest structure at both the fine- (<4 ha) and mid-scales (4–400 ha) and assess specific objectives of a restoration thinning project. I found that estimates of fine-scale forest structure were most accurate in low-density conditions, with

significantly degraded accuracies in high-density conditions. Mid-scale estimates of forest structure behaved similarly across the density gradient. Overall, I found that a majority of the prescription objectives were met in the post-thinning conditions, demonstrating the effectiveness of UAV image data in quantifying forest structure changes from thinning treatments. Next, I use UAV multispectral imagery and SfM models to quantify snow cover dynamics and examine the effects of forest structure shading on persistent snow cover. I first develop a method with 90.2% accuracy to identify persistent snow cover using repeat UAV imagery ($n = 11$ dates) across the 76-ha forest. Using the SfM-derived trees (98% accuracy, $n = 1,280$ trees) and forest structure variables, I show that forest canopy shading was a significant driver of persistent snow cover patches ($R^2 = 0.70$). Overall, my results indicate that UAV image-derived forest structure metrics can be used to accurately predict snow patch size and persistence, providing insight into the importance of forest canopy shading in the amount and distribution of persistent seasonal snow cover. Finally, I use dense soil water potential time-series data across the same thinned forest site to assess soil moisture availability and persistence in response to seasonal drought and forest structure conditions. Using terrestrial lidar data, I assess how fine-scale forest structure components drive differences in the timing, magnitude, and amount of soil drying across soil depths during the seasonal drought period. Results show significant differences in soil moisture response between two abnormally dry years, across all soil depths (25, 50, and 100 cm), and from specific forest structure metrics. Taken together, these studies provide a detailed methodological assessment of the efficacy of high-resolution remote sensing datasets in quantifying forest structure changes from thinning-based restoration and impacts of forest structure on specific ecohydrological components, and importantly how forest management can be used to optimize the availability of water resources in the semi-arid ponderosa pine forests.

ACKNOWLEDGEMENTS

My PhD work was supported and ultimately made possible by many people, and I would like to take this opportunity to express my deepest appreciation. The chair of my committee, Dr. Temuulen Sankey, helped me craft and complete this research from the ground up. Her encouragement for me to push the boundaries of current applied remote sensing techniques helped me feel like an active participant in innovation. My committee members, Dr. John Bradford, Dr. Joel Biederman, Dr. Scott Goetz, and Dr. Thomas Kolb all provided me with their domain-specific wisdom that helped my research successfully reach between disciplines and provide insight into complex ecological, hydrological, and remote sensing issues. I would also like to thank Paul Heinrich for his continual support in field work and ultimately helping me collect a truly unique dataset. The funding for this dissertation work was provided by The Nature Conservancy and the Salt River Project, both of which understood the value in promoting cutting-edge science and budding scientists.

I would also like to express my deepest gratitude for my family and friends for their encouragement and understanding as I embarked on this journey. Finally, I would like to thank my dearest friend and fiancé, Megan, for being a constant force of encouragement and enthusiasm. Her perseverance and patience cannot be overstated, and her ability to help me see the forest through the trees always kept us moving in the right direction.

TABLE OF CONTENTS

PREFACE.....	ii
ABSTRACT.....	ii
ACKNOWLEDGEMENTS.....	v
TABLE OF CONTENTS.....	vi
LIST OF TABLES.....	x
LIST OF FIGURES.....	xii
CHAPTER 1: INTRODUCTION.....	1
1.1 Southwestern semi-arid forest ecosystems: Importance, conditions, and outlook.....	1
1.2 Ecohydrological health indicators in southwesetern ponderosa pine forests.....	4
1.3 Spatial variability in ecohydrological variables.....	7
1.4 Remote sensing of forest structure and ecohydrology.....	9
1.5 Motivations.....	10
1.6 Objectives.....	11
1.7 References.....	14
CHAPTER 2: UAV-derived estimates of forest structure to inform ponderosa pine forest restoration.....	34
2.1 Abstract.....	34
2.2 Introduction.....	35

2.2.1 Quantifying forest biophysical variables	37
2.3 Materials and Methods.....	40
2.3.1 Study area and treatment description.....	40
2.3.2 UAV images and pre-processing	43
2.3.3 UAV image analysis	45
2.3.4 Field-based validation dataset.....	46
2.3.5 Fine-scale forest structure metrics	47
2.3.6 Mid-scale forest structure metrics.....	49
2.4 Results.....	51
2.4.1 Fine-scale forest structure metrics	51
2.4.2 Mid-scale forest structure metrics.....	55
2.4.3 Restoration treatment effects	57
2.5 Discussion.....	61
2.5.1 Estimating fine-scale forest metrics.....	61
2.5.2 Estimating mid-scale forest metrics.....	63
2.5.3 Restoration treatment outcomes.....	64
2.5.4 Other considerations for UAV applications.....	65
2.6 Conclusions and Management Implications	68
2.7 References.....	69

CHAPTER 3: UAV-based estimate of snow cover dynamics: Optimizing semi-arid forest structure for snow persistence.....	81
3.1 Abstract.....	81
3.2 Introduction.....	82
3.3 Materials and Methods.....	85
3.3.1 Study area.....	85
3.3.2 Data description and processing	87
3.3.3 Data analysis	96
3.4 Results.....	100
3.4.1 Snow cover classification and persistent snow patches.....	100
3.4.2 Forest structure metrics summary	104
3.4.3 Relationship between snow and forest structure.....	105
3.5 Discussion.....	108
3.6 Conclusions.....	113
3.7 References.....	115
CHAPTER 4: Soil moisture response to seasonal drought conditions and forest structure in a thinned semi-arid forest	133
4.1 Abstract.....	133
4.2 Introduction.....	133
4.3 Materials and methods	139

4.3.1 Study site description.....	139
4.3.2 Soil water potential data.....	141
4.3.3 Forest structure metrics.....	144
4.3.4 Data analysis	147
4.4 Results.....	148
4.4.1 Soil moisture data summary.....	148
4.4.2 Forest structure - soil moisture differences.....	151
4.5 Discussion.....	157
4.5.1 Multi-year drought impact.....	157
4.5.2 Forest structure effects.....	159
4.5.3 Management implications.....	163
4.6 Conclusions.....	164
4.7 References.....	166
CHAPTER 5: DISCUSSION.....	184
5.1 Management Implications.....	187
CHAPTER 6: CONCLUSIONS	190

LIST OF TABLES

Table 2.1: Summary of UAV flight data collection and SfM image reconstruction parameters used in our study, and relevant product characteristics.....	44
Table 2.2: Individual tree omission and commission errors in the low-, medium- and high-density classes, with the overall scores across each density class provided. Analysis parameters included were the true positive (TP), false negative (FN), false positive (FP) trees, as well as the recall (r), precision (p) and F-score (F). TPH, trees per hectare; CC, canopy cover.	52
Table 2.3: A summary of the UAV image-derived individual tree height and canopy diameter estimates, grouped by density classes, and compared to the US Forest Service Common Stand Exam (CSE) acceptable accuracy ranges. The reported values for each acceptable accuracy range indicate the percent of the total trees estimated from the UAV data within that range.	54
Table 2.4: Patch and interspace metrics from the treated portion of the study area. Patch contiguity is a unitless metric, ranging from 0 to 1 where 0 is a single pixel patch and it approaches 1 as patch shape complexity and patch boundary configuration increase. Fractal dimension index is a unitless metric, ranging from 1 to 2 where 1 is a patch with a simple shape (e.g., square) and 2 is a patch with a more convoluted boundary. Euclidean nearest random point distance (ENRPD) is an assessment of the shortest straight-line distance between randomly generated points and is used to measure the prevalence and size of forest gaps.....	58

Table 2.5: A selection of the restoration treatment objectives outlined for the study area. The restoration treatment outcomes were estimated from the post-treatment UAV image-derived datasets. TPH, trees per hectare. 60

Table 3.1: Three storm events, subsequent image collection dates, and weather conditions. The total snowfall indicates the snow recorded for the storm event, while the mean temperatures and wind speeds are cumulative means between the image dates. Each storm event was imaged several times from full snow coverage on the first day until the snow cover nearly melted off. The individual image dates were selected considering daily weather conditions and study site access. Periods of near-freezing daily temperatures yielded longer image date intervals so that noticeable changes in snow coverage could be observed. In contrast, periods of higher mean temperature values required more frequent image date intervals as the snow melted rapidly. Weather data were recorded at the regional National Weather Service Forecast office, approximately 15 km from the study site and compiled from NOAA’s Climate Data Online service.87

Table 3.2: Accuracy of the snow/non-snow classification across the 76-ha study site. The image used to generate the error matrix included an even amount of snow and non-snow pixels, providing the least biased estimation of classification error. 100

LIST OF FIGURES

- Figure 2.1:** Overview of the study site within the state of Arizona and accompanying US Forest Service land (panel A). The 46.5 ha study area with the field plot locations and an example of a single field plot are shown in panel B, whereas the eBee UAV platform used for all UAV-derived data collection is shown in panel C. Base imagery used in panel B is the post-treatment UAV multispectral orthomosaic image..... 41
- Figure 2.2:** Examples of our field plots from each of the low- (A), medium- (B) and high- (C) density classes. The top row shows the UAV orthomosaic images overlaid with both the field-measured and UAV-derived tree locations as well as their corresponding crown diameters. The bottom row shows the Structure-from-Motion (SfM) point cloud data that corresponds to each plot above, as well as the SfM-derived tree locations placed on each respective tree..... 52
- Figure 2.3:** Linear regression models established between the field-measured and UAV image-derived individual tree height estimates. The dashed line is a 1:1 reference line and solid black line is the overall fitted regression model (adj. $R^2 = 0.71$). In addition, separate regression models were fit to each density class and the regression lines are colored accordingly..... 54
- Figure 2.4:** Linear regression models established between field-based measurements and UAV image-derived estimates of tree canopy cover. The dashed line is a 1:1 reference line and solid black line is the overall fitted regression model (adj. $R^2 = 0.79$). In addition, separate regression models were fit to each density class and the regression lines are colored accordingly. Data points here are the individual 10 m cells ($n = 153$) from the

field-measured plots, which were summarized from the high-resolution (15 cm) binary canopy raster layers and are colored by density condition. 57

Figure 2.5: A comparison of pre-treatment (A) and post-treatment (B) forest patches illustrating substantial changes in horizontal structure and the creation of new forest patches.

Toward the center of panel B, the vegetation not highlighted as a patch is fallen timber awaiting removal. The base map images are the respective UAV orthomosaic images in 15 cm resolution used for canopy cover and forest patch delineation. 58

Figure 3.1: An overview of the study site highlighting the locations and extents of the UAV Structure-from-Motion (SfM) data, terrestrial laser scanner (TLS) data, and field-based validation data. (A) shows an example of the field-measured and TLS validated plots. (B) shows the distribution of all field-measured and TLS validated plots within the SfM data extent, which includes both thinned and unthinned portions of the forest. A majority of our ground-based measurements are distributed across the larger, thinned portion of the study site. (C) shows the UAV and TLS instruments used in this study. 86

Figure 3.2: UAV multispectral image analysis workflow. First, the original multispectral bands and the calculated indices were stacked into a single raster image, one for each image date (n = 11) and classified using a supervised random forest model to generate binary snow/non-snow classes. From the binary classification from each image date, the pixels with 10 or 11 snow-covered days (out of 11) were grouped to create the boundaries of individual persistent snow patches. 92

Figure 3.3: Calculating the individual tree metrics for the final analysis involved using both the field-measured and terrestrial laser scanner (TLS) point cloud-derived datasets.

Individual trees detected in the TLS point cloud were compared to field-measured trees for an omission and commission analysis. Their crown height (CH), average crown diameter (CD), and crown base heights (CBH) were compared to assess the accuracy of the TLS point cloud-derived estimates. The same comparison was made between matching trees in the TLS point cloud and Structure-from-Motion (SfM)-derived point cloud datasets, with the only difference being the addition of crown volume (CV). 95

Figure 3.4: A persistent snow patch and the trees influencing it at the three different ranges: 1, 1.5, and 2 times the height (CH) of the tree. A tree was included within each respective tree shading influence area (TSIA), if its CH multiplied by 1, 1.5, or 2 was extended into the snow patch and if the bearing of its location (XY) to the patch was within the range of daily solar angles. 98

Figure 3.5: The percent of the treated and untreated regions of the study site that are classified SCA for each UAV snow-series image following a storm. This data is grouped by storm, and partitioned by forest treatment condition to illustrate the reductions in SCA within and across the storms. SCA patterns following storm events show a greater SCA reduction in the treated portion of the study site than in the untreated portion. Evident also are the relatively similar initial amounts of classified SCA on the first image date after a storm in the treated portion, contrasting the initial amounts in the untreated portion. 102

Figure 3.6: Each UAV image (n = 11) was classified into snow/non-snow pixels (A) and the resulting rasters were assembled into a single composite, in which persistent snow patches were identified (B). The orthomosaic image used as the base imagery is from storm 2, day 3 (1 May 2019) and its binary snow classification (A) was used for the classification accuracy assessment because it contained a nearly even snow/non-snow (49/51%) area distribution..... 103

Figure 3.7: Variable importance scores calculated for the forest structure metric predictor variables used in fitting the final MARS model framework. The variable importance score ranges from 0 to 100, with higher scores indicating that the predictor was more influential in model construction (n = 500). The chart depicts the frequency with which each forest structure metric was within the respective range of the importance score. The data are partitioned by tree shading influence area (TSIA) size to better illustrate the interaction with forest structure metric. Overall, the most influential forest structure metric predictors are canopy cover (CC), mean solar radiation footprint (SRF) value, and mean trees per hectare (TPH). 106

Figure 3.8: A collection of the simple linear relationships reflecting each model’s predictive ability for the TSIA 1.5. Each line represents the prediction accuracy of a single model, and the red points are the value pairs for the predicted vs. observed persistent snow patch sizes (m²). The mean performance statistics for the entire set of prediction models in TSIA 1.5 is R² = 0.70 and a RMSE = 267 m². 107

Figure 3.9: A comparison of trees and their shadows with different vertical structure metrics, namely CBH:CH and CV. The perceived difference in forest canopy shading between trees with high CBH:CH and low CV values (Panel A) are compared to those trees

with overall larger crowns (Panel B). These canopy shading differences were expected to result in vertical forest structure metrics being significant in the modeling of persistent snow patch size. 111

Figure 4.1: Total accumulated precipitation for Flagstaff, AZ area beginning at the start of the water year (October 1). The mean accumulated precipitation values are summarized beginning for the water year of 2000 and ending for values recorded in early 2021.....138

Figure 4.2: Study site map showing the location and extent of soil moisture and forest structure field data collection across the study site (Panel B), which is within the larger 4FRI forest restoration area near Flagstaff, AZ, USA (Panel C). All soil water potential sensors are connected to data loggers (n = 16) (Panel A) located in areas with varying forest density. Forest structure data collection was centered on each data logger, with lidar and validation datasets overlapping to facilitate accuracy assessment..... 141

Figure 4.3: The complete soil moisture (SWP) and temperature (ST) time-series datasets for 2019 and 2020, with the respective fore-summer drought seasons depicted with dashed lines. Precipitation and air temperature data from the nearest (5.6 km away) National Oceanic and Atmospheric Administration (NOAA) climate data station (GHCND:USS0011P02S) is also shown for the full time frame. Since precipitation data are often localized during monsoonal storms, the soil moisture response recorded at the study site varies from the precipitation recorded at the NOAA station. However, it provides insight consistent with soil moisture responses as well as context for inter-annual trends. Importantly, both 2019 and 2020 precipitation totals were among the

lowest on record, 77% and 59% of normal in 2019 and 2020 respectively, likely exacerbating the underlying drought conditions at the study site. 143

Figure 4.4: Forest structure metrics were calculated using plot-level lidar data collected at each soil moisture data logger location (n = 16). Additionally, validation measurements were collected in 30x30 m plots to assess the accuracy of lidar-derived forest structure estimates. Panel A depicts a segmented tree from the lidar point cloud data, while Panel B provides an illustration of all the lidar-derived forest structure metrics estimated at a single plot. Panel C shows the terrestrial laser scanner (TLS) instrument and one of the ground targets used during data collection. 147

Figure 4.5: Soil moisture time-series data from 2019 and 2020 fore-summer drought seasons, with the x-axis day of year for the start of the fore-summer drought period (April 1) being day 91 and day 92 for 2019 and 2020 respectively. Each line shows the mean daily soil water potential (SWP) measurement (colored by depth) and illustrates the soil ‘drying down’ between spring snow melt (April 1) and late summer monsoon. Rain events can be observed when a curve sharply turns upward toward 0 MPa, which indicates soil becoming more saturated. The critical drying threshold (CDT) depicted at -1.0 MPa is the point at which ponderosa pine trees begin to experience moisture-related stress. 149

Figure 4.6: Mean differences in each soil moisture metric by depth, with Panel A showing differences for Onset Day (DOY), Panel B showing differences for the number of days spent under the CDT, and Panel C showing differences in the mean SWP (MPa). Significant were found for each depth-level comparison. 151

Figure 4.7: Histograms of the forest structure metric summaries calculated at each sensor location (n = 84), with sensor depths differentiated by color. Key indicators of the post-treatment forest structure are apparent in the distributions of mean canopy cover (CC), basal area (SBA), and trees per hectare (TPH), all of which reflect the overall lower forest density conditions across the study site compared to the conditions observed prior to the restoration thinning project (Belmonte et al., 2019)..... 152

Figure 4.8: Differences in Onset day (Panel A), number of critical drying threshold days (Panel B), and mean SWP (Panel C) related to tree crown height (CH). Significant Tukey’s pairwise comparisons are shown by the starred bars. Mean tree crown height was the most prevalent predictor of soil moisture metric differences across all sensor depths. 154

Figure 4.9: Notable forest structure-driven differences in each soil moisture metric. For Onset day (Panel A), basal area (BA) had significant pairwise differences for sensors at 25 & 50 cm, with higher BA translating to significantly earlier drying Onset day. Additionally, there were significant pairwise differences in tree diameter at breast height related to the number of critical drying threshold days (Panel B) and mean SWP (Panel C) for sensors at 25 cm. Here, trees with larger diameter at breast height contributed to more days spent under the threshold and lower (drier) overall SWP values..... 154

Figure 4.10: Illustration of four different 100 cm soil matric potential (MPa) time-series data, two from the plots with the lowest forest density conditions (panels A and B) and two from the highest forest density conditions (panels B and C). Soil matric potential data (middle panel) was averaged across both fore-summer drought seasons for each sensor

to illustrate the soil moisture response at that location. Trees per hectare (TPH), basal area (BA), canopy cover (CC), average tree crown height (CH), and average diameter at breast height (DBH) were summarized across the 20 m radius area centered on each sensor. 161

PREFACE

This dissertation consists of three manuscripts that examine the relationships between forest structure and ecohydrological processes in a thinned semi-arid ponderosa pine forest ecosystem. Two of these manuscripts are published and one will be soon submitted for peer review and publication to a leading remote sensing and ecohydrology journal. These manuscripts have been or will be reviewed by all co-authors prior to submission for publication. Formatting of all manuscripts is consistent throughout this document, and references are provided at the end of each manuscript for clarity. Chapter 1 consists of a comprehensive review of the literature relevant to all manuscripts. Chapter 2 is the first published manuscript on a novel method for inventorying and assessing the changes from a restoration thinning treatment in a semi-arid ponderosa pine forest in northern Arizona in the journal *Remote Sensing in Ecology and Conservation* (<https://zslpublications.onlinelibrary.wiley.com/doi/full/10.1002/rse2.137?af=R>). Chapter 3 is the second published manuscript about a novel method of quantifying persistent snow cover and assessing the relationships with forest structure in the journal of Remote Sensing (<https://www.mdpi.com/2072-4292/13/5/1036>). Chapter 4 is a manuscript that examines the response of the timing, magnitude, and extent of soil drying during seasonal drought and to forest structure conditions. Chapter 5 provides a brief discussion of the results from these chapters and summarizes the main findings and implications. Chapter 6 summarizes the overall conclusions of the dissertation.

CHAPTER 1: INTRODUCTION

1.1 Southwestern semi-arid forest ecosystems: Importance, conditions, and outlook

Forest ecosystems are integral to the health and functioning of our planet. They cover about 28% (3.7 billion ha) of the total land area on Earth and provide fundamental services to our natural and sociopolitical systems (FAO, 2015; Pearce, 2001). Specifically, forests harbor extensive plant and animal biodiversity, drive global carbon sequestration, and moderate the hydrologic cycle at the local and planetary scales. In addition, forest ecosystems provide many goods and services to humankind, resulting in extensive direct and indirect valuations underpinning economic markets (Mori et al., 2017; Pearce, 2001; Hawksworth & Kalin-Arroyo, 1995). The cumulative loss of forest ecosystems from direct human intervention and the anticipated losses from the effects of climate change has prompted the international community to begin prioritizing conservation and restoration of forest resources (Stanturf et al., 2014).

There are an estimated 7.48 million hectares of forested land across the Southwestern U.S., containing roughly 3.98 billion live trees (<https://www.fia.fs.fed.us/>). Across this region, mid-elevation ponderosa pine (*Pinus ponderosa*) forests have endured significant changes in their structure, composition, and ecological functioning since European-American settlement (hereafter pre-settlement) (Cooper, 1960; Fulé et al., 1997). These changes are a result of many different factors including wildfire suppression, selective logging, and livestock grazing (Altschul & Fairley, 1989; Cooper, 1960; Madany & West, 1983; Schubert, 1974). As a result, overly dense forests have replaced the low-density, park-like pre-settlement conditions, increasing fuel loads and creating conditions that promote net ecosystem moisture loss and a propensity for catastrophic wildfire.

The natural range in variability of forest structure and composition in pre-settlement forests was reflected by diversity in tree age and structure with forest patches and large, irregularly shaped interspaces (Cooper, 1960, 1961; Mast et al., 1999; Pearson, 1923; Sanchez-Meador et al., 2011; White, 1985, Woolsey, 1911). These conditions yielded an ecosystem adapted to and tolerant of frequent (every 2-26 years), low-severity wildfires and other naturally occurring disturbances such as insect and disease outbreaks (Castello et al., 1995; Dahms & Geils, 1997; Fitzgerald, 2005; Schubert, 1974). Currently, a majority of the region's ponderosa pine forests are characterized by higher canopy cover, comprised of trees homogeneous in both age and stature (Larson & Churchill, 2012; Moore et al., 2004; Reynolds et al., 2013). These conditions have altered the historical ecological functioning, health, and resilience of the entire ecosystem (Kolb et al., 1994; Swetnam, 1999; Swetnam & Betancourt, 1998). Reintroducing the natural range of variability of and promoting long-term ecological health in these forests are now recognized as important management goals (Allen et al., 2002; Covington & Moore, 1994; Covington et al., 1997; Fulé, 2008; Landres et al. 1999; White & Walker, 1997).

With overly dense forests dominating federally managed lands in the western U.S. and wildland firefighting costs nearly tripling to \$3 billion since the early 1990's, scientific community and natural resource managers called for a comprehensive ecosystem management strategy (Allen et al., 2002; Covington & Moore, 1994; Covington et al., 1997; Grumbine, 1994). Taken together, this spurred the United States Congress to pass the Forest Landscape Restoration Act (FLRA) in 2008-2009 (Fitch et al., 2018; Schultz et al., 2012; US GAO, 2007). This enabled the United States Forest Service (USFS) to establish the Collaborative Forest Landscape Restoration Program (CFLRP) and allocate funding to a number of large-scale forest management programs (Day et al., 2006; Weldon, 2014). As one of the first and the largest

CFLRP projects, the Four Forests Restoration Initiative (4FRI) in Arizona focuses on improving and sustaining watershed health, wildlife habitat, and biodiversity, while also reducing the risk of catastrophic wildfire across the Apache-Sitgreaves, Coconino, Kaibab and Tonto National Forests (<http://4fri.org/>). Spanning more than 20 years and covering almost a million hectares, 4FRI will design and implement restoration treatments that selectively harvest and thin dense forests and gradually reintroduce natural fire across the treated areas. As the threat of widespread and catastrophic wildfire to forests looms across the western United States, thinning- focused restoration practices have garnered increased public support and funding (Fitch et al., 2018; Schultz et al., 2012). In addition to reducing the risk of catastrophic wildfire, thinning practices also fulfill a suite of other ecologically oriented goals (Ziegler et al., 2017). For example, thinning can enhance wildlife habitat, promote vegetation health, and stabilize the water balance in treated forests. As more forest is earmarked for thinning, an operational understanding of how thinning patterns influence forest health and ecohydrological dynamics can further restoration efforts.

Continued monitoring and adaptive management strategies are critical for 4FRI's long term success (Schultz & Coelho, 2012; Williamson et al., 2011; Four Forests Restoration Initiative, 2013). Extensive data collection is needed to plan restoration treatments, assess adaptive management benchmarks, and monitor long-term progress. Doing so has traditionally relied on time intensive and costly field surveys, which provides thorough, fine-scale measurements at the plot-level (0.5 ha) (United States Forest Service, 2005). However, given the vast extent of the current and planned restoration treatments, remote sensing-based methodologies are needed for their flexible temporal and spatial resolutions. While the scope of forest restoration projects is often at the landscape-scale (400+ ha), individual restoration

treatments are designed and implemented at the mid-scale (4-400 ha) as funding and project logistics allow. This leaves a gap in forest mensuration and inventorying required for adaptive management and monitoring. Also established were specific monitoring frameworks and goals, each having distinct spatial and temporal scales. For example, an assessment of pre- and post-treatment forest structure characteristics need to be conducted annually at a scale of 10's to 100's of hectares. When coupled with a treatment plan including ~12,000 ha per year for 10 years, as outlined in 4FRI's initial NEPA documents, the need for a comprehensive and transparently structured monitoring protocol helps ensure stakeholder involvement and the program's long-term survival (Schultz & Coelho, 2012).

1.2 Ecohydrological health indicators in southwesetern ponderosa pine forests

Surface streamflow in the world's semi-arid regions provides water for drinking and agricultural uses for roughly one-sixth of the population and contributes trillions of dollars to the global economy (Barnett et al., 2005; Sturm et al., 2017). In the western U.S., significant reduction in surface streamflow within the Colorado River Watershed could manifest in up to \$1.5 billion in economic losses across the Southwestern U.S. (James et al., 2014). Critical to global and regional hydrologic cycles, near-surface water resources help moderate the land-atmosphere interactions responsible for redistributing water along the soil-vegetation-atmosphere continuum (Entekhabi, et al., 1996; Hong & Kalnay, 2000; Koster et al., 2004; Thornthwaite, 1952; van der Schrier & Barkmeijer, 2007). Additionally, these resources are critical to the health and distribution of vegetation and aquatic ecosystems across the landscape, as well as influence the partitioning of water into surface runoff and deep aquifer storage (Bales et al., 2011; French & Binley, 2004; Newman et al., 1998; Price & Hendrie, 1983; Rieman et al., 2003; Sandvig &

Phillips, 2006; Seyfried et al., 2005; Wilcox, Breshears, & Allen, 2003; Wilcox et al., 1997). Applied ecohydrology lies at the nexus of atmosphere-vegetation-hydrology interactions and seeks to explain these relationships by quantifying the distribution and persistence of water throughout the unsaturated zone of the soil horizon (Vose et al., 2011). This dissertation aims to further our current understanding of these relationships in high-elevation ponderosa pine forests of the Southwestern U.S.

Throughout semi-arid ecosystems, like those in the Southwestern U.S., limited precipitation inputs contribute to relatively low baseline soil water levels, making the loss of soil water a critical consideration in the total ecosystem water budget (Yaseef et al., 2010; Stoy et al., 2019; Wang et al., 2014; Wei et al., 2017). Soil water loss is largely governed by fluxes in near-surface soil water evaporation and vegetation transpiration, which can account for up to 100% of the precipitation inputs in semi-arid forests (Allen et al., 1998; Newman et al., 1997; Yaseef et al., 2012; Yaseef et al., 2009; Zhang et al., 2001). The relationship between near-surface soil water and vegetation water stress is crucial to quantifying broader ecosystem health and functioning in these water limited environments (Koepke & Kolb, 2013; Porporato et al., 2001). This has prompted scientists and land managers to seriously consider the effects of soil water limitation across the landscape and prioritize water management in forest ecosystems to reduce water stress and preserve productivity and resilience (Grant et al., 2013). Subsequently, this dissertation focuses on the effects of forest management on various components of the forest ecohydrological cycle.

Forests regulate surface streamflow timing and magnitude, snow accumulation and ablation, ground surface evaporation, and groundwater infiltration through interception,

transpiration, and ground shading (Essery et al., 2003; Lundquist et al., 2013; Price 2011; Vose et al., 2016). In the high-elevation (1,500-3,000 m) semi-arid ponderosa pine forests of the Southwestern U.S., about half of the annual precipitation falls as rain during the summer, while the other half as snow during the winter via extensive slow-moving Pacific storms (Hereford, 2014). Accumulated winter snow percolates into the soil column and functions as a reservoir for perennial evergreen vegetation throughout the growing season (Ehleringer et al., 1991; Forzieri et al., 2011). For mature ponderosa pine trees in particular, water from snowpack is the dominant source of water throughout the year (Ehleringer & Dawson, 1992; Kerhoulas et al., 2013).

As snowmelt concludes, the transition into the spring and early summer seasons heralds the driest months in the Southwestern U.S., and often referred to as the fore-summer drought period. This period is bookended by the disappearance of snow and the onset of the North American Monsoon in mid to late summer, and is characterized by high atmospheric water demand, increased evapotranspiration, and large fluctuations in soil moisture availability (Hereford, 2014; Loik et al., 2004). Persistent soil moisture deficits in the root zone during the growing season will negatively impact the physiological processes controlling vegetation functioning, structure, and overall health (Chapin, 1991; Chapin et al., 1987; Maherali & DeLucia, 2001; Williams et al., 2001). These negative effects can be further exacerbated by periodic or prolonged drought conditions (Adams et al., 2009).

While seasonal and multi-year drought conditions are not abnormal in these water-limited forests, climate-change-driven increases in air temperature and variability in vapor pressure deficit are likely contributing to hotter and more frequent droughts (Breshears et al., 2005; Palmer, 1965; Vicente-Serrano et al., 2010; Vicente-Serrano et al., 2013). Despite this evolved

tolerance to drought conditions, the presence of ongoing multi-year and hotter drought leads to unsustainable levels of tree water stress and eventually coincides with or contributes to widespread mortality from naturally occurring insect, pathogen, and wildfire (Allen et al., 2015; Clark et al., 2016; Ganey & Vojta, 2011; Gaylord et al., 2006; Kolb et al., 2016; Mueller et al., 2005; Pinol & Sala, 2000; Williams et al., 2010; Zhang et al., 1997). Given the currently ongoing multi-year drought conditions, this dissertation addresses the impacts of both the seasonal and multi-year drought periods.

1.3 Spatial variability in ecohydrological variables

Vegetation presence, stress, and mortality are not evenly distributed throughout semi-arid forests in part due to high spatial variability in snow cover and soil moisture levels across the landscape (Andrews et al., 2020; Huxman et al., 2004; Yaseef et al., 2010; Snyder & Tartowski, 2006; Teuling, 2005; Weltzin et al., 2003). Forest cover is central to governing the accumulation and ablation of snow on the ground surface, primarily by controlling canopy interception and subsequent sublimation (Essery et al., 2003; Molotch et al., 2007, 2009; Roth & Nolin, 2017; Varhola et al., 2010). Discontinuous forests and those with low overall canopy cover tend to have higher rates of snow accumulation and ablation than forests with continuous cover and with higher canopy cover (Dickerson-Lange et al., 2017; Gottfried & Ffolliott, n.d.; Revuelto et al., 2015). Additionally, the size, shape, spacing, and tree structure of forest patches greatly influences snow accumulation and ablation processes both within patches and in adjacent forest gaps (Davis et al., 1997; Dickerson-Lange et al., 2015; Essery et al., 2008; Lawler & Link, 2011). In addition, individual tree structure and the spatial patterns of tree groups directly influence the accumulation and ablation of snow throughout semi-arid forests, articulating the

spatial heterogeneity of soil moisture (Davis et al., 1997; Essery et al., 2008; Essery et al., 2003; Molotch et al., 2009; Roth & Nolin, 2017).

Forest canopy shading and individual tree structure also exacerbate spatial heterogeneity of soil moisture. As spring snowmelt occurs, areas with the most persistent and deeper snow saturate the shallow soil depths, translating into non-uniform soil water inputs across the landscape (Newman et al., 2004). Higher rates of soil water evaporation are observed in unshaded versus shaded areas, which can result in increased water yield from areas with higher cover (D'Odorico et al., 2007; Duff et al., 1997; Qubaja et al., 2020; Sahin & Hall, 1996; Tyagi et al., 2013). There are also significant effects attributed to fine-scale differences in tree structure and forest patch characteristics (Breshears et al., 1997; Gray et al., 2002; Teng-Chiu Lin et al., 1992). For example, within forest patches with high canopy cover, there is increased interception of precipitation but also more water uptake from transpiration, translating into lower soil moisture levels. Interspaces directly adjacent to tree groups show the opposite response, a direct benefit from canopy shading.

Quantifying the forest structure-driven differences in snowpack and soil moisture can help resource managers promote ecosystem resilience as both human-caused and natural disturbances change the structure and composition of these dry forests. Previous research has exhibited increases in snowpack-derived water resources from forest cover changes related to insect, drought, wildfire, and thinning-based forest management (Biederman et al., 2014; Broxton et al., 2020; Ffolliott et al., 1989; Ffolliott & Gottfried, 2003; Goeking & Tarboton, 2020.; Gottfried & Ffolliott, n.d.; Harpold et al., 2014; Pugh & Small, 2012; Sankey et al., 2015;

Winkler, 2011; Woods et al., 2006). This dissertation further addresses these relationships using novel, high resolution UAV time-series datasets from thinned and unthinned forests.

1.4 Remote sensing of forest structure and ecohydrology

Accurate and timely forest inventory data are essential to forest management, providing insight into individual tree and larger forest patch age, species composition, and structure. In particular, implementing forest restoration plans relies on quantifying forest structure to both create treatments and assess their effectiveness. Specific restoration prescriptions utilize this information with the goals to reduce fire, insect, and disease risk, while promoting other wildlife and stand diversity metrics such as interlocking canopies and old-growth tree retention (Allen et al., 2002; Covington et al, 1997; Mast et al., 1999). Planning for, implementing, and evaluating restoration treatments require quantitative data at a variety of spatial scales, which relies upon the accurate and efficient location and measurement of trees throughout a representative portion of the forest in question (Husch et al., 2003).

Forest structure metrics important to restoration planning and assessment include, but are not limited to, stand-level canopy height, diameter at breast height, basal area, trees per hectare, canopy cover, as well as more specific forest patch and interspace metrics. Traditional methods for providing estimates of these metrics require a combination of sample-driven field measurements of individual trees and statistical modeling techniques (Huffman et al., 2001). These methods tend to be expensive, time-intensive, and only viable at the fine-scale (< 4 ha). In an effort to alleviate these shortcomings, remotely sensed data products have emerged as a viable alternative across all spatial scales. This dissertation demonstrates applications using both airborne multispectral and ground-based lidar sensors. In addition to quantifying fine-scale (<4

ha) forest structure, UAV datasets can also be used to measure snow cover and depth (Harder et al., 2016; Lendzioch et al., 2019; Miziński & Niedzielski, 2017). While satellite remote sensing can provide temporally dense and spatially extensive measurements of snow-covered area (SCA), the generally coarse spatial resolutions, fixed time intervals, and cloud interference can limit its applications (Sankey et al., 2015). However, applying similar methodologies used in satellite remote sensing to derive SCA, UAV datasets can yield high resolution and near real-time SCA observations (Niedzielski et al., 2018). This offers a flexibility essential to capturing both ongoing forest structure changes as well as the often-day-to-day variability of snow cover, which rapidly melts in semi-arid Southwestern forests (Sankey et al., 2015).

1.5 Motivations

As the climate of Southwestern U.S. trends toward hotter and drier conditions, it is essential to better understand and manage for landscape-scale ecohydrological health. The region's semi-arid forests are critical to broader ecological health and remain vulnerable to a suite of natural and human-caused threats. As such, these forests have been the focus of costly and extensive management action for decades. Managers aim to curb stress and mortality in forests using different combinations of thinning- and burning-based treatments to promote natural ecosystem functioning. While this management strategy explicitly promotes a diverse suite of objectives, such as improvement of wildlife habitat and reduction of catastrophic wildfire potential, it lacks a framework to specifically manage for water resources and broader ecohydrological health.

Key to establishing and maintaining adaptive management strategies are accurate, detailed, and easily reproducible methodologies and data. For example, gauging the success of a restoration treatment and informing future treatments are reliant on measuring forest structure

changes at fine- to mid-scales and their impact on the ecohydrological processes. Doing so remains challenging given the scale and pace of restoration thinning projects. Importantly, methods for quantifying the response of ecohydrological components, like snowpack and soil moisture, in response to thinned forest conditions are not well documented. Further research into using remote sensing technology for rapid and scalable forest structure measurement will directly serve operational forest management throughout the region. Research into the remote sensing of near-surface water resources in thinned forests will help tailor future restoration efforts to maximize snow cover and soil moisture.

1.6 Objectives

The overarching goal of this dissertation research focuses on developing UAV and lidar remote sensing methods for operationalizing forest restoration assessment and investigating the complex relationships between ecohydrological processes and post-restoration forest structure. This research is divided into three distinct and interconnected chapters that use cutting-edge remote sensing techniques to: 1) quantify a mechanically thinned ponderosa pine forest structure in northern Arizona, 2) measure and relate snow cover dynamics to forest structure, and 3) assess seasonal soil moisture deficits in response to forest structure. Two of the three chapters have already resulted in peer-reviewed articles in the journals *Remote Sensing in Ecology and Conservation* (chapter 2) and *Remote Sensing* special issue *Ecohydrological Remote Sensing* (chapter 3).

Chapter 2 in this dissertation and the first publication focuses on quantifying forest structure changes from a mechanical thinning restoration treatment at a 76-ha study site and providing a framework for future management operations. I use UAV-borne photogrammetry to

examine the structural changes to a high-density forest that underwent a prescribed mechanical thinning restoration treatment. More specifically, I develop a methodology for measuring forest structure at the fine- and mid-scales to quantify the changes resulting from the treatment and determine whether this methodology is a viable tool for monitoring prescription-based forest restoration treatments. I use UAV high-resolution multispectral imagery and structure from motion (SfM) models to quantify vertical and horizontal forest structure metrics at the fine-scale across a gradient of density conditions. Then, I use the UAV-derived data to assess the effectiveness of the restoration thinning prescription.

The second publication, which is chapter 3 in this dissertation, focuses on quantifying snowpack dynamics in the thinned and unthinned portions of the same study site, and evaluates the benefits of thinning on snowpack. I use UAV multispectral orthomosaic image time-series to quantify snow cover and areas of persistent snowpack. In addition, I use UAV-derived SfM models to examine the effects of forest structure on snowpack persistence. Snow cover was quantified using data from three separate winter storms and persistent snow cover was identified using a novel classification scheme. The effects of forest structure shading on snow persistence were assessed using a novel approach to quantifying fine-scale tree shading with multivariate adaptive regression splines (MARS).

The third and final paper (chapter 4) focuses on measuring soil moisture availability and its persistence throughout fore-summer seasonal drought. I generate and use unprecedented, spatially- and temporally-extensive soil moisture time-series data to investigate soil moisture relationships to forest structure conditions. I use data from 112 soil matric potential sensors to quantify soil moisture along the top 100 cm of the soil profile during two consecutive seasonal

drought periods. Sensors were located across the same 76 ha study site and cover the gradient of forest density available from heavily thinned to overly dense unthinned conditions. I use high resolution lidar data from a terrestrial laser scanner to assess how fine-scale forest structure components drive differences in the timing, magnitude, and amount of soil drying.

The objectives of this study can be summarized as follows:

1. To develop a rapid and accurate methodology for measuring and assessing forest structure changes at fine- and mid-scales resulting from a restoration thinning project, using UAV high-resolution multispectral imagery and photogrammetric SfM point cloud data.
2. To quantify and predict the spatial extent of persistent snowpack as it relates to forest structure resulting from the restoration thinning project using UAV image time-series and photogrammetric SfM point cloud data.
3. To measure the soil moisture response to seasonal drought and to assess its relationship to fine-scale forest structure in the recently thinned forest using high-resolution soil matric potential measurements and terrestrial lidar datasets.

1.7 References

- Adams, H. D., Guardiola-Claramonte, M., Barron-Gafford, G. A., Villegas, J. C., Breshears, D. D., Zou, C. B., Troch, P. A., & Huxman, T. E. (2009). Temperature sensitivity of drought-induced tree mortality portends increased regional die-off under global-change-type drought. *Proceedings of the National Academy of Sciences of the United States of America*, *106*(17), 7063–7066. <https://doi.org/10.1073/pnas.0901438106>
- Allen, C. D., Breshears, D. D., & McDowell, N. G. (2015). On underestimation of global vulnerability to tree mortality and forest die-off from hotter drought in the Anthropocene. *Ecosphere*, *6*(8), 1–55. <https://doi.org/10.1890/ES15-00203.1>
- Allen, C. D., Savage, M., Falk, D. A., Suckling, K. F., Swetnam, T. W., Schulke, T., Stacey, P. B., Morgan, P., Hoffman, M., & Klingel, J. T. (2002). Ecological Restoration of Southwestern Ponderosa Pine Ecosystems: A Broad Perspective. *Ecological Applications*, *12*(5), 1418–1433. [https://doi.org/10.1890/1051-0761\(2002\)012\[1418:EROSPP\]2.0.CO;2](https://doi.org/10.1890/1051-0761(2002)012[1418:EROSPP]2.0.CO;2)
- Allen, R. G., Pereira, L. S., Raes, D., & Smith, M. (1998). *Crop evapotranspiration-Guidelines for computing crop water requirements-FAO irrigation and drainage paper 56*. [https://doi.org/ISBN 92-5-104219-5](https://doi.org/ISBN%2092-5-104219-5)
- Altschul, J. H., & Fairley, H. C. (1989). *Man, Models and Management: An Overview of the Archaeology of the Arizona Strip and the Management of its Cultural Resources*. SRI Press. <https://doi.org/doi:10.6067/XCV8DV1M7H>
- Andrews, C. M., D'Amato, A. W., Fraver, S., Palik, B., Battaglia, M. A., & Bradford, J. B. (2020). Low stand density moderates growth declines during hot-droughts in semi-arid

forests. *Journal of Applied Ecology*, September 2019, 1–14. <https://doi.org/10.1111/1365-2664.13615>

Bales, R. C., Hopmans, J. W., O'Geen, A. T., Meadows, M., Hartsough, P. C., Kirchner, P., Hunsaker, C. T., & Beaudette, D. (2011). Soil Moisture Response to Snowmelt and Rainfall in a Sierra Nevada Mixed-Conifer Forest. *Vadose Zone Journal*, 10(3), 786. <https://doi.org/10.2136/vzj2011.0001>

Barnett, T. P., Adam, J. C., & Lettenmaier, D. P. (2005). Potential impacts of a warming climate on water availability in snow-dominated regions. In *Nature* (Vol. 438, Issue 7066, pp. 303–309). <https://doi.org/10.1038/nature04141>

Breshears, D. D., Cobb, N. S., Rich, P. M., Price, K. P., Allen, C. D., Balice, R. G., Romme, W. H., Kastens, J. H., Floyd, M. L., Belnap, J., Anderson, J. J., Myers, O. B., & Meyer, C. W. (2005). Regional vegetation die-off in response to global-change-type drought. *Proceedings of the National Academy of Sciences of the United States of America*, 102(42), 15144–15148. <https://doi.org/10.1073/pnas.0505734102>

Breshears, D. D., Rich, P. M., Barnes, F. J., & Campbell, K. (1997). Overstory-imposed heterogeneity in solar radiation and soil moisture in a semiarid woodland. *Ecological Applications*, 7(4), 1201–1215. [https://doi.org/10.1890/1051-0761\(1997\)007\[1201:OIHISR\]2.0.CO;2](https://doi.org/10.1890/1051-0761(1997)007[1201:OIHISR]2.0.CO;2)

Broxton, P. D., van Leeuwen, W. J. D., & Biederman, J. A. (2020). Forest cover and topography regulate the thin, ephemeral snowpacks of the semiarid Southwest United States. *Ecohydrology*. <https://doi.org/10.1002/eco.2202>

- Castello, J. D., Leopold, D. J., & Smallidge, P. J. (2006). Pathogens, Patterns, and Processes in Forest Ecosystems. *BioScience*, *45*(1), 16–24. <https://doi.org/10.2307/1312531>
- Chapin, F. S. (1991). Integrated Responses of Plants to Stress. *BioScience*, *41*(1), 29–36. <https://doi.org/10.2307/1311538>
- Chapin, F. S., Bloom, A. J., Field, C. B., & Waring, R. H. (1987). Plant Responses to Multiple Environmental Factors. *BioScience*, *37*(1), 49–57. <https://doi.org/10.2307/1310177>
- Clark, J. S., Iverson, L., Woodall, C. W., Allen, C. D., Bell, D. M., Bragg, D. C., D'Amato, A. W., Davis, F. W., Hersh, M. H., Ibanez, I., Jackson, S. T., Matthews, S., Pederson, N., Peters, M., Schwartz, M. W., Waring, K. M., & Zimmermann, N. E. (2016). The impacts of increasing drought on forest dynamics, structure, and biodiversity in the United States. *Global Change Biology*, *22*(7), 2329–2352. <https://doi.org/10.1111/gcb.13160>
- Cooper, C. F. (1960). Changes in Vegetation, Structure, and Growth of Southwestern Pine Forests since White Settlement. *Ecological Monographs*, *30*(2), 129–164. <https://doi.org/10.2307/1948549>
- Covington, W. W., & Moore, M. M. (2006). Postsettlement Changes in Natural Fire Regimes and Forest Structure. *Journal of Sustainable Forestry*, *2*(1–2), 153–181. https://doi.org/10.1300/j091v02n01_07
- Covington, W. Wallace, Fule, P. Z., Moore, M. M., Hart, S. C., Kolb, T. E., Mast, J. N., Sackett, S. S., & Wagner, M. R. (1997). Restoring Ecosystem Health in Ponderosa Pine Forests of the Southwest. *Journal of Forestry*, *95*(4), 23–29.
- D'Odorico, P., Caylor, K., Okin, G. S., & Scanlon, T. M. (2007). On soil moisture-vegetation

feedbacks and their possible effects on the dynamics of dryland ecosystems. *Journal of Geophysical Research: Biogeosciences*, 112(4), n/a-n/a.

<https://doi.org/10.1029/2006JG000379>

Dahms, C. W., & Geils, B. W. (1997). An assessment of forest ecosystem health in the Southwest. *Gen Technical Rep Rm-Gtr-295 Fort Collins Co U S Dep Agric For Serv Rocky Mt For Range Exp Stn 97 P*, 295. <https://doi.org/10.2737/rm-gtr-295>

Davis, R. E., Hardy, J. P., Ni, W., Woodcock, C., McKenzie, J. C., Jordan, R., & Li, X. (1997). Variation of snow cover ablation in the boreal forest: A sensitivity study on the effects of conifer canopy. *Journal of Geophysical Research Atmospheres*, 102(24), 29389–29395. <https://doi.org/10.1029/97jd01335>

Day, K., Berg, J., Brown, H., Crow, T., Morrison, J., Nowacki, G., Puckett, D., Sallee, R., Schenck, T., & Wood, B. (2006). *Ecosystem Restoration: A Framework for Restoring and Maintaining the National Forests and Grasslands*. https://www.fs.fed.us/restoration/documents/RestFramework_final_010606.pdf

Dickerson-Lange, S. E., Gersonde, R. F., Hubbart, J. A., Link, T. E., Nolin, A. W., Perry, G. H., Roth, T. R., Wayand, N. E., & Lundquist, J. D. (2017). Snow disappearance timing is dominated by forest effects on snow accumulation in warm winter climates of the Pacific Northwest, United States. *Hydrological Processes*, 31(10), 1846–1862. <https://doi.org/10.1002/hyp.11144>

Dickerson-Lange, S. E., Lutz, J. A., Martin, K. A., Raleigh, M. S., Gersonde, R., & Lundquist, J. D. (2015). Evaluating observational methods to quantify snow duration under diverse forest

canopies. *Water Resources Research*, 51(2), 1203–1224.

<https://doi.org/10.1002/2014WR015744>

Ehleringer, J. R., & Dawson, T. E. (1992). Water uptake by plants: perspectives from stable isotope composition. *Plant, Cell and Environment*, 15, 1073–1082.

Ehleringer, J. R., Phillips, S. J., Schuster, W. S. F., & Sandquist, D. S. (1991). Differential utilization of summer rains by desert plants. *Oecologia*, 88, 430–434.

Entekhabi, D., Rodriguez-Iturbe, I., & Castelli, F. (1996). Mutual interaction of soil moisture state and atmospheric processes. *Journal of Hydrology*, 184(1–2), 3–17.

[https://doi.org/10.1016/0022-1694\(95\)02965-6](https://doi.org/10.1016/0022-1694(95)02965-6)

Essery, R., Bunting, P., Hardy, J., Link, T., Marks, D., Melloh, R., Pomeroy, J., Rowlands, A., & Rutter, N. (2008). Radiative transfer modeling of a coniferous canopy characterized by airborne remote sensing. *Journal of Hydrometeorology*, 9(2), 228–241.

<https://doi.org/10.1175/2007JHM870.1>

Essery, R., Pomeroy, J., Parviainen, J., Storck, P., Essery, R., Pomeroy, J., Parviainen, J., & Storck, P. (2003). Sublimation of Snow from Coniferous Forests in a Climate Model.

[Http://Dx.Doi.Org/10.1175/1520-0442\(2003\)016<1855:SOSFCF>2.0.CO;2](Http://Dx.Doi.Org/10.1175/1520-0442(2003)016<1855:SOSFCF>2.0.CO;2).

[https://doi.org/10.1175/1520-0442\(2003\)016<1855:SOSFCF>2.0.CO;2](https://doi.org/10.1175/1520-0442(2003)016<1855:SOSFCF>2.0.CO;2)

FAO: Food and Agriculture Organization of the United Nations. (2015). Global Forest Resources Assessment 2015. Retrieved from <http://www.fao.org/3/a-i4808e.pdf>

Ffolliott, P. F., & Gottfried, G. J. (2003). Contributions of Snow Research To Forest Watershed Management in the Southwestern United States. *Proceedings of the 71st Annual Meeting of*

the Western Snow Conference.

[http://www.westernsnowconference.org/proceedings/pdf_Proceedings/2003 WEB/Ffolliott, P. et al_Contributions of Snow Research to Forest.pdf](http://www.westernsnowconference.org/proceedings/pdf_Proceedings/2003%20WEB/Ffolliott,%20P.%20et%20al_Contributions%20of%20Snow%20Research%20to%20Forest.pdf)

Ffolliott, P. F., Gottfried, G. J., & Baker, M. B. (1989). Water yield from forest snowpack management: Research findings in Arizona and New Mexico. *Water Resources Research*, 25(9), 1999–2007. <https://doi.org/10.1029/WR025i009p01999>

Fitch, R. A., Kim, Y. S., Waltz, A. E. M., & Crouse, J. E. (2018). Changes in potential wildland fire suppression costs due to restoration treatments in Northern Arizona Ponderosa pine forests. *Forest Policy and Economics*, 87, 101–114. <https://doi.org/10.1016/j.forpol.2017.11.006>

Fitzgerald, S. a. (2005). Fire Ecology of Ponderosa Pine and the Rebuilding of Fire-Resilient Ponderosa Pine. *USDA Forest Service General Technical Report*, 97756, PSW-GTR-198.

Forzieri, G., Castelli, F., & Vivoni, E. R. (2011). Vegetation Dynamics within the North American Monsoon Region. *American Meteorological Society*, 1763–1783. <https://doi.org/10.1175/2010JCLI3847.1>

French, H., & Binley, A. (2004). Snowmelt infiltration: Monitoring temporal and spatial variability using time-lapse electrical resistivity. *Journal of Hydrology*, 297(1–4), 174–186. <https://doi.org/10.1016/j.jhydrol.2004.04.005>

Fulé, P. Z. (2008). Does it make sense to restore wildland fire in changing climate? *Restoration Ecology*, 16(4), 526–532. <https://doi.org/10.1111/j.1526-100X.2008.00489.x>

Fulé, P. Z., Covington, W. W., & Moore, M. M. (1997). Determining reference conditions for

- ecosystem management of southwestern ponderosa pine forests. *Ecological Applications*, 7(3), 895–908. [https://doi.org/10.1890/1051-0761\(1997\)007\[0895:drcfem\]2.0.co;2](https://doi.org/10.1890/1051-0761(1997)007[0895:drcfem]2.0.co;2)
- Ganey, J. L., & Vojta, S. C. (2011). Tree mortality in drought-stressed mixed-conifer and ponderosa pine forests, Arizona, USA. *Forest Ecology and Management*, 261, 162–168. <https://doi.org/10.1016/j.foreco.2010.09.048>
- Goeking, S. A., & Tarboton, D. G. (2020). Forests and Water Yield: A Synthesis of Disturbance Effects on Streamflow and Snowpack in Western Coniferous Forests. *Journal of Forestry*, 2020, 1–21. <https://doi.org/10.1093/jofore/fvz069>
- Gottfried, G. J., & Ffolliott, P. F. (2009). Snowpack dynamics in an opening and a thinned stand in a ponderosa pine forest. In *Hydrology and Water Resources in Arizona and the Southwest* (Vol. 39).
- Grant, G. E., Tague, C. L., & Allen, C. D. (2013). Watering the forest for the trees: An emerging priority for managing water in forest landscapes. *Frontiers in Ecology and the Environment*, 11(6), 314–321. <https://doi.org/10.1890/120209>
- Gray, A. N., Spies, T. A., & Easter, M. J. (2002). *Microclimatic and soil moisture responses to gap formation in coastal Douglas-fir forests*. <https://doi.org/10.1139/X01-200>
- Grumbine, E. R. (1994). What Is Ecosystem Management? *Conservation Biology*, 8(1), 27–38. <https://doi.org/10.1046/j.1523-1739.1994.08010027.x>
- Harder, P., Schirmer, M., Pomeroy, J., & Helgason, W. (2016). Accuracy of snow depth estimation in mountain and prairie environments by an unmanned aerial vehicle. *The*

Cryosphere, 10, 2559–2571. <https://doi.org/10.5194/tc-10-2559-2016>

Harpold, A. A., Biederman, J. A., Condon, K., Merino, M., Korgaonkar, Y., Nan, T., Sloat, L. L., Ross, M., & Brooks, P. D. (2014). Changes in snow accumulation and ablation following the Las Conchas Forest Fire, New Mexico, USA. *Ecohydrology*, 7(2), 440–452. <https://doi.org/10.1002/eco.1363>

Hereford, R. (2007). Climate Variation at Flagstaff, Arizona - 1950 to 2007. In *Open-File Report* (Version 1.). <https://doi.org/10.3133/ofr20071410>

Hong, S. Y., & Kalnay, E. (2000). Role of sea surface temperature and soil-moisture feedback in the 1998 Oklahoma-Texas drought. *Nature*, 408(6814), 842–844. <https://doi.org/10.1038/35048548>

Huffman, D. W., Moore, M. M., Covington, W. W., Crouse, J. E., & Fulé, P. Z. (2001). Ponderosa Pine Forest Reconstruction: Comparisons with Historical Data. *Ponderosa Pine Ecosystems Restoration and Conservation: Steps Towards Stewardship*, 3–8.

Husch, B., Beers, T. W., & Kershaw, J. A. (2003). *Forest Mensuration* (4th ed.). John Wiley and Sons.

Huxman, T. E., Smith, M. D., Fay, P. A., Knapp, A. K., Shaw, M. R., Lolk, M. E., Smith, S. D., Tissue, D. T., Zak, J. C., Weltzin, J. F., Pockman, W. T., Sala, O. E., Haddad, B. M., Harte, J., Koch, G. W., Schwinning, S., Small, E. E., & Williams, D. G. (2004). Convergence across biomes to a common rain-use efficiency. *Nature*, 429(6992), 651–654. <https://doi.org/10.1038/nature02561>

- James, T., Evans, A., Madly, E., & Kelly, C. (2014). *The Economic Importance of the Colorado River to the Basin Region*. <https://businessforwater.org/wp-content/uploads/2016/12/PTF-Final-121814.pdf>
- Kerhoulas, L. P., Kolb, T. E., & Koch, G. W. (2013). Tree size, stand density, and the source of water used across seasons by ponderosa pine in northern Arizona. *Forest Ecology and Management*, 289, 425–433. <https://doi.org/10.1016/j.foreco.2012.10.036>
- Koepke, D. F., & Kolb, T. E. (2013). Species variation in water relations and xylem vulnerability to cavitation at a forest-woodland ecotone. *Forest Science*, 59(5), 524–535. <https://doi.org/10.5849/forsci.12-053>
- Kolb, TE E, Wagner, M. R., & Covington, W. W. (1994). Concepts of forest health: utilitarian and ecosystem perspectives. *Journal of Forestry*, 92(2), 10–15. <http://scholarsarchive.library.oregonstate.edu/xmlui/handle/1957/17277>
- Kolb, Thomas E, Fettig, C. J., Ayres, M. P., Bentz, B. J., Hicke, J. A., Mathiasen, R., Stewart, J. E., & Weed, A. S. (2016). Observed and anticipated impacts of drought on forest insects and diseases in the United States q. *Forest Ecology and Management*, 380, 321–334. <https://doi.org/10.1016/j.foreco.2016.04.051>
- Koster, R. D., Dirmeyer, P. A., Guo, Z., Bonan, G., Chan, E., Cox, P., Gordon, C. T., Kanae, S., Kowalczyk, E., Lawrence, D., Liu, P., Lu, C. H., Malyshev, S., McAvaney, B., Mitchell, K., Mocko, D., Oki, T., Oleson, K., Pitman, A., ... Yamada, T. (2004). Regions of strong coupling between soil moisture and precipitation. *Science*, 305(5687), 1138–1140. <https://doi.org/10.1126/science.1100217>

- Laio, F., Porporato, A., Ridolfi, L., & Rodriguez-Iturbe, I. (2001). Plants in water-controlled ecosystems: Active role in hydrologic processes and response to water stress II. Probabilistic soil moisture dynamics. *Advances in Water Resources*, 24(7), 707–723. [https://doi.org/10.1016/S0309-1708\(01\)00005-7](https://doi.org/10.1016/S0309-1708(01)00005-7)
- Landres, P. B., Morgan, P., & Swanson, F. J. (1999). Overview of the use of natural variability concepts in managing ecological systems. *Ecological Applications* 1, 9(4), 1179–1188.
- Larson, A. J., & Churchill, D. (2012). Tree spatial patterns in fire-frequent forests of western North America, including mechanisms of pattern formation and implications for designing fuel reduction and restoration treatments. *Forest Ecology and Management*, 267, 74–92. <https://doi.org/10.1016/j.foreco.2011.11.038>
- Lawler, R. R., & Link, T. E. (2011). Quantification of incoming all-wave radiation in discontinuous forest canopies with application to snowmelt prediction. *Hydrological Processes*, 25(21), 3322–3331. <https://doi.org/10.1002/hyp.8150>
- Lendzioch, T., Langhammer, J., & Jenicek, M. (2019). Estimating Snow Depth and Leaf Area Index Based on UAV Digital Photogrammetry. *Sensors*, 19(5), 1027. <https://doi.org/10.3390/s19051027>
- Loik, M. E., Breshears, D. D., Lauenroth, W. K., & Belnap, J. (2004). A multi-scale perspective of water pulses in dryland ecosystems: Climatology and ecohydrology of the western USA. In *Oecologia* (Vol. 141, Issue 2, pp. 269–281). <https://doi.org/10.1007/s00442-004-1570-y>
- Lundquist, J. D., Dickerson-Lange, S. E., Lutz, J. A., & Cristea, N. C. (2013). Lower forest density enhances snow retention in regions with warmer winters: A global framework

- developed from plot-scale observations and modeling. *Water Resources Research*, 49(10), 6356–6370. <https://doi.org/10.1002/wrcr.20504>
- Maherali, H., & DeLucia, E. H. (2001). Influence of climate-driven shifts in biomass allocation on water transport and storage in ponderosa pine. *Oecologia*, 129, 481–491.
- Mast, J., Fulé, P. Z., Moore, M. M., Covington, W. W., & Waltz, A. E. M. (1999). Restoration of Presettlement Age Structure of an Arizona Ponderosa Pine Forest. *Ecological Applications*, 9(1), 228–239. [https://doi.org/10.1890/1051-0761\(1999\)009\[0228:ropaso\]2.0.co;2](https://doi.org/10.1890/1051-0761(1999)009[0228:ropaso]2.0.co;2)
- Miziński, B., & Niedzielski, T. (2017). Fully-automated estimation of snow depth in near real time with the use of unmanned aerial vehicles without utilizing ground control points. *Cold Regions Science and Technology*, 138, 63–72.
<https://doi.org/10.1016/j.coldregions.2017.03.006>
- Molotch, N. P., Blanken, P. D., Williams, M. W., Turnipseed, A. A., Monson, R. K., & Margulis, S. A. (2007). Estimating sublimation of intercepted and sub-canopy snow using eddy covariance systems. *Hydrological Processes*, 21(12), 1567–1575.
<https://doi.org/10.1002/hyp.6719>
- Molotch, N. P., Brooks, P. D., Burns, S. P., Litvak, M., Monson, R. K., McConnell, J. R., & Musselman, K. (2009). Ecohydrological controls on snowmelt partitioning in mixed-conifer sub-alpine forests. *Ecohydrology*, 2(2), 129–142. <https://doi.org/10.1002/eco.48>
- Moore, M. M., Huffman, D. W., Fulé, P. Z., Wallace Covington, W., & Crouse, J. E. (2004). Comparison of Historical and Contemporary Forest Structure and Southwestern Ponderosa Pine Forests. *Forest Science*, 50(2), 162–176.

- Mori, A. S., Lertzman, K. P., & Gustafsson, L. (2017). Biodiversity and ecosystem services in forest ecosystems: a research agenda for applied forest ecology. *Journal of Applied Ecology*, *54*(1), 12–27. <https://doi.org/10.1111/1365-2664.12669>
- Mueller, R. C., Scudder, C. M., Porter, M. E., Talbot Trotter, R., Gehring, C. A., & Whitham, T. G. (2005). Differential tree mortality in response to severe drought: Evidence for long-term vegetation shifts. *Journal of Ecology*, *93*(6), 1085–1093. <https://doi.org/10.1111/j.1365-2745.2005.01042.x>
- Newman, B. D., Campbell, A. R., & Wilcox, B. P. (1998). Lateral subsurface flow pathways in a semiarid Ponderosa pine hillslope. *Water Resources Research*, *34*(12), 3485–3496. <https://doi.org/10.1029/98WR02684>
- Newman, B. D., Wilcox, B. P., & Graham, R. C. (2004). Snowmelt-driven macropore flow and soil saturation in a semiarid forest. *Hydrological Processes*, *18*(5), 1035–1042. <https://doi.org/10.1002/hyp.5521>
- Niedzielski, T., Spallek, W., & Witek-Kasprzak, M. (2018). Automated Snow Extent Mapping Based on Orthophoto Images from Unmanned Aerial Vehicles. *Pure and Applied Geophysics*, *175*(9), 3285–3302. <https://doi.org/10.1007/s00024-018-1843-8>
- Palmer, W. C. (1965). Meteorological Drought. In *U.S. Weather Bureau, Res. Pap. No. 45* (p. 58). <https://www.ncdc.noaa.gov/temp-and-precip/drought/docs/palmer.pdf>
- Pearce, D. W. (2001). The Economic Value of Forest Ecosystems. *Ecosystem Health*, *7*(4), 284–296. <https://doi.org/10.1046/j.1526-0992.2001.01037.x>

- Pearson, G. A. (1923). Natural reproduction of western yellow pine in the Southwest. In *Bulletin of the U.S. Department of Agriculture; no.1105*. U.S. Department of Agriculture.
<https://doi.org/10.5962/bhl.title.64666>
- Price, A. G., & Hendrie, L. K. (1983). Water motion in a deciduous forest during snowmelt. *Journal of Hydrology*, 64(1–4), 339–356. [https://doi.org/10.1016/0022-1694\(83\)90076-8](https://doi.org/10.1016/0022-1694(83)90076-8)
- Price, K. (2011). Effects of watershed topography, soils, land use, and climate on baseflow hydrology in humid regions: A review. *Progress in Physical Geography: Earth and Environment*, 35(4), 465–492. <https://doi.org/10.1177/0309133311402714>
- Pugh, E., & Small, E. (2012). The impact of pine beetle infestation on snow accumulation and melt in the headwaters of the Colorado River. *Ecohydrology*, 5(4), 467–477.
<https://doi.org/10.1002/eco.239>
- Qubaja, R., Amer, M., Tatarinov, F., Rotenberg, E., Preisler, Y., Sprintsin, M., & Yakir, D. (2020). Partitioning evapotranspiration and its long-term evolution in a dry pine forest using measurement-based estimates of soil evaporation. *Agricultural and Forest Meteorology*, 281, 107831. <https://doi.org/10.1016/j.agrformet.2019.107831>
- Raz-Yaseef, N., Rotenberg, E., & Yakir, D. (2010). Effects of spatial variations in soil evaporation caused by tree shading on water flux partitioning in a semi-arid pine forest. *Agricultural and Forest Meteorology*, 150(3), 454–462.
<https://doi.org/10.1016/j.agrformet.2010.01.010>
- Raz-Yaseef, Naama, Yakir, D., Rotenberg, E., Schiller, G., & Cohen, S. (2010). Ecohydrology of a semi-arid forest: Partitioning among water balance components and its implications for

predicted precipitation changes. *Ecohydrology*, 3(2), 143–154.

<https://doi.org/10.1002/eco.65>

Raz-Yaseef, Naama, Yakir, D., Schiller, G., & Cohen, S. (2012). Dynamics of evapotranspiration partitioning in a semi-arid forest as affected by temporal rainfall patterns. *Agricultural and Forest Meteorology*, 157, 77–85.

<https://doi.org/10.1016/j.agrformet.2012.01.015>

Revuelto, J., López-Moreno, J. I., Azorin-Molina, C., & Vicente-Serrano, S. M. (2014). Topographic control of snowpack distribution in a small catchment in the central Spanish Pyrenees: Intra- and inter-annual persistence. *Cryosphere*, 8(5), 1989–2006.

<https://doi.org/10.5194/tc-8-1989-2014>

Reynolds, R. T., Meador, A. J. S., Youtz, J. A., Nicolet, T., Matonis, M. S., Jackson, P. L., DeLorenzo, D. G., & Graves, A. D. (2013). Restoring composition and structure in southwestern frequent-fire forests. *USDA Forest Service, RMRS-GTR-3*.

Rieman, B., Lee, D., Burns, D., Gresswell, R., Young, M., Stowell, R., Rinne, J., & Howell, P. (2003). Status of native fishes in the western United States and issues for fire and fuels management. *Forest Ecology and Management*, 178(1–2), 197–211.

[https://doi.org/10.1016/S0378-1127\(03\)00062-8](https://doi.org/10.1016/S0378-1127(03)00062-8)

Roth, T. R., & Nolin, A. W. (2017). Forest impacts on snow accumulation and ablation across an elevation gradient in a temperate montane environment. *Hydrol. Earth Syst. Sci*, 21, 5427–5442. <https://doi.org/10.5194/hess-21-5427-2017>

Sahin, V., & Hall, M. J. (1996). The effects of afforestation and deforestation on water yields. In

Journal of Hydrology ELSEVIER Journal of Hydrology (Vol. 178).

Sánchez Meador, A. J., & Moore, M. M. (2011). Reprint of: Lessons from long-term studies of harvest methods in southwestern ponderosa pine–Gambel oak forests on the Fort Valley Experimental Forest, Arizona, U.S.A. *Forest Ecology and Management*, 261(5), 923–936. <https://doi.org/10.1016/J.FORECO.2010.11.010>

Sandvig, R. M., & Phillips, F. M. (2006). Ecohydrological controls on soil moisture fluxes in arid to semiarid vadose zones. *Water Resources Research*, 42(8). <https://doi.org/10.1029/2005WR004644>

Sankey, T., Donald, J., McVay, J., Ashley, M., O'Donnell, F., Lopez, S. M., & Springer, A. (2015). Multi-scale analysis of snow dynamics at the southern margin of the North American continental snow distribution. *Remote Sensing of Environment*, 169, 307–319. <https://doi.org/10.1016/j.rse.2015.08.028>

Schubert, Gilbert H. 1974. Silviculture of southwestern ponderosa pine: The status of our knowledge. Res. Pap. RM-123. Fort Collins, CO: U.S. Department of Agriculture, Forest Service, Rocky Mountain Forest and Range Experiment Station. 71 p.

Schultz, C. A., Coelho, D. L., & Beam, R. D. (2014). Design and Governance of Multiparty Monitoring under the (USDA) Forest Service's Collaborative Forest Landscape Restoration Program. *Journal of Forestry*, 112(2), 198-206(9). <https://doi.org/10.5849/jof.13-070>

Schultz, C. A., Jedd, T., & Beam, R. D. (2012). The Collaborative Forest Landscape Restoration Program: A History and Overview of the First Projects. *Journal of Forestry*, 110(7), 381–391. <https://doi.org/10.5849/jof.11-082>

- Seyfried, M. S., Schwinning, S., Walvoord, M. A., Pockman, W. T., Newman, B. D., Jackson, R. B., & Phillips, F. M. (2005). Ecohydrological control of deep drainage in arid and semiarid regions. *Ecology*, *86*(2), 277–287. <https://doi.org/10.1890/03-0568>
- Snyder, K. A., & Tartowski, S. L. (2006). Multi-scale temporal variation in water availability: Implications for vegetation dynamics in arid and semi-arid ecosystems. *Journal of Arid Environments*, *65*(2), 219–234. <https://doi.org/10.1016/j.jaridenv.2005.06.023>
- Stanturf, J. A., Palik, B. J., & Dumroese, K. R. (2014). Contemporary forest restoration: A review emphasizing function. *Forest Ecol Manag*, *331*, 292–323. <https://doi.org/10.1016/j.foreco.2014.07.029>
- Stoy, P. C., El-Madany, T. S., Fisher, J. B., Gentine, P., Gerken, T., Good, S. P., Klosterhalfen, A., Liu, S., Miralles, D. G., Perez-Priego, O., Rigden, A. J., Skaggs, T. H., Wohlfahrt, G., Anderson, R. G., Coenders-Gerrits, A. M. J., Jung, M., Maes, W. H., Mammarella, I., Mauder, M., ... Wolf, S. (2019). Reviews and syntheses: Turning the challenges of partitioning ecosystem evaporation and transpiration into opportunities. *Biogeosciences*, *16*(19), 3747–3775. <https://doi.org/10.5194/bg-16-3747-2019>
- Sturm, M., Goldstein, M. A., & Parr, C. (2017). Water and life from snow: A trillion dollar science question. *Water Resources Research*, *53*(5), 3534–3544. <https://doi.org/10.1002/2017WR020840>
- Swetnam, T. W., & Allen, C. D. (1999). Applied historical ecology: using the past to manage for the future. *Ecological Applications*.
- Swetnam, T. W., & Betancourt, J. L. (2010). Mesoscale Disturbance and Ecological Response to

Decadal Climatic Variability in the American Southwest. In *Advances in Global Change Research* (Vol. 41, pp. 329–359). Springer International Publishing.

https://doi.org/10.1007/978-90-481-8736-2_32

Teng-Chiu Lin, by, Rich, P. M., Heisler, D. A., & Barnes, F. J. (1992). *Influences of Canopy Geometry on Near-Ground Solar Radiation and Water Balances of Pinyon-Juniper and Ponderosa Pine Woodlands*. American Society for Photogrammetry and Remote Sensing 1992 Annual Meeting. Albuquerque, NM, pp. 285-294.

Teuling, A. J. (2005). Improved understanding of soil moisture variability dynamics.

Geophysical Research Letters, 32(5), L05404. <https://doi.org/10.1029/2004GL021935>

Thornthwaite, C. W. (1952). Evaporation in the Hydrologic Cycle. In *The Physical and Economic Foundation of Natural Resources: The Physical Basis of Water Supply and Its Principal Uses* (pp. 25–35). Interior and Insular Affairs Committee House of Representatives, United States Congress.

Tyagi, J. V, Qazi, N., Rai, • S P, Singh, • M P, & Rai, S. P. (2013). Analysis of soil moisture variation by forest cover structure in lower western Himalayas, India. *Journal of Forestry Research*, 24(2), 317–324. <https://doi.org/10.1007/s11676-013-0355-8>

van der Schrier, G., & Barkmeijer, J. (2007). North American 1818-1824 drought and 1825-1840 pluvial and their possible relation to the atmospheric circulation. *Journal of Geophysical Research: Atmospheres*, 112(D13), n/a-n/a. <https://doi.org/10.1029/2007JD008429>

Varhola, A., Coops, N. C., Weiler, M., & Moore, R. D. (2010). Forest canopy effects on snow accumulation and ablation: An integrative review of empirical results. In *Journal of*

Hydrology (Vol. 392, Issues 3–4, pp. 219–233). Elsevier.

<https://doi.org/10.1016/j.jhydrol.2010.08.009>

Vicente-Serrano, S. M., Beguería, S., & López-Moreno, J. I. (2010). A multiscalar drought index sensitive to global warming: The standardized precipitation evapotranspiration index.

Journal of Climate, 23(7), 1696–1718. <https://doi.org/10.1175/2009JCLI2909.1>

Vicente-Serrano, S. M., Gouveia, C., Camarero, J. J., Beguería, S., Trigo, R., López-Moreno, J.

I., Azorín-Molina, C., Pasho, E., Lorenzo-Lacruz, J., Revuelto, J., Morán-Tejeda, E., &

Sanchez-Lorenzo, A. (2013). Response of vegetation to drought time-scales across global

land biomes. *Proceedings of the National Academy of Sciences of the United States of*

America, 110(1), 52–57. <https://doi.org/10.1073/pnas.1207068110>

Vose, J. M., Miniati, C. F., Luce, C. H., Asbjornsen, H., Caldwell, P. V., Campbell, J. L., Grant,

G. E., Isaak, D. J., Loheide, S. P., & Sun, G. (2016). Ecohydrological implications of

drought for forests in the United States. *Forest Ecology and Management*, 380, 335–345.

<https://doi.org/10.1016/j.foreco.2016.03.025>

Vose, J. M., Miniati, C. F., Luce, C. H., Asbjornsen, H., Caldwell, P. V., Campbell, J. L., Grant,

G. E., Isaak, D. J., Loheide II, S. P., & Sun, G. (2016). Ecohydrological implications of

drought for forests in the United States. *FOREST ECOLOGY AND MANAGEMENT*.

<https://doi.org/10.1016/j.foreco.2016.03.025>

Wang, L., Good, S. P., & Caylor, K. K. (2014). Global synthesis of vegetation control on

evapotranspiration partitioning. *Geophysical Research Letters*, 41(19), 6753–6757.

<https://doi.org/10.1002/2014GL061439>

- Wei, Z., Yoshimura, K., Wang, L., Miralles, D. G., Jasechko, S., & Lee, X. (2017). Revisiting the contribution of transpiration to global terrestrial evapotranspiration. *Geophysical Research Letters*, *44*(6), 2792–2801. <https://doi.org/10.1002/2016GL072235>
- Weldon, L. (2014). *Ecological Restoration in the United States. Speech Presented at Ecosystems, Economy, and Society*. <https://www.fs.fed.us/speeches/ecological-restoration-united-states>
- Weltzin, J. F., Loik, M. E., Schwinning, S., Williams, D. G., Fay, P. A., Haddad, B. M., Harte, J., Huxman, T. E., Knapp, A. K., Lin, G., Pockman, W. T., Shaw, M. R., Small, E. E., Smith, M. D., Smith, S. D., Tissue, D. T., & Zak, J. C. (2003). Assessing the Response of Terrestrial Ecosystems to Potential Changes in Precipitation. *BioScience*, *53*(10), 941. [https://doi.org/10.1641/0006-3568\(2003\)053\[0941:atrote\]2.0.co;2](https://doi.org/10.1641/0006-3568(2003)053[0941:atrote]2.0.co;2)
- White, A. S. (1985). Presettlement Regeneration Patterns in a Southwestern Ponderosa Pine Stand. *Ecology*, *66*(2), 589–594. <https://doi.org/10.2307/1940407>
- Wilcox, B. P., Breshears, D. D., & Allen, C. D. (2003). Ecohydrology of a resource-conserving semiarid woodland: Effects of scale and disturbance. *Ecological Monographs*, *73*(2), 223–239. [https://doi.org/10.1890/0012-9615\(2003\)073\[0223:EOARSW\]2.0.CO;2](https://doi.org/10.1890/0012-9615(2003)073[0223:EOARSW]2.0.CO;2)
- Wilcox, B. P., Newman, B. D., Brandes, D., Davenport, D. W., & Reid, K. (1997). Runoff from a semiarid Ponderosa pine hillslope in New Mexico. *Water Resources Research*, *33*(10), 2301–2314. <https://doi.org/10.1029/97WR01691>
- Williams, M., Law, B. E., Anthoni, P. M., & Unsworth, M. H. (2001). Use of simulation model and ecosystem flux data to examine carbon-water interactions in ponderosa pine. *Tree*

Physiology, 21, 287–298.

- Williamson, M., Rosenstock, S., & Kalies, L. (2011). *Four Forest Restoration Initiative: Stakeholders' Initial Science Needs Assessment*. {4FRI} Science and Monitoring Working Group.
- Winkler, R. D. (2011). Streamline Watershed Management Bulletin, Volume 14, Number 2. *Water Management Bulletin*, 14(2). <http://www.forrex.org/streamline>
- Woods, S. W., Ahl, R., Sappington, J., & McCaughey, W. (2006). Snow accumulation in thinned lodgepole pine stands, Montana, USA. *Forest Ecology and Management*, 235(1–3), 202–211. <https://doi.org/10.1016/j.foreco.2006.08.013>
- Woolsey, T. S. (1911). *Western Yellow Pine in Arizona and New Mexico*. United States Department of Agriculture. <https://www.fs.usda.gov/treesearch/pubs/37531>
- Zhang, L., Dawes, W. R., & Walker, G. R. (2001). Response of mean annual evapotranspiration to vegetation changes at catchment scale. *Water Resources Research*, 37(3), 701–708. <https://doi.org/10.1029/2000WR900325>
- Ziegler, J. P., Hoffman, C., Battaglia, M., & Mell, W. (2017). Spatially explicit measurements of forest structure and fire behavior following restoration treatments in dry forests. *Forest Ecology and Management*, 386, 1–12. <https://doi.org/10.1016/j.foreco.2016.12.002>

CHAPTER 2: UAV-derived estimates of forest structure to inform ponderosa pine forest restoration

2.1 Abstract

Restoring forest ecosystems has become an increasingly high priority for land managers across the American West. Millions of hectares of forest are in need of drastic yet strategic reductions in density (e.g., basal area). Meeting the restoration and management goals requires quantifying metrics of vertical and horizontal forest structure, which has relied upon field-based measurements, manned airborne or satellite remote sensing datasets. We used unmanned aerial vehicle (UAV) image-derived Structure-from-Motion (SfM) models and high-resolution multispectral orthoimagery in this study to quantify vertical and horizontal forest structure at both the fine- (<4 ha) and mid-scales (4–400 ha) across a forest density gradient. We then used these forest structure estimates to assess specific objectives of a forest restoration treatment. At the fine-scale, we found that estimates of individual tree height and canopy diameter were most accurate in low-density conditions, with accuracies degrading significantly in high-density conditions. Mid-scale estimates of canopy cover and forest density followed a similar pattern across the density gradient, demonstrating the effectiveness of UAV image-derived estimates in low- to medium-density conditions as well as the challenges associated with high-density conditions. We found that post-treatment conditions met a majority of the prescription objectives and demonstrate the UAV image application in quantifying changes from a mechanical thinning treatment. We provide a novel approach to forest restoration monitoring using UAV-derived data, one that considers varying density conditions and spatial scales. Future research should consider a more spatially extensive sampling design, including different restoration treatments,

as well as experimenting with different combinations of equipment, flight parameters, and data processing workflows.

2.2 Introduction

Forests cover roughly 28% (3.7 billion ha) of the land area on Earth and are cornerstone to the functioning of hydrologic, ecological and sociopolitical systems (FAO, 2015). In the American Southwest, specifically Arizona, there are an estimated 7.48 million hectares of forested land containing roughly 3.98 billion live trees (<https://www.fia.fs.fed.us/>). Across this region, ponderosa pine (*Pinus ponderosa*) forests have undergone significant changes in their structure, composition and ecological functioning since European-American settlement (hereafter pre-settlement) (Cooper, 1960; Fulé et al., 1997; Congalton and Green, 2008) due to wildfire suppression, selective logging and livestock grazing (Cooper, 1960; Altschul et al., 1989). Pre-settlement regional forest conditions were characterized by a mosaic of diversely aged and structured forest patches with large, irregularly shaped interspaces (Cooper, 1961; Sánchez Meador and Moore, 2011). Their distributions were dependent on site-specific conditions (Woolsey, 1911; Pearson, 1923; Cooper, 1960, 1961; White, 1985; Mast et al., 1999) and the natural variability of vertical and horizontal forest patch structure yielded an ecosystem adapted to and tolerant of frequent (every 2–26 years), low-severity wildfires and other naturally occurring disturbances such as insect and disease outbreaks (Schubert, 1974; Dahms and Geils, 1997; Fitzgerald, 2005; Castello et al., 2006).

The Southwestern ponderosa pine forests are now characterized by extensive closed canopy forests, comprised of trees usually homogeneous in both age and stature with few old-growth trees, and a uniform horizontal spatial distribution at the landscape scale (Moore et al.,

2004; Larson and Churchill, 2012; Reynolds et al., 2013). The current forest structure and composition have, in turn, altered the historical ecological functioning, health and resilience of the entire ponderosa pine ecosystem (Kolb et al., 1994; Swetnam et al., 1999; Swetnam and Betancourt, 2010). These changes to structure have increased and concentrated the amount of ground surface fuels and tree canopy fuels, leading to greater susceptibility to crown fire (Fulé et al., 2004; Reynolds et al., 2013). Reintroducing the ‘natural range of variability’ and promoting long-term ecological health of the Southwestern ponderosa pine forests are now recognized as important management goals (Allen et al., 2002; Covington & Moore, 2006; Fulé, 2008; Landres et al., 1999).

The United States Congress passed the Forest Landscape Restoration Act (FLRA) in 2008–2009 (Fitch et al., 2018; Schultz et al., 2012) and subsequently the Collaborative Forest Landscape Restoration Program (CFLRP) has allowed the United States Department of Agriculture Forest Service (USFS) to establish and fund a number of large-scale forest management programs (Day et al., 2006; Weldon, 2014). Given the collaborative foundations of the CFLRP, a diverse group of stakeholders in Arizona including federal, state, non-profit and private entities established the Four Forests Restoration Initiative (4FRI). As one of the first and the largest forest restoration efforts, 4FRI focuses on reducing the risk of catastrophic wildfire, improving and sustaining watershed health, wildlife habitat and biodiversity across the Apache-Sitgreaves, Coconino, Kaibab and Tonto National Forests (<http://4fri.org/>). Spanning more than 20 years and covering almost a million hectares, 4FRI will design and implement restoration treatments that selectively harvest and thin dense forests via mechanical thinning and reintroduce fire across the treated areas.

Continued monitoring of restoration treatments is critical in supporting adaptive management goals and ensure the long-term success of 4FRI (Williamson et al., 2011; Four Forests Restoration Initiative, 2013; Schultz et al., 2014). More specifically, quantitative data that catalog changes to forest cover and structure are necessary to evaluate the outcome and the success of a restoration treatment. These data allow managers to determine how well a specific treatment prescription is followed and how future treatments should be tailored to meet larger landscape-scale goals. Acquiring this data has traditionally relied on time-intensive and costly field surveys, which provides thorough, fine-scale measurements at the plot level (0.5 ha) (Smith, 2002; USGS, 2017). However, given the vast extent of the current and planned restoration treatments, remote sensing-based methodologies are needed for their cost-effectiveness and spatial extent coverage. Here, we assess unmanned aerial vehicle (UAV)-derived aerial imagery and Structure-from-Motion (SfM) models in evaluating the effectiveness of a forest restoration treatment.

2.2.1 Quantifying forest biophysical variables

Planning, implementing and evaluating restoration treatments can greatly benefit from quantitative datasets that summarize pre- and post-treatment conditions in a stand or across the landscape, regardless of the forest restoration objective and desired outcomes (Patton, 1977; Covington et al., 1997; Mast et al., 1999; Allen et al., 2002; Kalies and Rosenstock, 2013; Bottero et al., 2017; Matonis and Binkley, 2018). Evaluating individual treatments with accurate, quantitative datasets helps determine their contribution to the larger restoration plan and associated changes to the plan. Commonly used forest mensuration metrics in restoration planning and assessment are individual tree diameters at breast height (DBH), and stand-level

estimates of basal area (BA), trees per hectare (TPH), canopy cover (CC), as well as tree patch and interspace size and shape. Tree patches are groups of trees with similar vegetation composition and structure while interspaces are un-treed ‘areas not under the vertical projection of the outermost tree canopies’ (Reynolds et al. 2013, p. 71). Traditional field-based methods for these variables rely on trained field personnel, specialized measurement devices, and often lengthy site visits to produce detailed stem maps and stand-level summaries that are used for implementing and monitoring treatments. Additionally, quantifying stand-level metrics requires a combination of sample-driven field measurements of individual trees and statistical modeling techniques (Huffman et al. 2001). To facilitate standardization of data collection, the USFS developed the Common Stand Exam (CSE) guideline, which provide a step-by-step field measurement methodology and acceptable accuracy standards for collection of individual tree and plot-level vegetation data. We use the accuracy standards from the CSE Field Guide for Region 3 (Southwestern Region) as a baseline in evaluating the UAV-derived estimates of forest metrics.

In contrast to the traditional field-based forest mensuration methods, which tend to cover relatively small spatial extents, airborne lidar (light detection and ranging) data are commonly used to capture structural detail at the landscape level (400 + ha) (Næsset, 2004; Reutebuch et al., 2005; Hudak et al., 2006). The continued high costs associated with airborne lidar data acquisition make it unattractive for fine- (0–4 ha) and mid-scale (4–400 ha) projects. This has fostered interest in UAV-borne photogrammetric Structure-from-Motion (SfM) modeling as a viable, cost-effective alternative for fine- and mid-scale assessments (Iizuka et al., 2018; Puliti et al., 2015; White et al., 2013; Alonzo et al., 2018; Carr and Snyder, 2018; Diaz-Varela et al., 2016). SfM algorithms construct three-dimensional (3D) models with high point densities and

include spectral information. When compared to lidar 3D point cloud data, SfM models often provide similar accuracies in estimating individual tree canopy heights, diameter and volumes (Thiel and Schmulius, 2006; Wallace et al., 2016; Sankey et al., 2019). However, SfM photogrammetry in forested environments has unique challenges affecting the quality of data products and their overall accuracies are not well quantified across a gradient of forest conditions (Bohlin et al., 2017; Rupnik et al., 2017; Snavely et al., 2006). More specifically, Iglhaut et al. (2019) reported that uniform forest canopy textures and common patterns could hamper the ability of SfM algorithm, which negatively affect the quality of the data products. The untreated, highly dense forests typical of the 4FRI region might present large areas of tree and ground occlusion, which is expected to limit scene reconstruction. Here, we use UAV-borne photogrammetry to examine the structural changes to a high-density forest that underwent a prescribed mechanical thinning restoration treatment. Specifically, we develop a methodology for measuring forest structure at the fine- and mid-scales to quantify the changes resulting from the treatment, and determine whether this methodology is a viable tool for monitoring prescription-based forest restoration treatments.

Our first objective was to assess UAV-derived high-resolution multispectral imagery and SfM models in quantifying forest vertical and horizontal structural elements at the fine-scale (<4 ha) across a gradient of density conditions. We first hypothesized that the UAV-derived estimates of individual tree location, tree height (m) and crown diameter (m) would not differ significantly from corresponding field-based measurements. Specifically, all of the UAV-derived estimates of tree height and crown diameter would fall within the acceptable error rates used in USFS Common Stand Exam (CSE) protocol. Second, we hypothesized that as tree density,

measured in trees per hectare (TPH), and canopy cover increased along a density gradient, the accuracy of all UAV-derived individual tree level estimates would significantly decrease.

Our second objective was to evaluate UAV-derived vertical and horizontal forest structural measurements at the mid-scale (4–400 ha); first by quantifying the forest density and structure metrics before and after the mechanical thinning treatment, and then by comparing post-treatment conditions to the restoration prescription guidelines to determine if treatment objectives were met. We hypothesized that the lower, post-treatment forest density would allow accurate estimates of stand-level basal area (BA), canopy cover, and forest patch and interspace metrics. Additionally, that our workflow, when applied to the post-treatment UAV-image derived datasets, would allow forest managers to efficiently assess restoration treatment objectives.

2.3 Materials and Methods

2.3.1 Study area and treatment description

Situated on the southern edge of the Colorado Plateau in northern Arizona, the study area is located in the Coconino National Forest, at the base of the San Francisco Peaks, about 6.5 km from the City of Flagstaff (12S 438346 N., 3901732 E. UTM) (Figure 1A). The study area includes 46 hectares of forested land, ranging in elevation between 2200 and 2270 m above sea level. It is characterized by relatively flat topography bisected by two distinct ephemeral drainages oriented toward the southwest, with slopes of 0–10% across a majority of the study area and slopes up to 25% found in the drainages. The climate is sub-humid and is characterized by distinct seasonal trends including early summer drought, with an average of 560 mm of

precipitation (<http://www.wrcc.dri.edu>) falling half as snow during winter months and half as rain during the mid-summer monsoon season.

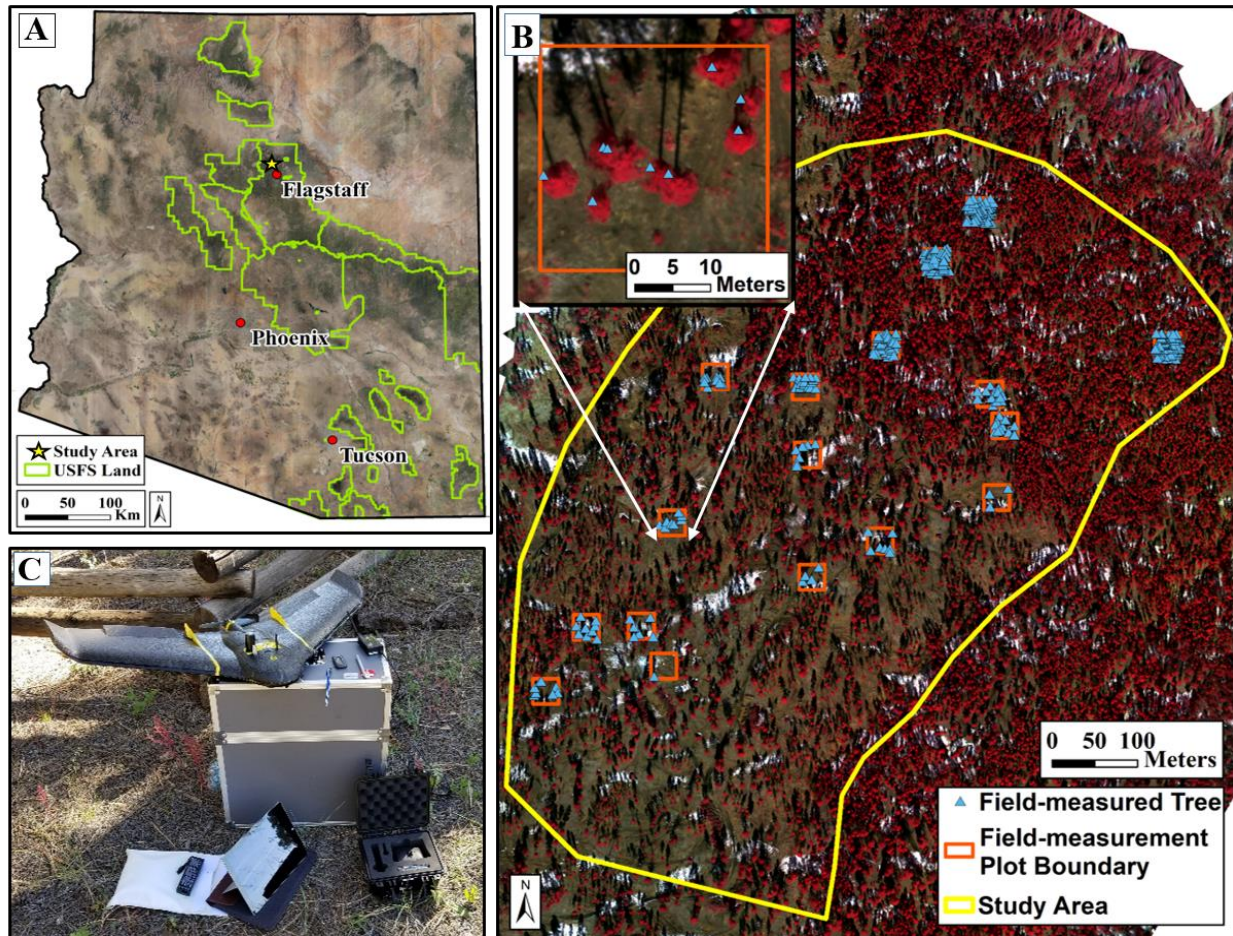


Figure 2.1: Overview of the study site within the state of Arizona and accompanying US Forest Service land (panel A). The 46.5 ha study area with the field plot locations and an example of a single field plot are shown in panel B, whereas the eBee UAV platform used for all UAV-derived data collection is shown in panel C. Base imagery used in panel B is the post-treatment UAV multispectral orthomosaic image.

The vegetation is characterized by ponderosa pine *Pinus ponderosa*, which dominates both the region and the study area, and includes intermittent Gambel oak *Quercus gambelii* and

Rocky Mountain juniper *Juniperus scopulorum*. The understory vegetation is typical of ponderosa pine-dominated forest in the immediate area and mainly consists of Arizona fescue *Festuca arizonica*, mountain muhly *Muhlenbergia montana*, mutton bluegrass *Poa fendleriana*, bottlebrush squirreltail *Elymus elymoides* and Buckbush *Ceanothus fendleri*. The site had been undisturbed since its last naturally occurring fire in 1876, except for selective historical firewood harvesting (Dieterich, 1980). However, the site was subjected to a prescribed fire in 1976 as a part of a study, in which 63% of the smaller surface fuels and 69% of the woody surface fuels (up to 8 cm in diameter) were consumed (Sackett, 1979).

Mechanical thinning operations across the study area began during the fall of 2017 and were completed by the spring of 2018. The study area spans two different restoration units and is divided into 30 ha treated and 16 ha untreated areas. Similar to other regional restoration treatments that promote diversity in tree group and interspace size, shape and spacing, this treatment aimed to reinstate pre-settlement forest conditions and included a range of thinning goals that would promote healthy overstory vegetation and the regeneration of understory vegetation (Allen et al., 2002; Larson and Churchill, 2012; Reynolds et al., 2013). Specifically, the treatment prescription at our study area emphasized irregular tree group delineation, expansion of interspace, retention of all non-ponderosa pine species (e.g., Gambel oak and juniper) and significant reductions in smaller ponderosa pine trees within groups and interspaces. The treatment was implemented using an approach called designation by prescription (DxP) and digital tree marking, which relied upon outfitting the tree harvesting equipment with tablet computers that use GPS. This supplied the harvesting personnel with location-specific prescription criteria to guide the cutting process. For this study, the same set of GPS-delineated polygons which guided thinning process was used to select for and quantify the patch and

interspaces. To assess whether the restoration treatment objectives were met or not, we used estimates of individual tree location and site-wide tree density in TPH and BA.

2.3.2 UAV images and pre-processing

We performed two sets of UAV flights, one before the treatment started (hereafter pre-treatment) during October 2017 and another set after the treatment was completed (hereafter post-treatment) during January 2018. We used the Parrot Sequoia multispectral sensor (Parrot Drones SAS, Paris) aboard a Sensefly eBee fixed-wing UAV platform (SenseFly, Lausanne, Switzerland) with a total payload of 690 gr in weight including the platform itself. With a wingspan of 96 cm, it can cover up to 12 km² in a single flight (www.sensefly.com/drone/abee-mapping-drone). All flights were planned and executed using Sensefly's eMotion 3 software (SenseFly, Lausanne, Switzerland), which enabled customized flight plans that controlled all flight and data parameters.

Site-specific characteristics known to cause issues in photogrammetric processing, such as dense forests and heavy shadowing, were carefully considered to ensure consistent data quality within and across flights (Puliti et al., 2015). Specifically, we used perpendicular and interlaced flight lines, high latitudinal and longitudinal overlaps (85% and 90%, respectively), and operated within 60 min of solar noon for all flights. During flight, each photo location included a total of five images; four individual 1.2MP images in the green (530–570 nm), red (640–680 nm), red edge (730–740 nm), and near infrared (770–810 nm) spectral bands, as well as a separate 16MP RGB composite image. Using on-board gyroscopic sensors, each image was assigned a unique set of GPS coordinates (X, Y and Z dimensions) as well as a location relative to the aircraft's principal axes: the x-axis (roll), y-axis (pitch) and z-axis (yaw). Using the

eMotion 3 software, this embedded information along with the flight log was used to geotag and georeference the images for all subsequent processing steps. The resulting pre-treatment dataset consisted of 1285 images per band (6425 total) covering 85 ha and the post-treatment dataset consisted of 1369 images per band (6845 total) covering 130 ha. We performed all flights at a consistent altitude of 122 meters above ground, which resulted in image spatial resolution of 15 cm. Specific flight parameters and environmental conditions are provided in Table 2.1.

Table 2.1: Summary of UAV flight data collection and SfM image reconstruction parameters used in our study, and relevant product characteristics.

	Pre-treatment Flight	Post-treatment Flight
UAV flight information		
Flight Date	10/14/2017	1/29/2018
Wind Speed	0.61 m/s	0.13 m/s
Cloud Cover	0%	0%
Total Flight Time	1:36:15	1:30:31
Number of Images	1285	1369
Total Coverage	0.85 km ²	1.45 km ²
Data processing parameter		
Photo Aligment Accuracy Setting	High	High
Key Point Limit Setting	60,000	60,000
Tie Point Setting	0 (maximum)	0 (maximum)
Generic Preselection	No	No
Reference Preselection	Yes	Yes
Dense Cloud Quality Setting	High	High
Depth Filtering Setting	Aggressive	Aggressive
Data output details		
Orthomosaic Ground Resolution	13.6 cm/pixel	15.7 cm/pixel
SfM Model Tie Points	6,496,677	5,406,209
SfM Dense Cloud Points	12,092,123	14,505,513
SfM Model Reprojection Error	0.33 pixel	0.31 pixel
XY Error	1.59 m	1.14 m
Z error	1.13 m	1.80 m

We established ground control points (GCPs) for each flight evenly spread across the study site using a combination of 1 m × 1 m vinyl checkerboard panels and large rocks that would remain visible above the snow in the winter season. Each GCP was mapped using a Trimble GeoXH handheld GPS unit and the data were differentially corrected using GPS Pathfinder Office software. The post-corrected GPS positional accuracies ranged between 0 and 50 cm for 87.5% and 96.5% of the total points for pre- and post-treatment datasets, respectively. Error estimates in the orthomosaic imagery are described in Table 2.1.

2.3.3 UAV image analysis

Post-processing of individual images into final data products was accomplished using the Agisoft PhotoScan v1.4.0 photogrammetric processing software (Agisoft LLC, St. Petersburg, Russia). In Agisoft, all images from the flights were scanned for matching ‘tie-points’, oriented in three-dimensional space via bundle-adjustment, and then mosaicked together based on unique overlapping points and spectral similarities (Dandois and Ellis, 2013). The general workflow in the software includes image alignment to create a sparse point cloud, incorporation of GCP locations, image alignment optimization, gradual filtering out of inaccurate and error-inducing points, and lastly a full image realignment before data product creation (Puliti et al., 2015; USGS, 2017). Final data products for this study included an undistorted, high-resolution orthomosaic image of the entire study site in 15 cm spatial resolution and four spectral bands, and dense three-dimensional (3D) point cloud data photogrammetrically generated from the high-resolution images using Structure-from-Motion (SfM) algorithms. A full list of parameters used for all image processing steps is provided in Table 2.1.

2.3.4 Field-based validation dataset

To assess the accuracy of the UAV-derived forest measurements, a total of 17 field plots were established throughout the study area and were inventoried during the summer of 2018, approximately 5 months after the post-treatment UAV flights. The field plots were each selected to represent a specific forest condition along the canopy cover and stem density gradient, capturing as much variability in forest density across the study area as possible. To assess the effects of forest conditions on UAV image-derived tree measurements, we divided the field-measured plots ($n = 17$) into groups of varying stem density conditions, which was expressed in trees per hectare (TPH). These density conditions included low (1–89 TPH; $n = 5$ plots), medium (100–211 TPH; $n = 8$ plots) and high (467–856 TPH; $n = 4$ plots). Each plot was 30 m \times 30 m in dimension (0.09 ha). Together, the field plots covered roughly 2% (1.53 ha) of the total study area.

Within each plot, the geographic location (X, Y coordinates), height (Z), two canopy widths (widest and narrowest) and the diameter at breast height (DBH) of each tree were measured for all trees taller than 1.37 m. The DBH measurements were used to estimate basal area (BA) at the plot level. Stems less than 1.37 in height were considered as seedlings and not measured due to their low abundance. All trees were stem-mapped using a Trimble Geo7X handheld GPS unit with the Laser Rangefinder module, with 95.6% of all recorded point locations having <2 m accuracy. A total of 392 individual trees were located and measured across the 17 plots (Figure 2.1).

2.3.5 Fine-scale forest structure metrics

Using the UAV image-derived point cloud data, we segmented individual trees and estimated their location (X, Y coordinates), tree height (Z in m), and crown diameter (m). First, the raw SfM point cloud was filtered using the statistical outlier removal tool in CloudCompare software (CloudCompare, 2.9.1, 2018) and then classified into ground versus non-ground points using the Cloth Simulation Filter (CSF) model (Zhang et al., 2016). We performed all steps of the individual tree segmentation (ITS) process using the lidR and rLiDAR packages (Mohan et al., 2017; Roussel et al., 2017) implemented in RStudio. A digital terrain model (DTM) was produced using the post-treatment classified ground points dataset, which was superior to the pre-treatment dataset due to the greater amount of classified ground points. The overall accuracy of the DTM ($R^2 = 0.95$, RMSE = 2.98 m) was assessed by comparing points extracted from the DTM to the corresponding points from the differentially corrected GPS elevation values (Z) of the trees in the field-based validation dataset. This DTM was then used to normalize both the pre- and post-treatment point clouds prior to tree segmentation.

Using the ITS algorithm developed by Li et al. (2012), a collection of points was grouped into a tree from the top of the tree crown down using thresholds controlling the relative spacing between trees, the changes in that spacing throughout the height of the tree and the relationship between point distances. The ideal parameters were achieved by iteratively and incrementally testing them with our data and based on the results from previous research (Shin et al., 2018). The final parameters were as follows: distance threshold (DT) 1 of 1.4 m, DT 2 of 1.7 m, minimum height of 2 m, individual point height for triggering DT value of 12 m and the search radius of 0 m. The segmentation and associated tree metric calculation processes yielded a list of

all trees segmented with their unique identification number, their geographic coordinates (UTM in meters), heights (m) and two opposing canopy diameters (m).

An accuracy assessment was performed to determine which of the field-measured trees ($n = 392$) were correctly identified and segmented in the UAV-derived point cloud data. The accuracy assessment consisted of an analysis of omission and commission error rates (Mohan et al. [2017](#); Shin et al. [2018](#)). The omission and commission analysis quantifies the rate of correctly identified trees or true positive (TP), omitted or false negative (FN) and incorrectly included trees or false-positive (FP) trees. These accuracy categories are summarized by calculating the recall (r), precision (p) and F-score (F) via the following equations:

$$r = \frac{TP}{TP + FN}$$

$$p = \frac{TP}{TP + FP}$$

$$F = 2 \times \frac{(r \times p)}{(r + p)}$$

The correctly identified trees in the UAV image-derived point cloud were then compared to the corresponding trees measured in the field using their height, and crown diameter via paired t tests and simple linear regression models. Differences in individual tree locations were quantified using a simple Euclidean distance from the field-measured GPS tree locations. The UAV image-derived estimates for each variable were also compared to a set of acceptable accuracy ranges utilized by the USFS during their common stand examination (CSE): $\pm 10\%$ for an intensive examination and $\pm 20\%$ for an extensive examination. Analysis of variance

(ANOVA) tests with unequal variances were used to compare individual tree metrics among the three density categories: low, medium and high.

2.3.6 Mid-scale forest structure metrics

We estimated stand-level basal area (BA), canopy cover, and forest patch and interspace metrics as well as the changes in these variables resulting from the mechanical thinning treatment. We first established a linear relationship between the field-measured tree density in trees per hectare (TPH) and BA (m²/ha) at the plot level (n = 17) using the following equation:

$$BA \left(\frac{m^2}{ha} \right) = 8.95 + 0.07 * TPH$$

This relationship yielded R² of 0.89 and RMSE of $347 \frac{m^2}{ha}$, when compared to the field-measured BA. We then extended this relationship to the entire study area using our UAV image-derived tree density estimate from the individual tree segmentation described above to estimate the site-wide BA.

Using the UAV orthomosaic image in the ENVI 5.3 software (Exelis Visual Information Solutions, Boulder, Colorado), we classified canopy cover. The four spectral bands were converted to reflectance and layer stacked together to create a single multispectral image, which was then used to calculate normalized difference vegetation index (NDVI). Using a NDVI value threshold along with a 2-m tree height threshold in the SfM point cloud data, we classified tree canopy versus non-tree canopy cover. Since our study area was dominated by a single, evergreen conifer species, NDVI provided a simple approach in distinguishing tree canopies from the herbaceous understory mixed with some bareground. The integration of the tree height

information allowed us to eliminate large piles of cut trees and vegetative material left behind from the mechanical thinning treatment operations. The resulting binary canopy/non-canopy classification was summarized in 10 m cells to estimate total tree canopy cover per cell (in percent). Field-measured canopy cover was calculated by rasterizing each tree's average crown diameter into 15 cm grid cells, then summarizing it into 10 m cells to facilitate direct comparison. The relationship between the field-measured and UAV-derived estimates of canopy cover was assessed using a simple linear regression model. We then quantified the changes in forest canopy cover and BA between the pre- and post-treatment conditions.

Other specific outcomes of the restoration prescription were also quantified using a set forest patch and interspace metrics: patch and interspace shape regularity, size and spacing (Pelz and Dickinson, 2014). First, a forest patch and interspace raster was created from the binary canopy cover classification by implementing a clustering algorithm in R-Studio (Girvetz and Greco, 2007). The patch summary raster is a binary classification of the pixels labeled by the algorithm as either a forest patch or non-patch (i.e., interspace). This was resampled to 5 m pixels and then used with the FragStats software (McGarigal et al., 2012) to estimate the following specific patch-level metrics: patch area (ha), patch perimeter (m), contiguity index (unitless) and Euclidean nearest random point distance (ENRPD) (m). The contiguity index quantifies the shape of a patch by measuring its contiguity of cells within a 3×3 cell neighborhood (McGarigal et al., 2012), whereas ENRPD quantifies the prevalence and size of gaps (Pelz and Dickinson, 2014). We summarized the patch-level metrics in both the pre- and post-treatment images and compared them to evaluate the restoration treatment.

2.4 Results

2.4.1 Fine-scale forest structure metrics

Our field plots included a total of 392 trees: the low-density plots ($n = 7$) contained 37 field-measured trees, the medium-density plots ($n = 6$) contained 75 trees and the high-density plots ($n = 4$) contained 280 trees. These field-measured trees were used for the assessment of fine-scale, individual-tree metrics derived from the SfM point cloud data (Figure 2.2). Overall, 64% of all the trees were correctly identified and segmented in the UAV SfM point cloud data: 92% from low-density, 71% from medium-density and 30% from high-density plots (Table 2.2). We compared Euclidean distances between tree X and Y coordinates across density classes. ANOVA results indicated there was a significant difference between the classes ($P < 0.01$) and the low- and high-density classes were significantly different.

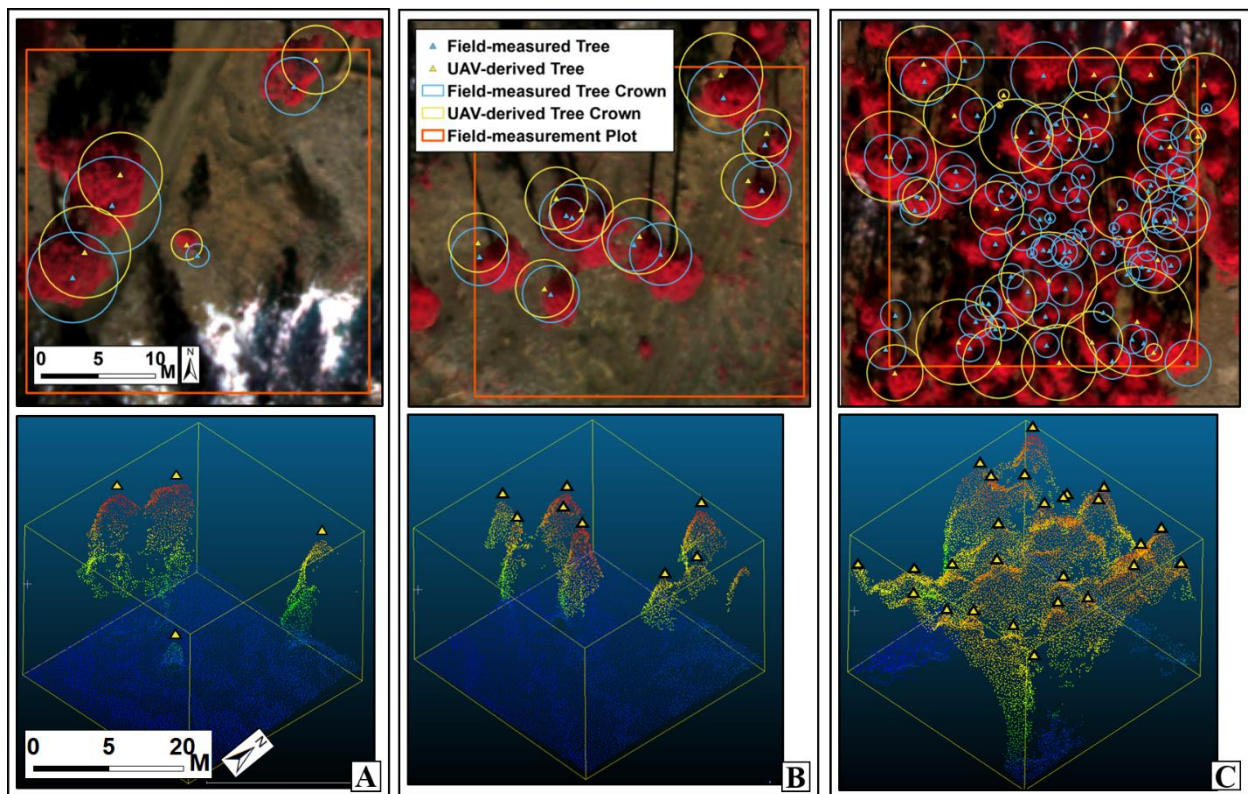


Figure 2.2: Examples of our field plots from each of the low- (A), medium- (B) and high- (C) density classes. The top row shows the UAV orthomosaic images overlaid with both the field-measured and UAV-derived tree locations as well as their corresponding crown diameters. The bottom row shows the Structure-from-Motion (SfM) point cloud data that corresponds to each plot above, as well as the SfM-derived tree locations placed on each respective tree.

Table 2.2: Individual tree omission and commission errors in the low-, medium- and high-density classes, with the overall scores across each density class provided. Analysis parameters included were the true positive (TP), false negative (FN), false positive (FP) trees, as well as the recall (r), precision (p) and F-score (F). TPH, trees per hectare; CC, canopy cover.

	Mean TPH	Mean CC (%)	Field-based measurement	UAV image- derived	TP	FN	FP	r	p	F
Low density (n = 7)	59	9	37	35	34	3	1	0.92	0.97	0.94
Medium density (n = 6)	139	17	75	57	53	22	4	0.71	0.93	0.80
High density (n = 4)	778	74	280	185	93	221	20	0.33	0.82	0.44

A simple linear regression model of all individual tree heights showed moderate overall agreement between field-based measurements and UAV image-derived estimates (Figure 2.3). Furthermore, a paired t test indicated no significant overall difference ($P = 0.51$) between the field-based measurements ($M = 17.52$ m; $sd = 4.58$ m) and UAV image-derived estimates ($M =$

17.39 m; sd = 4.65 m). In contrast, comparison of all individual tree crown diameters showed a significant difference ($P < 0.01$) between the field-based measurements ($M = 4.48$ m; sd = 1.66 m) and UAV image-derived estimates ($M = 5.96$ m; sd = 2.46 m). The UAV image-derived crown diameters tended to be overestimated. When we compared the UAV image-derived estimates to USFS Common Stand Exam (CSE) acceptable error rates, 86% of the overall tree height estimations fell within the $\pm 20\%$ range and 63% fell within the $\pm 10\%$ range (Table 2.3). However, only 29% of the UAV image-derived tree crown diameter estimates was within the $\pm 20\%$ range (Table 2.3). Both the UAV image-derived individual tree height and crown diameter estimates differed between density classes, with the low- and high-density classes consistently being the most and least accurate estimates, respectively (Table 2.3).

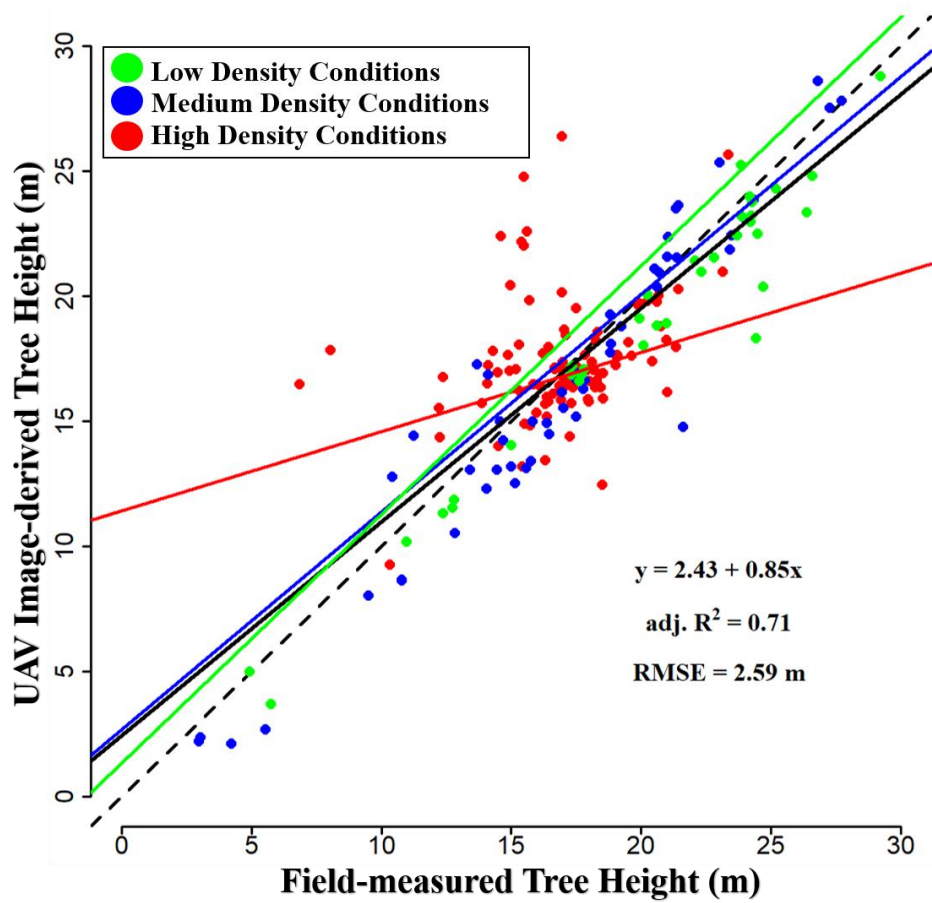


Figure 2.3: Linear regression models established between the field-measured and UAV image-derived individual tree height estimates. The dashed line is a 1:1 reference line and solid black line is the overall fitted regression model (adj. $R^2 = 0.71$). In addition, separate regression models were fit to each density class and the regression lines are colored accordingly.

Table 2.3: A summary of the UAV image-derived individual tree height and canopy diameter estimates, grouped by density classes, and compared to the US Forest Service Common Stand Exam (CSE) acceptable accuracy ranges. The reported values for each acceptable accuracy range indicate the percent of the total trees estimated from the UAV data within that range.

	Tree Height		Crown Diameter	
	CSE $\pm 10\%$	CSE $\pm 20\%$	CSE $\pm 10\%$	CSE $\pm 20\%$
UAV image-derived estimates within CSE accuracy ranges				
Low Density (n = 34)	29 (85.3%)	32 (94.1%)	9 (26.5%)	21 (61.7%)
Medium Density (n = 53)	30 (56.6%)	45 (84.9%)	13 (24.5%)	22 (41.5%)
High Density (n = 93)	54 (58.0%)	77 (82.7%)	4 (4.3%)	10 (10.7%)
Overall (n = 180)	113 (62.7%)	154 (85.5%)	26 (14.4%)	53 (29.4%)

In the low-density class, 92% (n = 34) of the trees was correctly identified as True Positives (TP), with a recall (r) score of 0.92 (0.75–1.00), an overall precision (p) of 0.97 (0.86–1.00) and an F-Score of 0.94 (0.80–1.00) (Table 2.2). When we compared the location of these trees in the low-density class to the field-based GPS data, the mean difference in the coordinates' Euclidean distances was 2.44 m. A simple linear regression model comparing the field-based and UAV image-derived individual tree heights showed strong agreement with an adjusted $R^2 = 0.95$

(RMSE = 1.77 m) for these trees, while the regression model of the crown diameters showed moderate agreement with an adjusted $R^2 = 0.61$ (RMSE = 1.27 m).

In the medium-density class, 71% ($n = 53$) of the trees was correctly identified as true positives, with slightly lower recall ($r = 0.71$), precision ($p = 0.93$) and F-score values ($F = 0.80$) than for the low-density class (Table 2.2). The mean difference in the coordinates' Euclidean distances was lower than that of the low-density class at 1.92 m. The regression model of individual tree heights had an adjusted $R^2 = 0.92$ (RMSE = 1.87 m) (Figure 2.3). The regression model of medium-density class crown diameters only had an adjusted $R^2 = 0.09$ (RMSE = 2.19 m).

In the high-density class, only 33% ($n = 93$) of the field-measured trees was correctly identified as true positives, with recall ($r = 0.30$), precision ($p = 0.82$) and F-score values ($F = 0.44$) lowest among the three density classes (Table 2.2). The lowest mean difference between the coordinates' Euclidean distances was observed for this density class at 1.54 m. The regression model of tree heights showed low agreement between the SfM-derived and field-measured heights with an adjusted $R^2 = 0.08$ (RMSE = 3.14 m) (Figure 2.3), while the model comparing canopy diameters exhibited similar behavior with an adjusted $R^2 = 0.005$ (RMSE = 3.94 m).

2.4.2 Mid-scale forest structure metrics

Field-measured canopy cover and UAV image-derived estimates showed good agreement overall (adj. $R^2 = 0.79$; RMSE = 15.4%) (Figure 2.4). When this agreement was assessed by density class, the medium-density relationship (adj. $R^2 = 0.78$; RMSE = 10.8%) was stronger than the low- (adj. $R^2 = 0.72$; RMSE = 10.7%) and high- (adj. $R^2 = 0.48$; RMSE = 27.1%) density classes.

ANOVA results indicated significant differences in UAV image-derived canopy cover estimates between the density classes ($F_{2,150} = 84.47$, $P < 0.01$): the high-density class had significantly greater canopy cover than both the medium- ($P < 0.01$) and low- ($P < 0.01$) density classes. When we similarly assessed the UAV image-derived tree density estimates, there was a significant difference ($P = 0.03$) in TPH between the field-measured ($M = 248.4$ TPH; $sd = 297.1$ TPH) and UAV image-derived estimates ($M = 129.4$ TPH; $sd = 107.6$ TPH). Significant differences were also found between density classes in both the field-measured ($F_{2,14} = 106.9$, $P < 0.01$) and UAV image-derived estimates ($F_{2,14} = 30$, $P < 0.01$). The UAV image-derived TPH estimate in the high-density class was significantly greater than both the medium- ($P < 0.01$) and low- ($P < 0.01$) density classes.

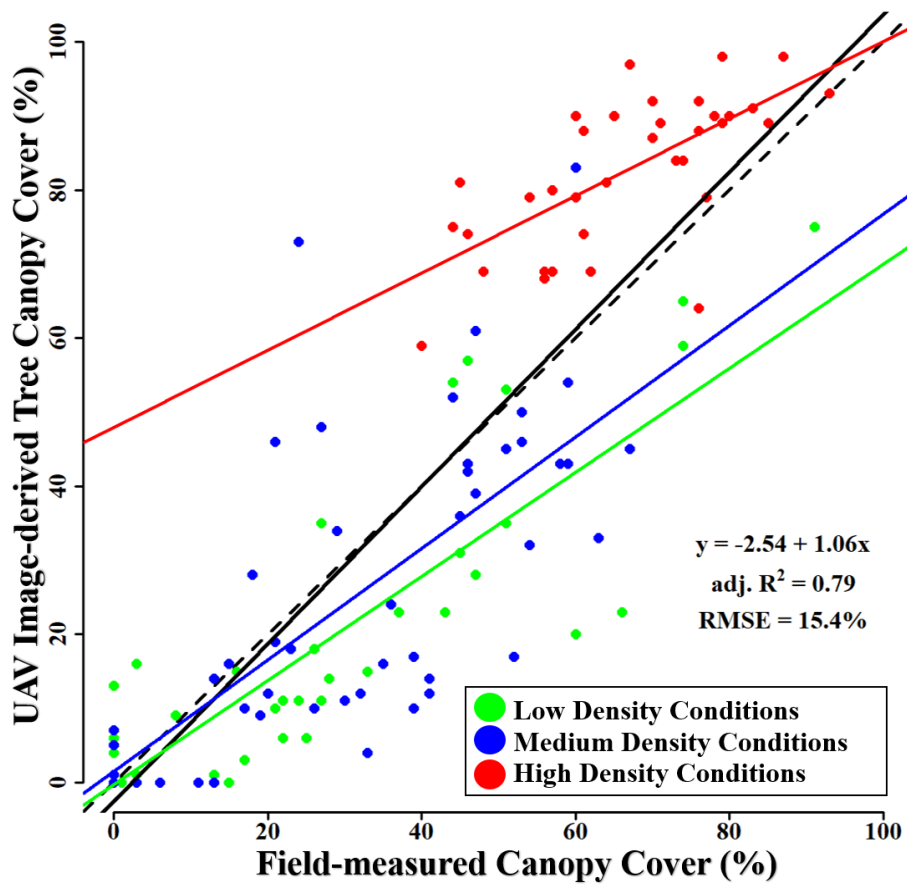


Figure 2.4: Linear regression models established between field-based measurements and UAV image-derived estimates of tree canopy cover. The dashed line is a 1:1 reference line and solid black line is the overall fitted regression model (adj. $R^2 = 0.79$). In addition, separate regression models were fit to each density class and the regression lines are colored accordingly. Data points here are the individual 10 m cells ($n = 153$) from the field-measured plots, which were summarized from the high-resolution (15 cm) binary canopy raster layers and are colored by density condition.

2.4.3 Restoration treatment effects

When the UAV image-derived canopy cover estimates were compared across the treated portion of the study area from the pre-treatment and post-treatment dates, the results indicated that the restoration treatment reduced the forest canopy cover from 39.4% to 9.6%. Similarly, our results indicated that stem density was reduced from 212.4 TPH to 64.5 TPH and the corresponding basal area was reduced from 22.9 m²/ha to 13.2 m²/ha. Our patch and interspace analysis results indicated that the treatment created considerable canopy openings by breaking up once continuous forest patches, often leaving single trees or groups of 2–3 trees behind (Figure 2.5). The restoration treatment increased the number of patches across the study site by 70.6%, while the mean patch area decreased by 80.8% to 0.13 ha (Table 2.4). The total patch area across the study site decreased by 39.6% with a corresponding 74% increase of interspace area. Measures of the average patch contiguity decreased overall, while both the average patch fractal dimension index value and the Euclidean nearest random point distance (ENRPD) increased. This indicates that the remaining patches are less contiguous to one another, have more complex shapes, and that there is more area between remaining patches, respectively (Table 2.4).

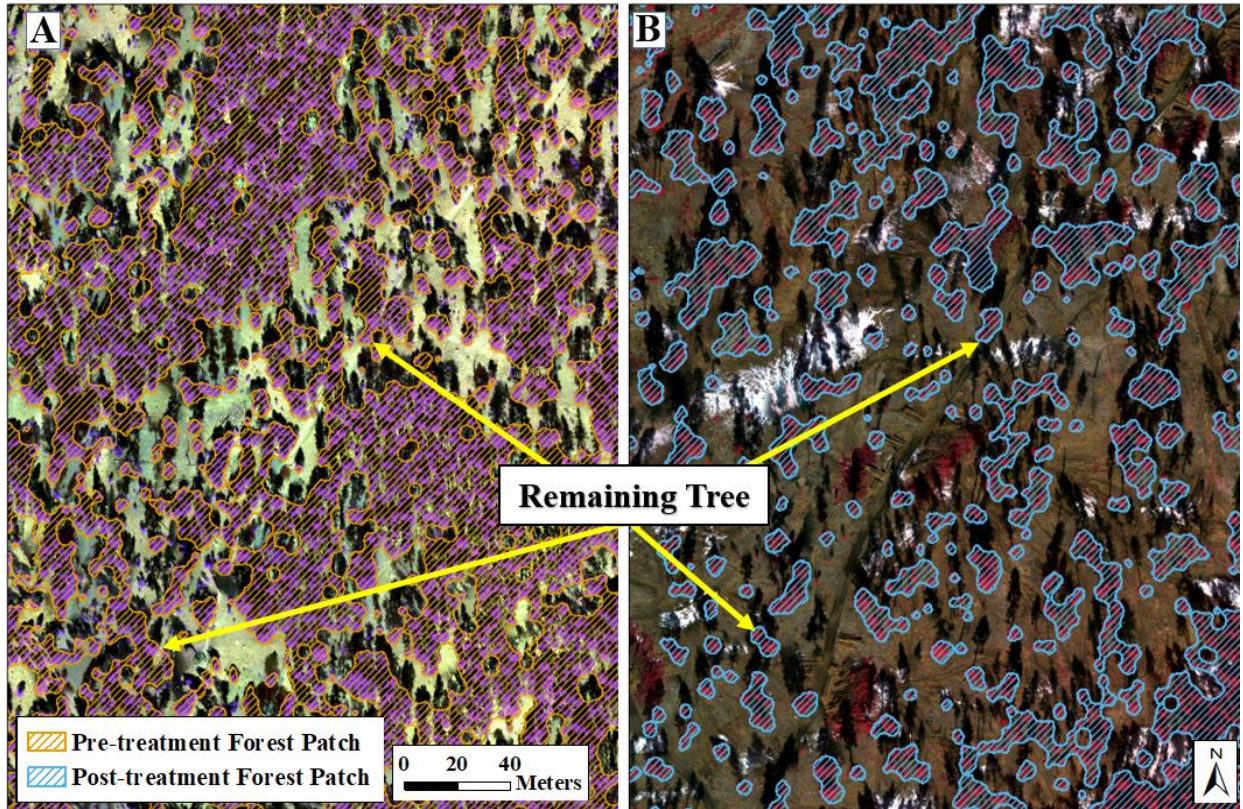


Figure 2.5: A comparison of pre-treatment (A) and post-treatment (B) forest patches illustrating substantial changes in horizontal structure and the creation of new forest patches. Toward the center of panel B, the vegetation not highlighted as a patch is fallen timber awaiting removal. The base map images are the respective UAV orthomosaic images in 15 cm resolution used for canopy cover and forest patch delineation.

Table 2.4: Patch and interspace metrics from the treated portion of the study area. Patch contiguity is a unitless metric, ranging from 0 to 1 where 0 is a single pixel patch and it approaches 1 as patch shape complexity and patch boundary configuration increase. Fractal dimension index is a unitless metric, ranging from 1 to 2 where 1 is a patch with a simple shape (e.g., square) and 2 is a patch with a more convoluted boundary. Euclidean nearest random point

distance (ENRPD) is an assessment of the shortest straight-line distance between randomly generated points and is used to measure the prevalence and size of forest gaps.

	No. of Patches	Total Patch Area (ha)	Total Interspace Area (ha)	Mean Patch Area (ha)	Fractal Dimension Index	ENRPD (m)
Patch and Interspace Metrics						
Pre-Treatment	39	15.2	12.5	0.68	1.12 (range=0.41)	3.5 (range=15.6)
Post-Treatment	133	5.9	21.8	0.13	1.16 (range=0.26)	7.1 (range=38.9)

	No. of Patches	Total Patch Area (ha)	Total Interspace Area (ha)	Mean Patch Area (ha)	Patch Contiguity	ENRPD (m)
Patch and Interspace Metrics						
Pre-Treatment	39	15.2	12.5	0.68	0.41 (range=0.35)	3.5 (range=15.6)
Post-Treatment	133	5.9	21.8	0.13	0.47 (range=0.60)	7.1 (range=38.9)

Next, we compared the UAV image-derived mid-scale forest structure metrics to the restoration treatment objectives stated in the forest restoration prescription (Table 2.5) to evaluate whether the objectives were achieved. Across the treated portion of the study area, the UAV image-derived estimates of BA showed a reduction from 22.9 m²/ha to 13.2 m²/ha, falling within the 11–14 m²/ha target range for the overall stand-level BA. Next, using a 5 m buffer along the stream course, we found that 138 trees were cut within this area. This reduction is more than the treatment objective, which emphasizes a retention of all stream course bank stabilization trees. The interspace areas, termed ‘regeneration openings’, cover roughly 9% of the study area,

and range in size from 0.07 to 0.33 ha, which fell outside of the 15% total area as targeted, but within the 0.2–0.4 ha range targets. There was an average of 5.3 trees per ‘regeneration’ polygon remaining after treatment and the target range was 3–5 trees. Similarly, the restoration goals in the different tree group areas were met, with the remaining groups being more irregularly shaped and smaller in area. However, the average spacing between tree groups was found to be lower (5.35 m) than the target (12–18 m). Finally, the interspace tree density was found to be higher (9.5 TPH) than intended (2–5 TPH).

Table 2.5: A selection of the restoration treatment objectives outlined for the study area. The restoration treatment outcomes were estimated from the post-treatment UAV image-derived datasets. TPH, trees per hectare.

Restoration Treatment Objective	Restoration Treatment Outcome
Final stand-level basal area (BA) = 11-14 m ² /ha	Final BA = 13.2 m ² /ha
Retain all streamcourse bank stabilization trees	Net loss of 138 trees
Regeneration Openings should:	
Be 15% of the treatment area	9% of treatment area
Range in size from 0.2-0.4 ha (up to 0.8 ha)	range: 0.07-0.33 ha
Retain 3-5 reserve trees in openings larger than 0.4 ha	Average of 5.3 trees
Tree Groups should:	
Be irregularly shaped	Fractal dimension index = 1.16 (range 0.26)
Range in size from 0.04-0.4 ha (averaging 0.1-0.2 ha)	Range: 0.03-0.37 ha (mean 0.13 ha)
Distance b/t groups should be 12-18 m	Avg. distance = 5.35 m
Cut all remaining interspace trees, leaving 2-5 TPH	Density = 9.5 TPH

2.5 Discussion

2.5.1 Estimating fine-scale forest metrics

We used high-resolution UAV-derived multispectral imagery and SfM models to quantify fine-scale vertical and horizontal forest structure across a gradient of forest density conditions. We found that forest density played a significant role in the accuracy of individual tree detection, height and canopy diameter estimation. Across the field plots of all densities, the UAV image-derived data initially identified 46% of all individual trees and resulted in an overall accuracy of 60%. However, once parsed by density condition, the average accuracy increased to 92% in low-density plots and 71% for medium-density plots, but remained low at 33% for high-density plots. While other studies reported higher rates of overall true positive tree identification, even with plot-level density class distinctions (Guerra-Hernández et al., 2016; Mohan et al., 2017; Shin et al., 2018), the high-density plots used in our study were on average much denser (up to 778 TPH) than the high-density conditions (>300 TPH) considered elsewhere. We provide the first accuracy assessment of UAV image and SfM data in very high-density conditions and note that when stem density increases beyond approximately 500 TPH, UAV image-derived estimates cannot provide adequate accuracies.

The location of individual trees provided by the ITS was accurate overall, but was dependent on density conditions. Interestingly, the location accuracy improved as the density increased, with the mean error in tree coordinates for low-, medium- and high-density conditions at 2.44 m, 1.92 m and 1.54 m, respectively. We speculate that this is due to a combination of tree canopy size and complexity as well as the stem density. For example, the ITS algorithm identifies tree tops, but many tree canopies are interlocked and tree tops are located closer

together in high-density conditions. In comparison, trees in the lower density conditions are much farther apart leading to larger mean errors in their locations. They are also most often the largest trees with big canopy diameters because they were intentionally left uncut during the restoration treatment.

The UAV-derived individual tree height estimates performed well overall, with no significant differences between the UAV-derived and field-measured pairs. Furthermore, 86% of the individual tree height estimates were within the 20% acceptable error range of the USFS Common Stand Exam guidelines. The 86% accuracy is also well within the accepted rates of remotely sensed data analysis (Congalton and Green, 2008). Taken together, these findings indicate that UAV image-derived methods can be used by forest restoration practitioners for estimating tree height. However, when parsed by density class, the relationships between the field-measured and UAV-image derived tree heights were notably different between both the low- and medium-density conditions versus the high-density conditions (Figure 2.3). The results of the low- and medium-density conditions are consistent with findings of other research (Zarco-Tejada et al., 2014; Panagiotidis et al., 2016; Wallace et al., 2016) and might be due to the relatively high point densities present in the SfM point clouds. The lack of agreement in the high-density conditions appears to result from a combination of incorrectly identified tree tops, outlier points in the UAV dataset, and higher DTM error.

Individual tree crown diameters were not well estimated overall, with high-density conditions being the driver behind UAV-derived and field-measured differences. Overall, the agreement was poor except for in low-density conditions. Other studies have reported more accurate SfM-derived estimates of canopy diameter, but they included consistent tree spacing,

higher spatial resolution data and less dense conditions (Zarco-Tejada et al., 2014; Díaz-Varela et al., 2015), none of which were present in this study. This underscores the notion that individual tree crown diameters, especially when measured using UAV-image-based techniques, are subject to bias and error. Field techniques require a technician to visually determine a canopy dripline to estimate the canopy diameter. Since the UAV-image derived point cloud is often noisy yet continuous in high-density conditions, the canopy edges are obscured leading to inaccurate estimates of crown diameters. Other individual tree metrics such as crown bulk density and height to crown are of interest to regional forest managers due to their use in fire modeling and allometric equation development. However, since restoration practices occur at the mid- to landscape-scales, canopy cover is a more important metric and further improvements in its estimates are needed.

When compared to traditional USFS CSE accuracy standards, UAV image-derived tree crown diameters were within the $\pm 10\%$ and $\pm 20\%$ acceptable accuracy ranges for only 14% and 29% of the observations, respectively. Importantly, the high-density conditions again provided less accurate estimation for both tree height and crown diameter. This highlights the need to refine UAV image-derived estimates, especially for crown diameter, to ensure they provide a viable augmentation to CSE field measurement. This is especially important as UAV-borne remote sensing methods continue to be leveraged in forest mensuration and inventorying applications.

2.5.2 Estimating mid-scale forest metrics

When estimating mid-scale forest structure metrics, the UAV image-derived estimates of canopy cover, TPH and BA in high-density conditions were consistently significantly different from

field-based estimates. In high-density conditions, canopy cover was consistently overestimated, while in low-density conditions it was underestimated (Figure 2.4). We believe that this arises from the fact that our field methods employed two measurements of canopy diameter to calculate an average estimate for each tree canopy, while UAV-image derived estimates provide full coverage at 15 cm resolution pixels. Despite both methods being summarized to a plot-level estimate, we believe that the UAV-image derived data naturally provide a more complete and repeatable estimation overall. Using at-nadir images with NDVI estimates can eliminate potential bias between different field-based approaches (Fiala et al. 2006). Compared with the field-based measurements of TPH and BA, the UAV-based measurements underestimated these metrics in high-density conditions. As mentioned previously, the high-density conditions we measured were the highest observed thus far and allowed for a more realistic understanding of the limits of this methodology. Our observations in these conditions also highlight obvious areas of future improvement and demonstrate the UAV potential for restoration practitioners.

2.5.3 Restoration treatment outcomes

A central motivation of this study was to provide forest managers with a realistic evaluation of UAV image-derived estimates and workflows as a tool for assessing mechanical forest restoration treatments and their outcomes. As is the case for other regional restoration projects, the treatment at our study site relied on a set of prescriptive guidelines and desired outcomes (Table 2.5). We found that the treatment led to a 70% reduction in TPH, 42% reduction in BA and a 30% reduction in percent canopy cover. This increased the number of forest patches by 70%, where the average patch sizes are smaller in size with more complex shapes. Additionally, the total amount and complexity of forest patch interspace increased.

Restoration treatment outcomes showed an overall agreement with the restoration objectives. Five of the nine treatment goals that we assessed were successfully achieved (Table 2.5). We believe that these are strong results especially since the other restoration treatment objectives were still relatively close to their goal and displayed the overall intended trend. For example, scrutiny of the net loss of bank-stabilization trees, while counter to a specific treatment objective, revealed that the thinning operations favored shorter trees. Since the trees cut in these stream bank areas were shorter, they were likely considered undesirable according to a broader site-wide goal. We also found that the creation of ‘regeneration opening’ areas was not as extensive as the prescription had intended, but the size and shape of the remaining ‘tree groups’ were on target. It is important to note that the prescription we assessed was developed for the entire 138 ha treatment unit, of which we only assessed 30 ha. Objectives not met in this analysis could, therefore, be met if the entire treatment unit was assessed following implementation. In addition, variability in metrics across the treatment unit is desired. While potentially not met in one part of the unit, the average condition or range in conditions across the unit may be met, when the whole unit is assessed. Future studies might benefit from assessing a greater portion of the area corresponding to the prescription.

2.5.4 Other considerations for UAV applications

High-resolution multispectral UAV orthoimagery and SfM models offer an exciting new approach for forest inventorying and monitoring. As with any emerging technology, there are a number of specific shortcomings that we encountered which warrant attention. Similar to other studies, we found that environmental conditions (e.g., sun angle, wind, high ground reflectance), sensor resolution and flight plan characteristics all contributed to data processing, the quality of

final data products, and the derived tree structure estimates (Dandois et al. 2015; Iglhaut et al., 2019; Iizuka et al. 2018; Puliti et al. 2015). Perhaps most importantly, the nearly continuous canopy cover in higher-density forest conditions provides significant uncertainty. Specifically, we observed a final (dense) 3D point cloud with little variability in texture across the dense forest canopy and not enough ground points. This yields a DTM with relatively homogenous values and lower accuracies in high-density conditions (RMSE = 3.52), which influenced the overall accuracy (RMSE = 2.98 m) of the final DTM. In comparison, the accuracies observed in the low- and medium-density conditions were greater (RMSE = 2.21). This is consistent with previous studies and indicates that the ground surface occlusion under dense canopy degrades DTM accuracy (Dandois and Ellis 2010; Wallace et al. 2016) and subsequently impacts estimates of individual tree locations and heights (Dandois et al. 2015; Wallace et al. 2016; Mohan et al. 2017).

The homogenous DTM values also impacted tree segmentation, which underperformed in higher-density areas. Tree height and crown diameter estimates were subsequently affected by the segmentation issues and interlocking canopies. Thus, improving the DTM accuracy would likely provide a more heterogeneous canopy in dense conditions, leading to improved tree location, height and canopy diameter estimates. Using a more accurate DTM from an alternate source, such as an airborne lidar dataset, would presumably provide more accurate tree location and estimations, although these alternatives are often too coarse in spatial resolution, publically unavailable, or prohibitively expensive.

We experimented with varying parameters of the ITS algorithm, other ITS algorithms, as well as parsing the point cloud by density conditions. In the end, we decided that an overly

complicated workflow might deter forest managers from adopting this methodology and applied the single best ITS algorithm and parameterization to the entire point cloud. We suggest that future attempts can improve ITS results and the subsequent tree height and crown diameter estimations by adopting lower flight altitudes, higher sensor resolution and by leveraging flight conditions with higher sun angles or overcast skies. These conclusions echo those of other similar work and underscore the importance of numerous data acquisition parameters on final product quality and accuracy (Dandois et al. 2015; Puliti et al. 2015). Our findings highlight that on-demand data acquisition, adaptable SfM workflows and a growing library of forest data-specific processing tools make UAV images a promising tool for estimating fine- and mid-scale forest structure metrics especially in low- and medium-density conditions.

As the need for forest restoration continues to increase, and the abilities of UAV-borne remote sensing are refined, the use of UAV-derived forest structure measurements has the potential to optimize restoration planning and monitoring. Restoration planning is often challenged with an accurate estimate of pre-treatment forest density conditions, which can now be rapidly acquired with a UAV. After an initial capital investment in UAV equipment and software of up to \$30,000, data can be acquired and processed on demand which continually lowers long-term operation costs. When compared to the costs of traditional plot-level field surveys (~US\$180 per plot), airborne lidar (\$7.50–\$6 per ha at 15,000–40,000 ha, respectively) or manned aerial imagery (\$200,000–\$500,000 over >10,000 ha), the costs associated with UAV-borne data acquisition are lower (Sankey et al. 2017). In our region, the pace, timing and implementation of restoration treatments are often dependent on weather and logging contractor availability. Having a flexible, standardized and cost-effective approach to assess and monitor restoration treatment outcomes can help forest managers operate more efficiently. Additionally,

the mid-scale forest metrics and methodology we presented in this study can be applied to monitoring a wider array of forest restoration outcomes including wildfire risk and potential behavior, wildlife habitat characteristics and drought resilience components of a post-restoration landscape. Providing such assessments at high spatial and temporal resolution could enable restoration planning and adaptive management to occur at both a faster pace and greater scale.

2.6 Conclusions and Management Implications

UAV applications provide three unique advantages in monitoring forest restoration. First, forest managers can acquire data for individual treatments to tailor subsequent treatments and achieve larger landscape-scale benchmarks. Second, UAV data can be used to accurately quantify post-treatment conditions and compare them to prescription objectives. We found the most accurate fine- and mid-scale estimates of forest structure to occur across low-density conditions, which often correspond to post-treatment conditions. Third, pre- and post-treatment conditions can be directly compared for mid-scale forest metrics, especially canopy cover. Our findings support previous findings that demonstrated coarser (1 m pixel) resolution manned aerial digital photography can be used at the landscape scale (400 ha +) to assess canopy cover and forest patch and interspace characteristics. UAV image-derived mid-scale metrics can be leveraged for the high spatial and temporal resolution to provide nearly continuous feedback to forest managers. Other study areas with understory shrub layers might also benefit from the high-resolution data that UAV sensors can provide, when classifying forest vegetation.

Future UAV-based research should focus on developing a spatially extensive sampling strategy to provide a more comprehensive evaluation of landscape-scale forest restoration. It is also important to include different treatment types and regionally relevant topographic and

vegetative characteristics. This would allow for the detection of differences between varying prescriptions, allow for the workflow to be tailored to site-specific conditions, and better facilitate landscape-scale restoration monitoring.

2.7 References

- Allen, C. D., Savage, M., Falk, D. A., Suckling, K. F., Swetnam, T. W., Schulke, T., ... Klingel, J. T. (2002). Ecological Restoration of Southwestern Ponderosa Pine Ecosystems: A Broad Perspective. *Ecological Applications*, *12*(5), 1418–1433. [https://doi.org/10.1890/1051-0761\(2002\)012\[1418:EROSPP\]2.0.CO;2](https://doi.org/10.1890/1051-0761(2002)012[1418:EROSPP]2.0.CO;2)
- Altschul, J. H., & Fairley, H. C. (1989). *Man, Models and Management: An Overview of the Archaeology of the Arizona Strip and the Management of its Cultural Resources*. <https://doi.org/doi:10.6067/XCV8DV1M7H>
- Bohlin, J., Bohlin, I., Jonzén, J., & Nilsson, M. (2017). Mapping forest attributes using data from stereophotogrammetry of aerial images and field data from the national forest inventory. *Silva Fennica*, *51*(2). <https://doi.org/10.14214/sf.2021>
- Bottero, A., D'amato, A. W., Palik, B. J., Bradford, J. B., Fraver, S., Battaglia, M. A., & Asherin, L. A. (2017). Density-dependent vulnerability of forest ecosystems to drought. *Journal of Applied Ecology*. <https://doi.org/10.1111/1365-2664.12847>
- Carr, J. C., & Snyder, J. B. (2018). Individual tree segmentation from a leaf-off photogrammetric point cloud. *International Journal of Remote Sensing*, *39*(15–16), 5195–5210.

- Castello, J. D., Leopold, D. J., & Smallidge, P. J. (2006). Pathogens, Patterns, and Processes in Forest Ecosystems. *BioScience*, *45*(1), 16–24. <https://doi.org/10.2307/1312531>
- Chianucci, F., Disperati, L., Guzzi, D., Bianchini, D., Nardino, V., Lastri, C., ... Corona, P. (2016). Estimation of canopy attributes in beech forests using true colour digital images from a small fixed-wing UAV. *International Journal of Applied Earth Observation and Geoinformation*, *47*, 60–68. <https://doi.org/10.1016/j.jag.2015.12.005>
- Churchill, D. J., Larson, A. J., Dahlgreen, M. C., Franklin, J. F., Hessburg, P. F., & Lutz, J. A. (2013). Restoring forest resilience: From reference spatial patterns to silvicultural prescriptions and monitoring. *Forest Ecol Manag*, *291*(Canadian Journal of Forest Research 39 2009), 442–457. <https://doi.org/10.1016/j.foreco.2012.11.007>
- Cooper, C. F. (1960). Changes in Vegetation, Structure, and Growth of Southwestern Pine Forests since White Settlement. *Ecological Monographs*, *30*(2), 129–164. <https://doi.org/10.2307/1948549>
- Cooper, C. F. (1961). Pattern in Ponderosa Pine Forests. *Ecology*, *42*(3), 493–499. <https://doi.org/10.2307/1932235>
- Covington, W. W., Fule, P. Z., Moore, M. M., Hart, S. C., Kolb, T. E., Mast, J. N., ... Wagner, M. R. (1997). Restoring Ecosystem Health in Ponderosa Pine Forests of the Southwest. *Journal of Forestry*, *95*(4), 23–29.
- Dahms, C. W., & Geils, B. W. (1997). An assessment of forest ecosystem health in the Southwest. *Gen Technical Rep Rm-Gtr-295 Fort Collins Co U S Dep Agriculture Forest*

Service Rocky Mountain Forest Range Experimental Station 97 P, 295.

<https://doi.org/10.2737/rm-gtr-295>

Dandois, J. P., & Ellis, E. C. (2013). High spatial resolution three-dimensional mapping of vegetation spectral dynamics using computer vision. *Remote Sensing of Environment*, 136, 259–276. <https://doi.org/10.1016/j.rse.2013.04.005>

Day, K., Berg, J., Brown, H., Crow, T., Morrison, J., Nowacki, G., ... Wood, B. (2006). *Ecosystem Restoration: A Framework for Restoring and Maintaining the National Forests and Grasslands*. Retrieved from https://www.fs.fed.us/restoration/documents/RestFramework_final_010606.pdf

Díaz-Varela, R. A., de la Rosa, R., León, L., & J, Zarco-Tejada, P. (2015). High-Resolution Airborne UAV Imagery to Assess Olive Tree Crown Parameters Using 3D Photo Reconstruction: Application in Breeding Trials. *Remote Sensing*, 7(4), 4213–4232. <https://doi.org/10.3390/rs70404213>

Diaz-Varela, R., Gonzalez-Ferreiro, E., Correia, A. C., Nunes, A., Tomé, M., Guerra-Hernandez, J., ... Fontes, L. (2016). Using high resolution UAV imagery to estimate tree variables in Pinus pinea plantation in Portugal. *Forest Systems*, 25(2), eSC09. <https://doi.org/10.5424/fs/2016252-08895>

Dickinson, Y., Pelz, K., Giles, E., & Howie, J. (2016). Have we been successful? Monitoring horizontal forest complexity for forest restoration projects. *Restoration Ecology*, 24(1), 8–17. <https://doi.org/10.1111/rec.12291>

- FAO: Food and Agriculture Organization of the United Nations. (2015). Global Forest Resources Assessment 2015. Retrieved from <http://www.fao.org/3/a-i4808e.pdf>
- Fitch, R. A., Kim, Y. S., Waltz, A. E. M., & Crouse, J. E. (2018). Changes in potential wildland fire suppression costs due to restoration treatments in Northern Arizona Ponderosa pine forests. *Forest Policy and Economics*, 87, 101–114.
<https://doi.org/10.1016/j.forpol.2017.11.006>
- Fitzgerald, S. a. (2005). Fire Ecology of Ponderosa Pine and the Rebuilding of Fire-Resilient Ponderosa Pine. *USDA Forest Service General Technical Report, 97756, PSW-GTR-198*.
- Four Forests Restoration Initiative. (2013) (4FRI) Adaptive Management, Biophysical and Socio-economic Monitoring Plan December 2013.
- Fulé, P. Z. (2008). Does it make sense to restore wildland fire in changing climate? *Restoration Ecology*, 16(4), 526–532. <https://doi.org/10.1111/j.1526-100X.2008.00489.x>
- Fulé, P. Z., Crouse, J. E., Cocke, A. E., Moore, M. M., & Covington, W. W. (2004). Changes in canopy fuels and potential fire behavior 1880-2040: Grand Canyon, Arizona. *Ecological Modelling*, 175(3), 231–248. <https://doi.org/10.1016/j.ecolmodel.2003.10.023>
- Fulé, P. Z., Covington, W. W., & Moore, M. M. (1997). Determining reference conditions for ecosystem management of southwestern ponderosa pine forests. *Ecological Applications*, 7(3), 895–908. [https://doi.org/10.1890/1051-0761\(1997\)007\[0895:drcfem\]2.0.co;2](https://doi.org/10.1890/1051-0761(1997)007[0895:drcfem]2.0.co;2)

- Girvetz, E. H., & Greco, S. E. (2007). How to define a patch: A spatial model for hierarchically delineating organism-specific habitat patches. *Landscape Ecology*, 22(8), 1131–1142.
<https://doi.org/10.1007/s10980-007-9104-8>
- Grumbine, E. R. (1994). What Is Ecosystem Management? *Conservation Biology*, 8(1), 27–38.
<https://doi.org/10.1046/j.1523-1739.1994.08010027.x>
- Guerra-Hernández, J., González-Ferreiro, E., Sarmiento, A., Silva, J., Nunes, A., Correia, A. C., ... Díaz-Varela, R. (2016). Using high resolution UAV imagery to estimate tree variables in *Pinus pinea* plantation in Portugal. *Forest Systems*, 25(2), 9.
<https://doi.org/10.5424/fs/2016252-08895>
- Hudak, A., Smith, A. M., Evans, J. G., & Falkowski, M. J. (2006). Estimating Coniferous Forest Canopy Cover from LiDAR and Multispectral Data. *American Geophysical Union, Fall Meeting 2006*.
- Huffman, D. W., Moore, M. M., Covington, W. W., Crouse, J. E., & Fulé, P. Z. (2001). Ponderosa Pine Forest Reconstruction: Comparisons with Historical Data. *Ponderosa Pine Ecosystems Restoration and Conservation: Steps Towards Stewardship*, 3–8.
- Husch, B., Beers, T. W., & Kershaw, J. A. (2003). *Forest Mensuration* (4th ed.). New York: John Wiley and Sons.
- Iizuka, K., Yonehara, T., Itoh, M., & Kosugi, Y. (2018). Estimating Tree Height and Diameter at Breast Height (DBH) from Digital surface models and orthophotos obtained with an

- unmanned aerial system for a Japanese Cypress (*Chamaecyparis obtusa*) Forest. *Remote Sensing*, 10(1), 13. <https://doi.org/10.3390/rs10010013>
- Kalies, E. L., & Rosenstock, S. S. (2013). Stand structure and breeding birds: Implications for restoring ponderosa pine forests. *Journal of Wildlife Management*, 77(6), 1157–1165. <https://doi.org/10.1002/jwmg.577>
- Kolb, T. E., Wagner, M. R., & Covington, W. W. (1994). Concepts of forest health: utilitarian and ecosystem perspectives. *Journal of Forestry*, 92(2), 10–15. Retrieved from <http://scholarsarchive.library.oregonstate.edu/xmlui/handle/1957/17277>
- Lagro, J. (1991). Assessing Patch Shape in Landscape Mosaics. *Photogrammetric Engineering & Remote Sensing*, 57(3), 285–293. Retrieved from https://www.asprs.org/wp-content/uploads/pers/1991journal/mar/1991_mar_285-293.pdf
- Landres, P. B., Morgan, P., & Swanson, F. J. (1999). Overview of the use of natural variability concepts in managing ecological systems. *Ecological Applications*, 9(4), 1179–1188.
- Larson, A. J., & Churchill, D. (2012). Tree spatial patterns in fire-frequent forests of western North America, including mechanisms of pattern formation and implications for designing fuel reduction and restoration treatments. *Forest Ecology and Management*, 267, 74–92. <https://doi.org/10.1016/j.foreco.2011.11.038>
- Lisein, J., Pierrot-Deseilligny, M., Bonnet, S., & Lejeune, P. (2013). A photogrammetric workflow for the creation of a forest canopy height model from small unmanned aerial system imagery. *Forests*, 4(4), 922–944. <https://doi.org/10.3390/f4040922>

- Mast, J., Fulé, P. Z., Moore, M. M., Covington, W. W., & Waltz, A. E. M. (1999). Restoration of Presettlement Age Structure of an Arizona Ponderosa Pine Forest. *Ecological Applications*, 9(1), 228–239. [https://doi.org/10.1890/1051-0761\(1999\)009\[0228:ropaso\]2.0.co;2](https://doi.org/10.1890/1051-0761(1999)009[0228:ropaso]2.0.co;2)
- Matonis, M. S., & Binkley, D. (2018). Not just about the trees: Key role of mosaic-meadows in restoration of ponderosa pine ecosystems. *Forest Ecology and Management*. <https://doi.org/10.1016/j.foreco.2018.01.019>
- McGarigal, K., Cushman, S. A., & Ene, E. (2012). *FRAGSTATS v4: Spatial Pattern Analysis Program for Categorical and Continuous Maps*. Amherst, MA.
- Mohan, M., Silva, C., Klauberg, C., Jat, P., Catts, G., Cardil, A., ... Dia, M. (2017). Individual Tree Detection from Unmanned Aerial Vehicle (UAV) Derived Canopy Height Model in an Open Canopy Mixed Conifer Forest. *Forests*, 8(9), 340. <https://doi.org/10.3390/f8090340>
- Moore, M. M., Huffman, D. W., Fulé, P. Z., Wallace Covington, W., & Crouse, J. E. (2004). Comparison of Historical and Contemporary Forest Structure and Southwestern Ponderosa Pine Forests. *Forest Science*, 50(2), 162–176.
- Næsset, E. (2004). Practical large-scale forest stand inventory using a small-footprint airborne scanning laser. *Scandinavian Journal of Forest Research*, 19(2), 164–179. <https://doi.org/10.1080/02827580310019257>
- Noss, R. F., Beier, P., Wallace Covington, W., Edward Grumbine, R., Lindenmayer, D. B., Prather, J. W., ... Vosick, D. J. (2006). Recommendations for Integrating Restoration Ecology and Conservation Biology in Ponderosa Pine Forests of the Southwestern United

States. *Restoration Ecology*, 14(1), 4–10. <https://doi.org/10.1111/j.1526-100X.2006.00099.x>

Panagiotidis, D., Abdollahnejad, A., Surovy, P., & Chiteculo, V. (2016). Determining tree height and crown diameter from high-resolution (UAV) imagery. *International Journal of Remote Sensing*, 1–19. <https://doi.org/10.1080/01431161.2016.1264028>

Patton, D. R. (1977). Managing Southwestern Ponderosa Pine for the Abert Squirrel. *Journal of Forestry*, 75(5), 264–267.

Pearson, G. A. (1923). Natural reproduction of western yellow pine in the Southwest. In *Bulletin of the U.S. Department of Agriculture; no.1105*. <https://doi.org/10.5962/bhl.title.64666>

Pelz, K., & Dickinson, Y. (2014). Monitoring forest cover spatial patterns with aerial imagery: A tutorial. *Technical Brief CFRI-TB-1401*, p. 50. Colorado State University.

Puliti, S., Orka, H. O., Gobakken, T., & Nasset, E. (2015). Inventory of small forest areas using an unmanned aerial system. *Remote Sensing*, 7(8), 9632–9654. <https://doi.org/10.3390/rs70809632>

Reutebuch, S. E., Andersen, H.-E., & McGaughey, R. J. (2005). Light Detection and Ranging (LIDAR): An Emerging Tool for Multiple Resource Inventory. *Journal of Forestry*, 103(6), 286–292. Retrieved from <https://academic.oup.com/jof/article-abstract/103/6/286/4598654>

- Reynolds, R. T., Meador, A. J. S., Youtz, J. A., Nicolet, T., Matonis, M. S., Jackson, P. L., ... Graves, A. D. (2013). Restoring composition and structure in southwestern frequent-fire forests. *USDA Forest Service, RMRS-GTR-3*.
- Roccaforte, J. P., Fulé, P. Z., & Covington, W. W. (2010). Monitoring Landscape-Scale Ponderosa Pine Restoration Treatment Implementation and Effectiveness. *Restoration Ecology, 18*(6), 820–833. <https://doi.org/10.1111/j.1526-100x.2008.00508.x>
- Roussel, J.-R., Caspersen, J., Béland, M., Thomas, S., & Achim, A. (2017). Removing bias from LiDAR-based estimates of canopy height: Accounting for the effects of pulse density and footprint size. *Remote Sensing of Environment, 198*, 1–16. <https://doi.org/10.1016/J.RSE.2017.05.032>
- Rupnik, E., Daakir, M., & Pierrot Deseilligny, M. (2017). MicMac – a free, open-source solution for photogrammetry. *Open Geospatial Data, Software and Standards, 2*(1), 14. <https://doi.org/10.1186/s40965-017-0027-2>
- Sánchez Meador, A. J., & Moore, M. M. (2011). Reprint of: Lessons from long-term studies of harvest methods in southwestern ponderosa pine–Gambel oak forests on the Fort Valley Experimental Forest, Arizona, U.S.A. *Forest Ecology and Management, 261*(5), 923–936. <https://doi.org/10.1016/J.FORECO.2010.11.010>
- Sankey, T., Donager, J., McVay, J., & Sankey, J. B. (2017). UAV lidar and hyperspectral fusion for forest monitoring in the southwestern USA. *Remote Sensing of Environment, 195*, 30–43. <https://doi.org/10.1016/j.rse.2017.04.007>

- Schubert, Gilbert H. 1974. Silviculture of southwestern ponderosa pine: The status of our knowledge. Res. Pap. RM-123. Fort Collins, CO: U.S. Department of Agriculture, Forest Service, Rocky Mountain Forest and Range Experiment Station. 71 p.
- Schultz, C. A., Jedd, T., & Beam, R. D. (2012). The Collaborative Forest Landscape Restoration Program: A History and Overview of the First Projects. *Journal of Forestry*, *110*(7), 381–391. <https://doi.org/10.5849/jof.11-082>
- Schultz, C. A., Coelho, D. L., & Beam, R. D. (2014). Design and Governance of Multiparty Monitoring under the (USDA) Forest Service’s Collaborative Forest Landscape Restoration Program. *Journal of Forestry*, *112*(2), 198-206(9). <https://doi.org/10.5849/jof.13-070>
- Shin, P., Sankey, T., Moore, M. M., & Thode, A. E. (2018). Evaluating Unmanned Aerial Vehicle Images for Estimating Forest Canopy Fuels in a Ponderosa Pine Stand. *Remote Sensing*, *10*(8), 1266. <https://doi.org/10.3390/rs10081266>
- Smith, W. B. (2002). Forest inventory and analysis: A national inventory and monitoring program. *Environmental Pollution*, *116*(SUPPL. 1), S233–S242. [https://doi.org/10.1016/S0269-7491\(01\)00255-X](https://doi.org/10.1016/S0269-7491(01)00255-X)
- Snavely, N., Seitz, S. M., & Szeliski, R. (2006). Photo tourism. In *ACM Transactions on Graphics* (Vol. 25). <https://doi.org/10.1145/1141911.1141964>
- Stanturf, J. A., Palik, B. J., & Dumroese, K. R. (2014). Contemporary forest restoration: A review emphasizing function. *Forest Ecol Manag*, *331*, 292–323. <https://doi.org/10.1016/j.foreco.2014.07.029>

- Swetnam, T. W., Allen, C. D., & Betancourt, J. L. (1999). Applied historical ecology: Using the past to manage for the future. *Ecological Applications*, 9(4), 1189–1206.
[https://doi.org/10.1890/1051-0761\(1999\)009\[1189:AHEUTP\]2.0.CO;2](https://doi.org/10.1890/1051-0761(1999)009[1189:AHEUTP]2.0.CO;2)
- Swetnam, T. W., & Betancourt, J. L. (2010). Mesoscale Disturbance and Ecological Response to Decadal Climatic Variability in the American Southwest. In *Advances in Global Change Research* (Vol. 41, pp. 329–359). https://doi.org/10.1007/978-90-481-8736-2_32
- Thiel, C., & Schullius, C. (2016). Comparison of (UAV) photograph-based and airborne lidar-based point clouds over forest from a forestry application perspective. *International Journal of Remote Sensing*, 1–16. <https://doi.org/10.1080/01431161.2016.1225181>
- USGS. (2017). Unmanned aircraft systems data post-processing. In *USGS National UAS Project Office*. Retrieved from <https://www.faa.gov/uas/>
- Wallace, L., Lucieer, A., Malenovsky, Z., Turner, D., & Vopěnka, P. (2016). Assessment of Forest Structure Using Two UAV Techniques: A Comparison of Airborne Laser Scanning and Structure from Motion SfM Point Clouds. *Forests*, 7(3), 62.
<https://doi.org/10.3390/f7030062>
- Weldon, L. (2014). *Ecological Restoration in the United States. Speech Presented at Ecosystems, Economy, and Society*. Retrieved from <https://www.fs.fed.us/speeches/ecological-restoration-united-states>
- White, A. S. (1985). Presettlement Regeneration Patterns in a Southwestern Ponderosa Pine Stand. *Ecology*, 66(2), 589–594. <https://doi.org/10.2307/1940407>

- White, J. C., Wulder, M. A., Vastaranta, M., Coops, N. C., Pitt, D., & Woods, M. (2013). The utility of image-based point clouds for forest inventory: A comparison with airborne laser scanning. *Forests*, 4(3), 518–536. <https://doi.org/10.3390/f4030518>
- Williamson, M., Rosenstock, S., & Kalies, L. (2011). *Four Forest Restoration Initiative: Stakeholders' Initial Science Needs Assessment*. {4FRI} Science and Monitoring Working Group.
- Woolsey, T. S. (1911). *Western Yellow Pine in Arizona and New Mexico*. Retrieved from <https://www.fs.usda.gov/treesearch/pubs/37531>
- Zahawi, R. A., Dandois, J. P., Holl, K. D., Nadwodny, D., Reid, L. J., & Ellis, E. C. (2015). Using lightweight unmanned aerial vehicles to monitor tropical forest recovery. *Biological Conservation*, 186, 287–295. <https://doi.org/10.1016/j.biocon.2015.03.031>
- Zarco-Tejada, P. J., Diaz-Varela, R., Angileri, V., & Loudjani, P. (2014). Tree height quantification using very high resolution imagery acquired from an unmanned aerial vehicle (UAV) and automatic 3D photo-reconstruction methods. *European Journal of Agronomy*, 55, 89–99. <https://doi.org/10.1016/j.eja.2014.01.004>

CHAPTER 3: UAV-based estimate of snow cover dynamics: Optimizing semi-arid forest structure for snow persistence

3.1 Abstract

Seasonal snow cover in the dry forests of the American West provides essential water resources to both human and natural systems. The structure of trees and their arrangement across the landscape are important drivers of snow cover distribution across these forests, varying widely in both space and time. We used unmanned aerial vehicle (UAV) multispectral imagery and Structure-from-Motion (SfM) models to quantify rapidly melting snow cover dynamics and examine the effects of forest structure shading on persistent snow cover in a recently thinned ponderosa pine forest. Using repeat UAV multispectral imagery ($n = 11$ dates) across the 76-ha forest, we first developed a rapid and effective method for identifying persistent snow cover with 90.2% overall accuracy. The SfM model correctly identified 98% ($n = 1280$) of the trees, when compared with terrestrial laser scanner validation data. Using the SfM-derived forest structure variables, we then found that canopy shading associated with the vertical and horizontal metrics was a significant driver of persistent snow cover patches ($R^2 = 0.70$). The results indicate that UAV image-derived forest structure metrics can be used to accurately predict snow patch size and persistence. Our results provide insight into the importance of forest structure, specifically canopy shading, on the amount and distribution of persistent seasonal snow cover in a typical dry forest environment. An operational understanding of forest structure effects on snow cover will help inform forest management that can target snow cover dynamics in addition to forest health.

3.2 Introduction

Runoff from seasonal snowpack in semi-arid regions provides drinking water and agricultural irrigation for at least one-sixth of the world's population (Barnett et al., 2005). Snowpack also provides important ecosystem services, including water for vegetation, aquatic ecosystems, and shallow groundwater recharge (Bales et al., 2011; French & Binley, 2004; Newman et al., 1998; Price & Hendrie, 1983; Wilcox et al., 1997). Throughout the western United States, higher annual mean temperatures and changes to winter air humidity are contributing to an earlier and faster spring snowmelt (Harpold & Brooks, 2018). Regional climate projections indicate that these effects will become more pronounced (Barnett et al., 2008; Hidalgo et al., 2009; Safeeq et al., 2016) and inconsistent snowpack will contribute to higher rates of drought-induced tree stress and mortality (Allen et al., 2015).

In the ponderosa pine (*Pinus ponderosa*) forests of northern and central Arizona, roughly half of the annual precipitation falls as rain during the summer, and the other half as snow during the winter (Hereford, 2014). For mature ponderosa pine trees, winter precipitation via snowpack is the dominant source of water throughout the year, underscoring the importance of snowpack to forest health (Ehleringer et al., 1991; Kerhoulas et al., 2013). In turn, forest cover influences the accumulation and ablation of snow on the ground surface, primarily by controlling canopy interception and by partitioning the solar radiation available at the ground surface (Essery et al., 2003; Harpold et al., 2014; Molotch et al., 2007, 2009; Roth & Nolin, 2017; Varhola et al., 2010). Additionally, the size, shape, spacing, and structure of forest patches (i.e., groups of trees) influence snow accumulation and ablation processes (Davis et al., 1997; Dickerson-Lange et al., 2015; Essery et al., 2008; Lawler & Link, 2011; Veatch et al., 2009).

At the landscape-scale, snowpack distribution, depth, and snow water equivalent (SWE) are most accurately estimated using airborne lidar datasets. Similarly, recent advances in forest inventorying and monitoring have leveraged both terrestrial and airborne lidar datasets to produce georeferenced and scaled measurements of individual trees at the landscape scale (400+ ha) (Bauwens et al., 2016; Calders et al., 2018; Dassot et al., 2011; Donager et al., 2018; Liang et al., 2019; Næsset, 2004; Reutebuch et al., 2005; Sankey, 2012; Sankey et al., 2013). However, lidar is often expensive to acquire. Optical remote sensing of snow-covered area (SCA) is a proven method that can provide accurate estimates of spatial and temporal snowpack accumulation and distribution (Kongoli et al., 2012; Nolin, 2011; T. Sankey et al., 2015). However, SCA estimates lack the snow depth and SWE dimensions. In addition, airborne and satellite-based optical images generally have coarse spatial resolutions, fixed time intervals, and cloud interference that limit their applications in the southwestern USA, where snow rapidly melts in <2 weeks following a storm (T. Sankey et al., 2015). It is important to identify alternative means to rapidly and cost effectively monitor landscape-scale snow extent and persistence for assessing the relationship between SCA and forest structure changes.

As a lower-cost alternative to airborne data, unmanned aerial vehicles (UAVs) are increasingly used to acquire high resolution images (Alonzo et al., 2018; Belmonte et al., 2019; Guerra-Hernández et al., 2016; Iizuka et al., 2018; Puliti et al., 2015; Sankey et al., 2017; Sankey et al., 2019; Sankey et al., 2021; Shin et al., 2018; White et al., 2013). UAV-borne photogrammetric Structure-from-Motion (SfM) modelling has also been successfully used in fine (0–4 ha) and mid-scale (4–400 ha) forest structure assessments (Belmonte et al., 2019; Carr & Slyder, 2018; Shin et al., 2018; Thiel & Schmulius, 2016; Wallace et al., 2016). Compared to lidar-derived 3D point cloud models, UAV SfM often provide similar accuracies in estimating

individual tree canopy heights, diameter, and volumes (Sankey et al., 2019; Thiel & Schnullius, 2016; Wallace et al., 2016). In addition to characterizing forest canopy cover, tree canopy height and diameter, tree density, patch and gap sizes and geometry (Alonzo et al., 2018; Belmonte et al., 2019; Sankey et al., 2019; Shin et al., 2018), UAV datasets can also be used to measure snow cover and depth (Harder et al., 2016; Lendzioch et al., 2019; Miziński & Niedzielski, 2017). UAVs can provide very high resolution and near real-time SCA data (Niedzielski et al., 2018) and can be examined with similar methodologies used in airborne and satellite optical remote sensing to derive SCA. UAVs offer a flexibility essential for capturing both ongoing forest structure changes as well as day-to-day variability of the highly dynamic snow cover in semi-arid Southwestern forests (Baker & Ffolliott, 2003; Belmonte et al., 2019; Sankey et al., 2019).

Here we quantify snowpack dynamics in a recently thinned and unthinned ponderosa pine forest to evaluate the potential benefits of the forest restoration treatment for snowpack. We use UAV-derived multispectral orthomosaic imagery to quantify snow cover dynamics and identify persistent snowpack, and three-dimensional Structure-from-Motion (SfM) models to examine the effects of forest structure, specifically via shading, on snowpack persistence. Our objectives were to:

1. Quantify snow cover following three different winter storms and identify persistent snowpack across the study site;
2. Examine forest structure shading effects on snowpack persistence;
3. Model and predict persistent snowpack using the most influential forest structure metrics.

To assess the importance of specific characteristics and their spatial distribution, forest structure metrics were separated into groups that emphasize vertical and horizontal characteristics. We hypothesized that horizontal forest structure metrics would be more influential for predicting persistent snowpack than vertical forest structure metrics due to the variation in ground shading exhibited by trees, no matter their size or shape. In addition, we hypothesized that crown base height and crown volume would be important for predicting the size of persistent snow patches.

3.3 Materials and Methods

3.3.1 Study area

Our study area is located in the Coconino National Forest in northern Arizona (Figure 3.1). The study area includes 76 ha of forest, characterized by relatively flat topography ranging in elevation between 2200 and 2275 m, with slopes of 0–10% across most of the study area. The vegetation is characterized by ponderosa pine (*Pinus ponderosa*), which dominates both the region and the study area, and includes sporadic Gambel oak (*Quercus gambelii*) and Rocky Mountain juniper (*Juniperus scopulorum*). The climate is sub-humid and characterized by distinct seasonal trends including early summer drought, with an average of 560 mm of precipitation (Western Regional Climate Center, 2020) falling half as snow during winter months and half as rain during the mid-summer monsoon season. The site had been undisturbed since its last naturally occurring fire in 1876, except for selective historical firewood harvesting (Sackett, 1980). However, the site was subjected to a prescribed fire in 1976, in which 63% of the smaller surface fuels and 69% of the woody surface fuels (up to 8 cm in diameter) were consumed (Sackett, 1980).

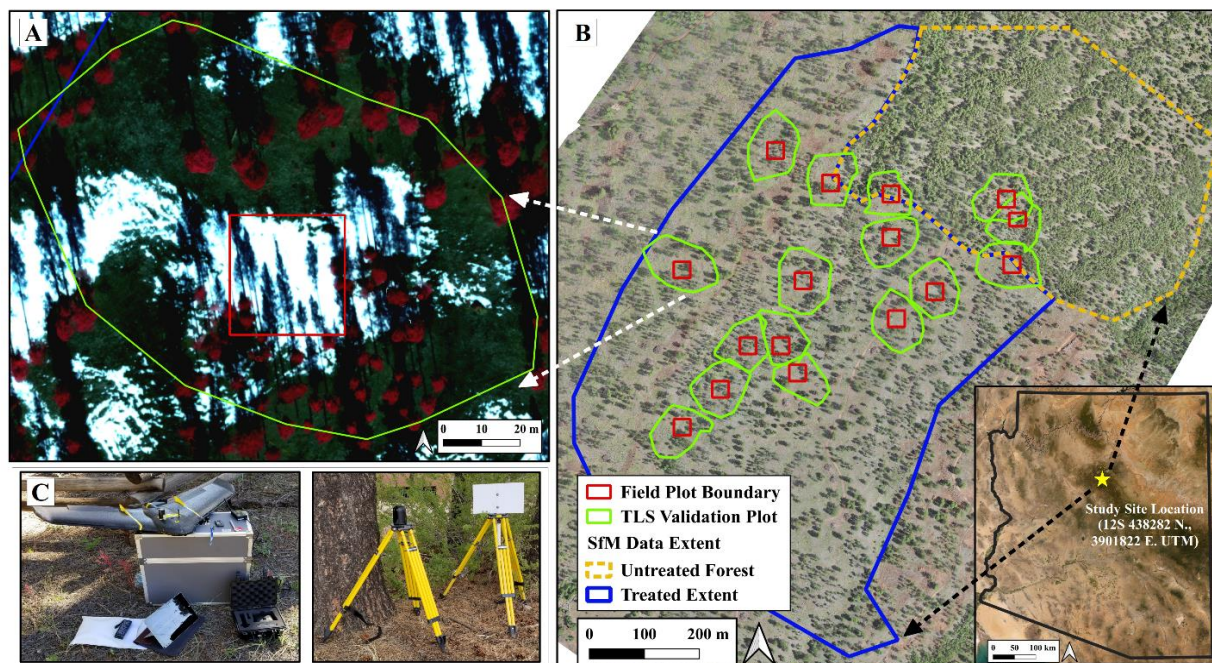


Figure 3.1: An overview of the study site highlighting the locations and extents of the UAV Structure-from-Motion (SfM) data, terrestrial laser scanner (TLS) data, and field-based validation data. (A) shows an example of the field-measured and TLS validated plots. (B) shows the distribution of all field-measured and TLS validated plots within the SfM data extent, which includes both thinned and unthinned portions of the forest. A majority of our ground-based measurements are distributed across the larger, thinned portion of the study site. (C) shows the UAV and TLS instruments used in this study.

A mechanical thinning restoration treatment at the study area began during the fall of 2017 and was completed by the spring of 2018, yielding a 53-ha treated portion and 23-ha untreated portion for this study (Figure 3.1). Similar to other regional restoration treatments that promote diversity in tree group and interspace size, shape, and spacing, this treatment aimed to reinstate pre-settlement forest conditions and included a range of thinning goals that would

promote healthy overstory vegetation and the regeneration of understory vegetation (Allen et al., 2002; Larson & Churchill, 2012; Reynolds et al., 2013; Sackett, 1980). Specifically, the restoration treatment prescription at our study area emphasized irregular tree group delineation, expansion of interspace, retention of all non-ponderosa pine species (e.g., Gambel oak and juniper), and significant reductions in smaller ponderosa pine trees within groups and interspaces.

3.3.2 Data description and processing

3.3.2.1 Snow covered area and persistent snow patches

Our examination of the relationship between persistent snow cover and forest structure began with quantifying snow covered area (SCA) across the entire study site throughout the melt-off period following three significant (>20 cm new snowfall depth) independent winter storm events during the winters of 2017–2018 and 2018–2019. For each storm, a set of 15-cm resolution multispectral UAV orthomosaic images were acquired from the first day following the storm (i.e., maximum SCA) until the snow cover had fully disappeared (i.e., minimum SCA). To capture temporal changes in SCA following each storm, the interval at which images were acquired depended on the weather conditions in the preceding days, but we attempted to keep image date intervals consistent among independent storm events (Table 3.1). The final SCA dataset consisted of three ‘snow-series’ (one snow-series per storm event), yielding a total of 11 different orthomosaic images.

Table 3.1: Three storm events, subsequent image collection dates, and weather conditions. The total snowfall indicates the snow recorded for the storm event, while the mean temperatures and wind speeds are cumulative means between the image dates. Each storm event was imaged

several times from full snow coverage on the first day until the snow cover nearly melted off. The individual image dates were selected considering daily weather conditions and study site access. Periods of near-freezing daily temperatures yielded longer image date intervals so that noticeable changes in snow coverage could be observed. In contrast, periods of higher mean temperature values required more frequent image date intervals as the snow melted rapidly. Weather data were recorded at the regional National Weather Service Forecast office, approximately 15 km from the study site and compiled from NOAA’s Climate Data Online service.

Storm Date	Snowfall (cm)	Image Date	Mean Daily High (°C)	Mean Daily Low (°C)	Mean Wind Speed (m/s)
01/20/2018	28.9	01/22/2018	0.7	-17.4	3.3
		01/24/2018	7.8	-15.8	2.1
		01/26/2018	5.8	-12.3	4.9
		01/29/2018	10.0	-9.8	3.6
12/27/2018	73.4	01/01/2019	0.4	-14.7	3.3
		01/03/2019	5.1	-17.1	3.6
		01/05/2019	11.1	-9.2	1.8
		01/14/2019	6.8	-5.7	2.6
02/05/19	93.9	02/07/2019	1.9	-10.3	5.9
		02/25/2019	4.1	-11.0	3.8
		03/04/2019	10.7	-4.3	3.6

Data comprising the snow-series orthomosaic images were collected using a Sensefly eBee RTK fixed-wing UAV platform (SenseFly, Lausanne, Switzerland) fitted with a Parrot Sequoia multispectral sensor (Parrot Drones SAS, Paris, France). Each flight mission was pre-programmed using Sensefly's proprietary software, which controlled flight plans and customized all flight and data parameters. Flight specifications included high latitudinal and longitudinal overlaps (85% and 90%, respectively) in order to generate the SfM outputs, an average flight altitude of 120 m, and operation centered around solar noon on each image date. There was an average of ~350 images captured for each flight based on the predetermined flight path, with wind conditions largely responsible for the total number of images collected. During each flight, four georeferenced images were recorded at each photo location in the green (530–570 nm), red (640–680 nm), red edge (730–740 nm), and near infrared (770–810 nm) spectral bands. These images were post-processed using Sensefly's eMotion 3 software, which automatically excluded a few distorted images from each flight (SenseFly, Lausanne, Switzerland).

The images were then used to create the final datasets in Agisoft PhotoScan v1.4.0 photogrammetric processing software (Agisoft LLC, St. Petersburg, Russia) for each image date. All images from each flight were scanned for matching 'tie-points', oriented in three-dimensional space via bundle-adjustment, and then mosaicked together (Belmonte et al., 2019). The general workflow in the software includes image alignment to create a sparse point cloud, incorporation of GCP locations, image alignment optimization, gradual filtering out of inaccurate and error-inducing points, and a full image realignment (Belmonte et al., 2019). This workflow generated a final orthomosaicked image in 15 cm spatial resolution in all four spectral bands and dense 3-dimensional (3D) point cloud data photogrammetrically generated from the high

resolution images using Structure-from-Motion (SfM) algorithms. We optimized the SfM algorithm parameters based on our previous results (Belmonte et al., 2019).

The snow-series images were used to first classify SCA across the study site in each image and subsequently delineate persistent snow cover patches. All images ($n = 11$) were classified into five classes: vegetation, sunlit bare ground, shaded bare ground, sunlit snow, and shaded snow, using a random forest supervised classification performed in Google Earth Engine (Massey et al., 2018; Sankey et al., 2018). The random forest classifier was parameterized based on previous remotely sensed image classification examples, with the number of trees set to 100 and the number of variables per split set to the square root of the number of variables (Massey et al., 2018; Sankey et al., 2018). The training dataset consisted of manually digitized polygons ($n = 492$ total) for each of the five classes. The image resolution (15 cm/pixel) allowed for the training dataset classes to be easily delineated. The final binary snow versus non-snow rasters were created by combining pixels classified as both sunlit and shaded snow into a single ‘snow’ class, while pixels in the remaining classes were combined into a single ‘non-snow’ class. The accuracy of this binary classification was assessed using a set of randomly generated snow/non-snow samples ($n = 500$) from the image with roughly half its pixels snow covered, allowing for an unbiased accuracy assessment. Image classification relied on a multi-band image stack created from the four original spectral bands (green, red, red edge, near infrared) and six additional bands derived from the original four: normalized difference vegetation index (NDVI) (Rouse, 1974), soil adjusted vegetation index (SAVI) (Huete, 1988), Gray Level Co-Occurrence Matrix (GLCM) (Haralick, 1973) variance, GLCM homogeneity, GLCM contrast, and GLCM entropy. The GLCM texture bands were included to increase the effectiveness of the

classification algorithm in discriminating the different combinations of bare ground, snow, and their shaded equivalents.

Finally, persistent snow cover was delineated using a single snow cover image composite. This image composite was created by stacking each binary classification ($n = 11$) and counting when each pixel was snow-covered out of the 11 total dates in the image composite. A simple post-processing procedure was used to eliminate spurious pixels and reduce noise along edges of snow pixels. Specifically, we conducted a progressive moving-window majority filtering using windows of 3×3 and 5×5 cells. From this image composite, persistent snow patches were identified by selecting isolated groups of adjacent pixels with snow cover in 10 or 11 out of the total 11 images (Figure 3.2). Groups of pixels less than 200 m^2 were numerous and observed to melt completely between image dates, thus they were eliminated from the analysis. The resulting patches were refined using a general boundary cleaning procedure to eliminate spurious edges, then vectorized and attributed with an identification number and an area estimate (m^2).

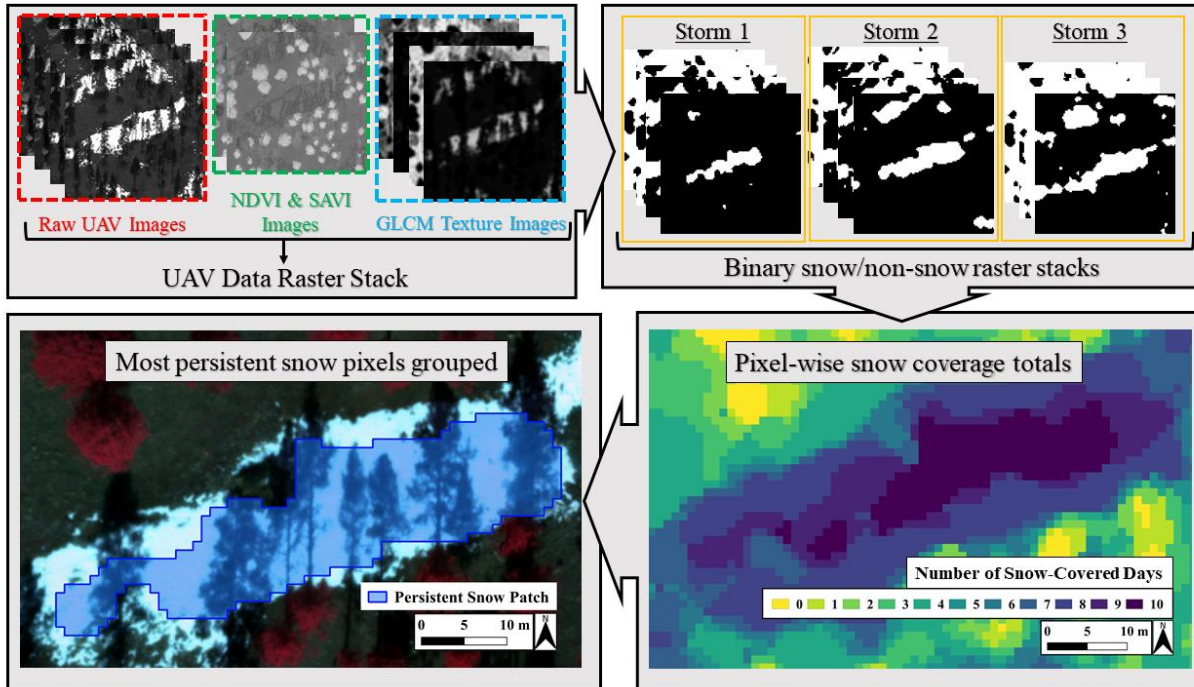


Figure 3.2: UAV multispectral image analysis workflow. First, the original multispectral bands and the calculated indices were stacked into a single raster image, one for each image date ($n = 11$) and classified using a supervised random forest model to generate binary snow/non-snow classes. From the binary classification from each image date, the pixels with 10 or 11 snow-covered days (out of 11) were grouped to create the boundaries of individual persistent snow patches.

3.3.2.2 Forest structure metrics

Forest structure metrics were quantified across the entire study site using the UAV SfM point cloud data and validated using both field measurements and a terrestrial laser scanner (TLS) point cloud dataset. The vertical forest structure metrics examined in our study are tree crown height (CH), crown diameter (CD), crown base height (CBH), the ratio of tree base height to crown height (CBH:Z), and crown volume (CV). The horizontal structure metrics in our study

include trees per hectare (TPH), canopy cover (%) per area (CC), average of five nearest neighbor distances (KNN), Clark and Evans Index (CEI), a canopy height-based solar radiation footprint (SRF), and an average distance from the northern canopy edge (NCE).

The UAV SfM point cloud data were collected across the entire study site with the same platform and sensor used for snow-series data collection and following completion of the mechanical thinning restoration treatment (Belmonte et al., 2019). The final orthomosaic has error estimates of 1.14 m and 1.80 in the X, Y, and Z dimensions, respectively (Belmonte et al., 2019). In addition, the SfM point cloud was used to create a digital terrain model (DTM) using the Cloth Simulation Filter (CSF) tool in CloudCompare v2.9.1 (Belmonte et al., 2019). The CSF tool was parameterized using ‘relief’ for Scenes, a Cloth Resolution of 1 m, and a Classification Threshold of 0.7 m. The accuracy of the DTM ($R^2 = 0.95$ and a RMSE = 2.98 m) was assessed by comparing points extracted from the DTM to corresponding points from differentially corrected Trimble GeoXH GPS elevation values collected from the trees in the field-based validation dataset.

Individual tree segmentation was performed on both the SfM and TLS point clouds using the Li et al. (Li et al., 2012) algorithm in the lidR package (Roussel et al., 2017) in RStudio (R-Studio Team, 2015). The segmented point clouds were then used to estimate each tree’s location (X, Y in UTM 12N m), maximum crown height (CH in m), and average of its widest and narrowest crown diameters (CD in m) using the rLiDAR package in R-Studio (Mohan et al., 2017). Each tree’s crown base height (CBH in m) was estimated from the point cloud data using a novel multiple changepoint detection algorithm (Runge et al., 2020). This algorithm used the area of two-dimensional convex hulls, which were calculated at every 50 cm along a tree’s

height to isolate the height at which trunk points transitioned into canopy points. Finally, each tree's CV (m^3) was then estimated by calculating the volume of the three-dimensional convex hull made from each tree's points above its CBH value.

3.3.2.3 Forest structure metrics validation

We assessed the accuracy of the SfM point-cloud-derived tree metrics by comparing them to both the field-measured and terrestrial laser scanner (TLS) point cloud-derived tree metrics (Figure 3.3). The TLS point cloud data provided accurate high-resolution estimates of all field-measured forest structure metrics and spatially extended the field-measured metrics while also alleviating known accuracy issues associated with UAV SfM-derived crown base height (CBH) and crown volume (CV) estimates (Shin et al., 2018). Since we used a newer TLS instrument that has not been previously evaluated, an assessment of the omission and commission error rates was performed between the field-measured and TLS-derived datasets as well as between the TLS- and SfM-derived datasets. This facilitated direct comparison between trees from the TLS and SfM point clouds.

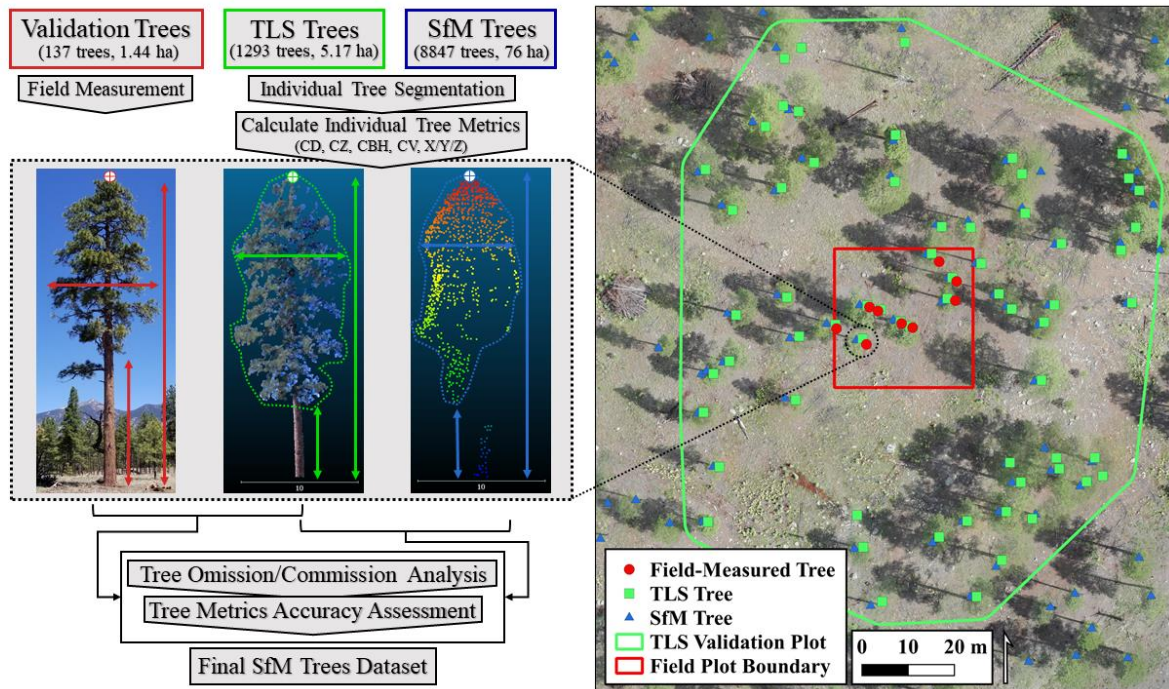


Figure 3.3: Calculating the individual tree metrics for the final analysis involved using both the field-measured and terrestrial laser scanner (TLS) point cloud-derived datasets. Individual trees detected in the TLS point cloud were compared to field-measured trees for an omission and commission analysis. Their crown height (CH), average crown diameter (CD), and crown base heights (CBH) were compared to assess the accuracy of the TLS point cloud-derived estimates. The same comparison was made between matching trees in the TLS point cloud and Structure-from-Motion (SfM)-derived point cloud datasets, with the only difference being the addition of crown volume (CV).

The TLS point cloud data was acquired within 0.64 ha field plots ($n = 16$) covering a total area of 5.17 ha and spread along a gradient of forest density present across the study site. The TLS data were collected using a Leica Geosystems BLK360 Imaging Laser Scanner (Leica Geosystems AG, 2020), which has a range of up to 60 m radius. The BLK360 captures 360,000

points per second at 830 nm wavelength with 300 and 360 degrees of vertical and horizontal field of view, respectively, and with 6mm-10m accuracies. Each TLS validation plot included at least three scans, which were tied together and georeferenced using four distinct reference targets. Reference targets were 50 × 50 cm reflective panels bolted to adjustable tripods at 1 m above ground, and their positions were recorded using a Trimble GeoXH GPS unit. We determined the locations and configuration of the scanner and reference targets using guidelines developed in our previous study (Donager et al., 2018). Using Cloud Compare software, the scans were co-registered using the target center points, then merged into a single point cloud and georeferenced using the GPS coordinates of the target; the overall X, Y, and Z positional accuracy of the 16 point clouds is 0.46 m. The average point spacing of all point clouds was 0.03 m with a range of 0.025–0.046 m, and each was subsampled to 0.01 m to reduce redundant points and ensure consistent point spacing across scans.

The TLS point cloud data were validated using field-based measurements taken from 137 trees within 30 × 30 m validation plots (n = 16), covering a total of 1.44 ha. The field-based validation plots were centered within the TLS validation plots, providing as much overlap between the datasets as possible. Using the Trimble GeoXH handheld GPS unit with an attached Trimble laser range finder module, each tree's geographic position (X,Y,Z coordinates), CH, CD, and CBH were measured and differentially corrected in GPS Pathfinder Office.

3.3.3 Data analysis

3.3.3.1 Forest structure predictor variables

The effect of forest canopy shading on persistent snow patches was quantified using distinct tree shading influence areas. Previous research shows that a tree's ground shading influence extends

between 1 and 2 times its crown height during the winter season in forests of the southwestern U.S. [55,69,70]. To support and refine this, we used three different spatial extents of localized tree shading to assess the size of persistent snow patches. These tree shading influence areas (TSIAs) were established with respect to each individual persistent snow patch and included trees located within a distance of 1, 1.5, and 2 times their crown heights. To ensure that only the trees capable of influencing a persistent snow patch were included, trees were selected based on whether their shadows were within solar azimuth angle extents specific to study site location and snow-series image date. The resulting minimum bounding extents were termed TSIA1.0, TSIA1.5, and TSIA2.0 (Figure 3.4). Once trees were selected in each TSIA, their vertical forest structure metrics were averaged to produce a final dataset.

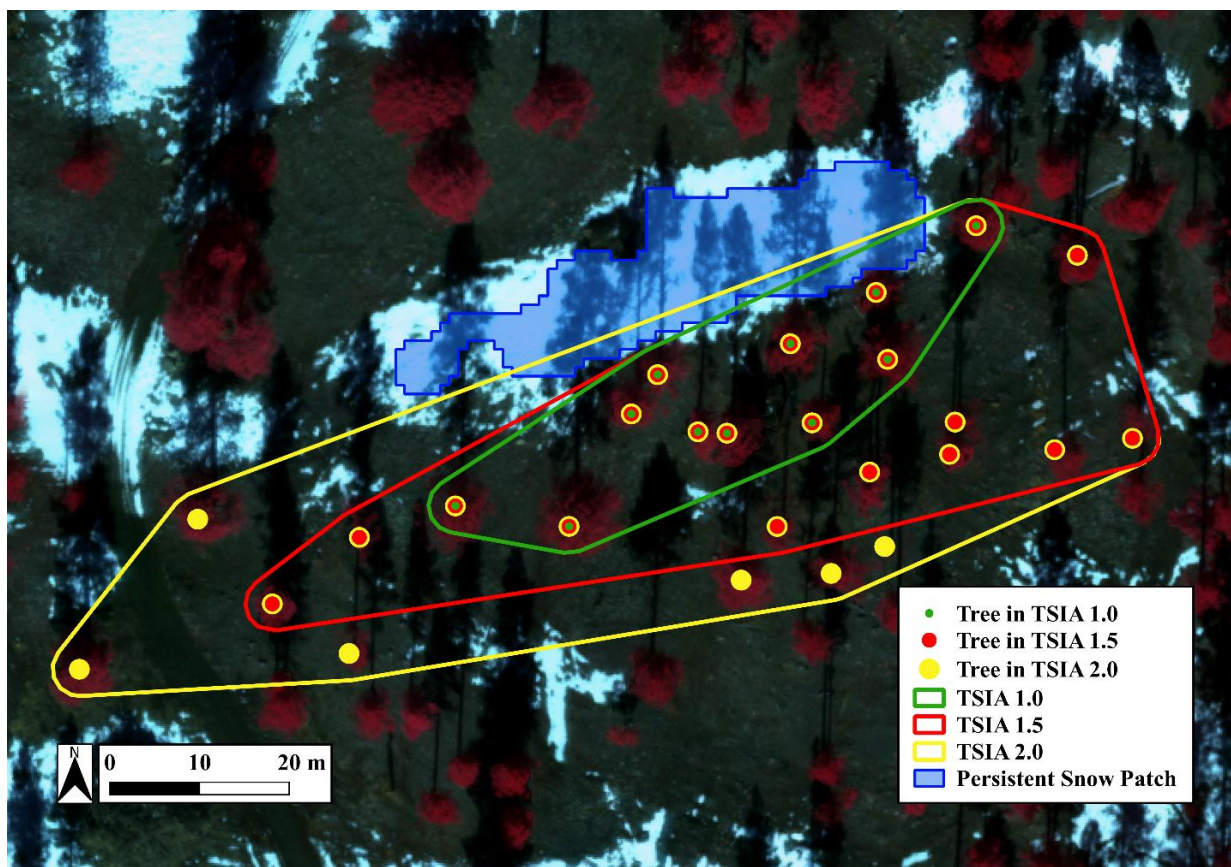


Figure 3.4: A persistent snow patch and the trees influencing it at the three different ranges: 1, 1.5, and 2 times the height (CH) of the tree. A tree was included within each respective tree shading influence area (TSIA), if its CH multiplied by 1, 1.5, or 2 was extended into the snow patch and if the bearing of its location (XY) to the patch was within the range of daily solar angles.

In addition to the vertical forest structure metric summaries, each TSIA was assigned a set of horizontal arrangement metrics to quantify the spatial distribution of trees. Forest density was estimated by calculating trees per hectare (TPH) and average canopy cover (CC) in percent, while spacing of trees was measured using the average nearest neighbor (KNN) distance in meters from each tree to its five nearest neighbors. The clustering of trees was measured using a unitless Clark and Evans Index (CEI) value, with values < 1 indicating ordering and values > 1 indicating clustering. The amount of ground shading was expressed using an average solar radiation footprint (SRF) value in w/m^2 for each TSIA polygon. The SRF was created using a sitewide canopy height model and the solar radiation toolset in ArcMap 10.8 to calculate the cumulative amount of incoming solar radiation (w/m^2) during each snowstorm event (Olpenda et al., 2018; Abdollahnejad et al., 2018). The ground surface pixel values were averaged across the three storms and then across each TSIA polygon. Finally, each pixel's distance to the northern canopy edge (DNCE) was calculated and averaged across each TSIA using a binary canopy cover raster based on the methodology developed by Mazzotti et al. 2019. The DNCE values provided a fine-scale metric that describes the directional within-stand differences of forest canopy spatial arrangement, and are well suited for assessing the effect of forest canopy radiative transfer.

3.3.3.2 Model framework

An initial exploratory data analysis revealed sources of significant multicollinearity between forest structure metrics (independent variables) as well as numerous complex and non-linear relationships with persistent snow patch area (dependent variable). A variable selection process was used to eliminate the highly correlated and less descriptive forest structure metrics using variable inflation factor (VIF) scoring. To find a suitable model, we parameterized generalized linear models, random forest, support vector machine, and Multivariate Adaptive Regression Spline (MARS) algorithms for regression and tested their predictive accuracies using the Caret package (Kuhn, 2008) in RStudio. We selected the MARS model framework since it provided both the most accurate predictive accuracy as well as offering variable importance scores, which helped us interpret results into meaningful forest management recommendations.

The MARS model performs nonparametric multivariate regression without underlying assumptions of the data and is useful for regression problems with high-dimensional datasets and multiple predictor variable interactions. Our modeling framework assessed the relationship between persistent snow patch size (m^2) and forest structure metrics for each of the three different tree shadow influence areas (TSIAs). Initial attempts at model fitting and prediction presented inconsistent results, with model hyperparameters and predictive accuracies fluctuating based on different randomly selected training and testing datasets, which can be apparent when using machine learning methods on smaller datasets (Breiman, 2001). Due to our relatively small sample size ($n = 99$), we adopted a split-sample validation procedure that was repeated 500 times. This provided 500 different randomly selected testing and training data partitions, model construction, and predictive accuracy assessments. While the number of repetitions is usually arbitrarily chosen, we found that 500 repetitions provided a large enough sample size to clearly

discriminate between trends in variable importance. Each model iteration utilized an exhaustive grid search to select the optimal set of hyperparameters, allowing for the inclusion of all possible predictors as well as for two-way interactions between predictors. An optimal model was then selected from each iteration by minimizing the generalized cross-validation error estimate, from which variable importance scores ranging from 0 to 100 were calculated for each model term.

Model results were summarized based on the frequency of both the hyperparameter value and the variable importance scores. Separately, the optimal model framework for each iteration was used for prediction on the testing dataset. Instead of arriving at a single ideal model that definitively explains the relationship between persistence snow patch area and forest structure, this approach provides a robust conceptual understanding of the relationship.

3.4 Results

3.4.1 Snow cover classification and persistent snow patches

The snow cover classification accuracy assessment was performed using the third image from the second storm due to its mostly even distribution of snow/non-snow pixels. The snow classification performed well, with an overall accuracy of 90.2% and a kappa coefficient of 0.80. Relatively low rates of omission error were observed for the non-snow and snow classes at 13% and 6%, respectively, while similar rates of commission error were observed for the non-snow and snow classes at 6% and 14%, respectively (Table 3.2).

Table 3.2: Accuracy of the snow/non-snow classification across the 76-ha study site. The image used to generate the error matrix included an even amount of snow and non-snow pixels, providing the least biased estimation of classification error.

Class Value	Non-Snow	Snow	Total	User's Accuracy
Non-Snow	236	14	250	94%
Snow	35	215	250	86%
Total	271	229	500	
Producer's Accuracy	87%	94%		
Overall Accuracy: 90.2%				

With the average daily high temperatures similar across all storm events (6.1 °C, 5.8 °C, and 5.7 °C for storms 1–3, respectively), storm 1 had the lowest initial snowfall amount (28.9 cm) and the lowest reduction in site-wide SCA (–51%) over 8 days. In contrast, storms 2 and 3 had greater initial snowfall amounts, 73.4 cm and 93.9 cm, respectively, and site-wide reductions in SCA were consistently higher and for longer time periods: –59% over 15 days and –70% over 26 days, respectively (Table 3.1).

The proportion of SCA in the treated portion of the study site on Day 1 was consistent across all storms, ranging from 91.2% to 89.4% to 90% for storms 1, 2, and 3, respectively. The proportion of SCA across the untreated portion of the study site on Day 1 of each storm was consistently lower, with values ranging from 43.4% to 62.3% to 58.1% for storms 1, 2, and 3, respectively. The effect of treatment condition on the magnitude of SCA reduction is evident both within and across storm events. The treated portion of the study site consistently exhibited a wider range of reductions in SCA within each storm compared to the narrower range in reductions observed in the untreated portion. The average of each storm's total SCA reduction in the treated portion was –76.5% compared to –38.6% in the untreated portion (Figure 3.5).

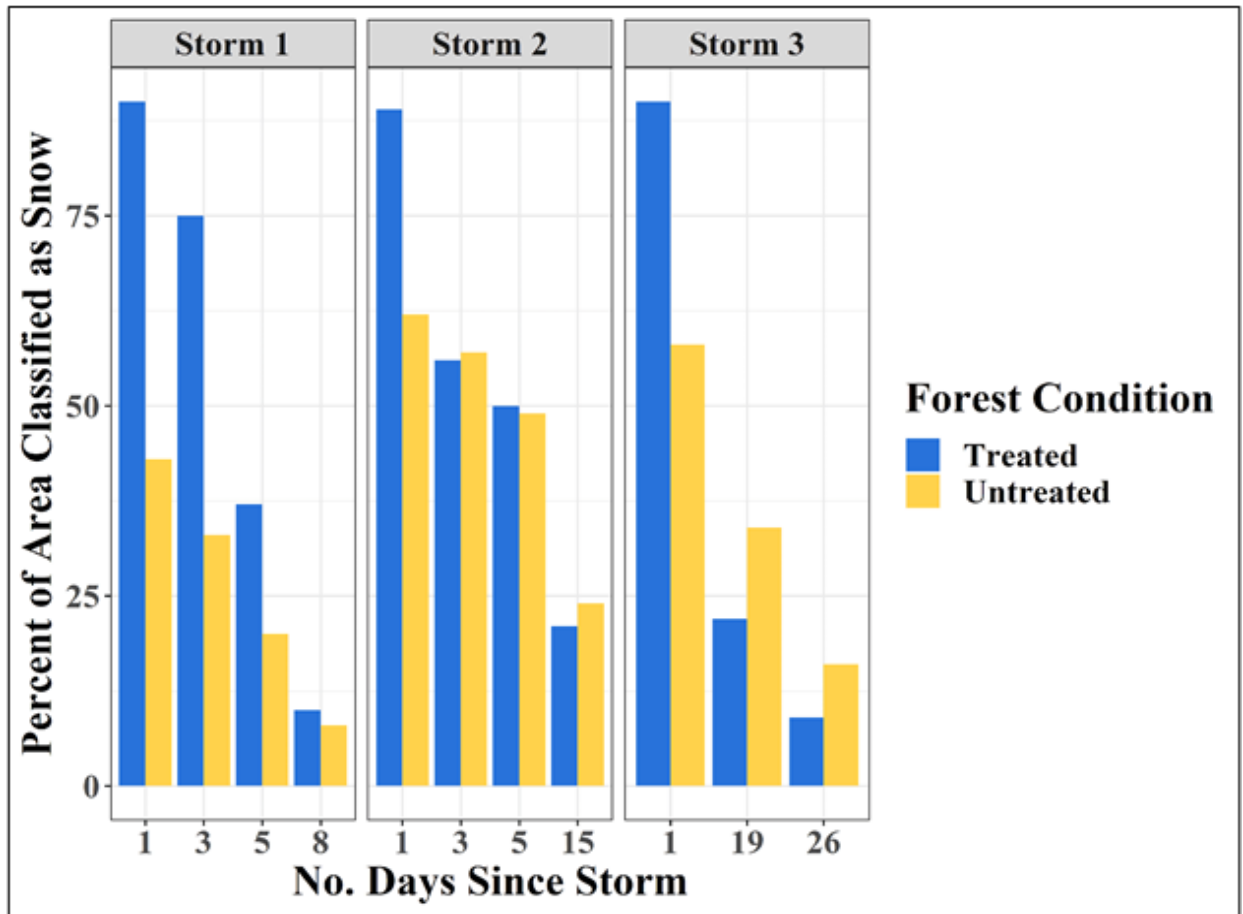


Figure 3.5: The percent of the treated and untreated regions of the study site that are classified SCA for each UAV snow-series image following a storm. This data is grouped by storm, and partitioned by forest treatment condition to illustrate the reductions in SCA within and across the storms. SCA patterns following storm events show a greater SCA reduction in the treated portion of the study site than in the untreated portion. Evident also are the relatively similar initial amounts of classified SCA on the first image date after a storm in the treated portion, contrasting the initial amounts in the untreated portion.

Distinct persistent snow patches were identified from the final composite of classified snow-series images from grouped pixels that were covered in snow for 10 or 11 of the total days

($n = 11$) (Figure 3.6A). A total of 99 individual snow patches were delineated across the entire study site, covering 8.4% (6.36 ha) of the total area and ranging in size from 203 to 2699 m^2 (SD = 469.7 m^2), with an average size of 646.9 m^2 and a majority (82%) being less than 1000 m^2 . The patches delineated across the treated portion of the study site ($n = 67$) had an average size of 722 m^2 and covered 9.2% (4.84 ha) of the treated area (Figure 3.6B). In contrast, the patches in the untreated portion of the study site ($n = 32$) had an average size of 474 m^2 and covered 6.6% (1.52 ha) of that area (Figure 3.6B).

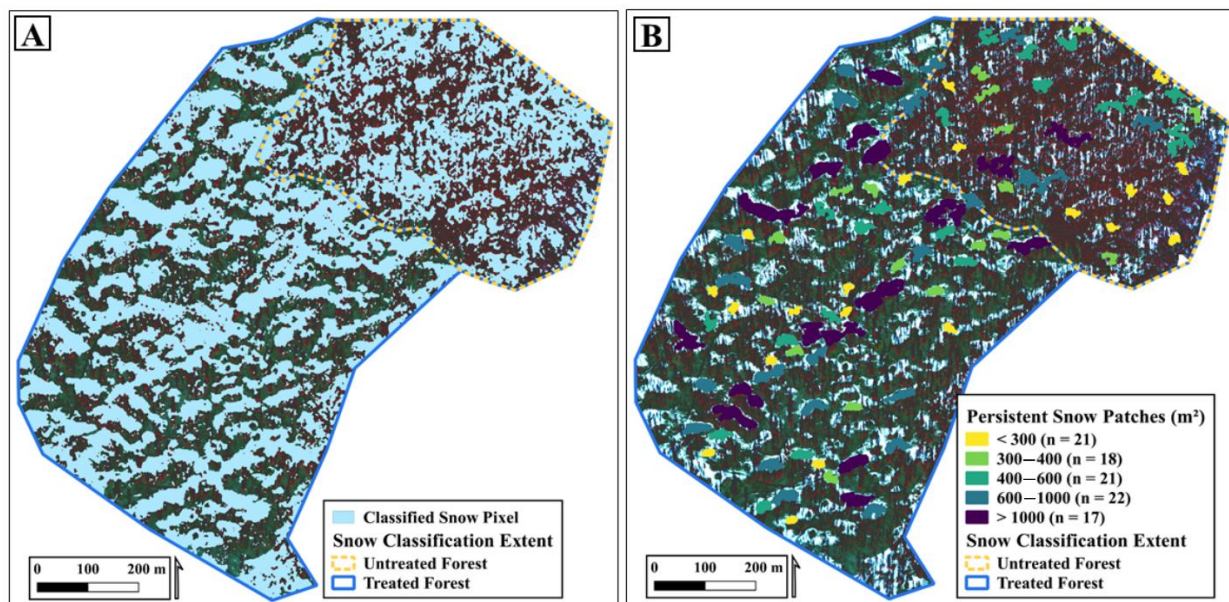


Figure 3.6: Each UAV image ($n = 11$) was classified into snow/non-snow pixels (A) and the resulting rasters were assembled into a single composite, in which persistent snow patches were identified (B). The orthomosaic image used as the base imagery is from storm 2, day 3 (1 May 2019) and its binary snow classification (A) was used for the classification accuracy assessment because it contained a nearly even snow/non-snow (49/51%) area distribution.

3.4.2 Forest structure metrics summary

The TLS-derived point cloud correctly identified 88% ($n = 120$) of trees from within the field-measured validation plots. The final TLS dataset consisted of 1293 trees identified within the TLS plot data extents ($n = 16$ validation plot, totaling 5.17 ha). The SfM-derived point cloud correctly identified 98% ($n = 1280$) trees within the TLS point cloud data extent, and the final dataset included a total of 8847 trees across the 76-ha study site. The individual tree metrics compared between all datasets are identical except for CV, which was calculated from TLS and SfM point clouds (Figure 3.2).

The accuracy of the individual tree structure metrics used in the final model are a product of a multi-scale accuracy assessment, which compared the field-measured, TLS-derived, and SfM-derived estimates. The relationships between the field-measured and TLS-derived tree metrics were generally strong, while the relationships between the TLS- and SfM-derived tree metrics varied.

The final set of forest structure predictors used for modeling were selected to balance both accurate tree dimension estimation as well as to maximize the model's predictive capacity. The vertical forest structure metrics were selected by first examining the relationships between SfM- and TLS-derived estimates, then by assessing their multicollinearity and variance inflation factor (VIF) scores. For example, the weak relationship between SfM- and TLS-derived CD ($R^2 = 0.14$; RMSE = 1.62 m) indicated that it should not be used as a predictor variable. In addition, CD was highly correlated with CV ($R^2 = 0.72$) and had a high VIF score (12.3), indicating that it would negatively impact model accuracy and interpretability. For the entire study site, the

complete set of vertical and horizontal forest structure metrics included as model predictors are summarized by TSIA size (1, 1.5, and 2).

3.4.3 Relationship between snow and forest structure

The most frequent number of model terms for TSIA 1.0 was 5 (50% of all model iterations), for TSIA 1.5 were 6 (35% of all model iterations), and for TSIA 2.0 were 7 (35% of all model iterations), while the most frequent interaction degree term was 1 for all TSIA groups. The average model error estimates calculated across all model iterations grouped by TSIA size were 0.14 for TSIA 1.0, 0.11 for TSIA 1.5, and 0.14 for TSIA 2.0. As the influence region size increased, more predictor variables were needed to stabilize the model and there was less consensus in the number of predictors selected.

For all TSIA sizes, the forest structure metrics with the highest variable importance scores were the mean canopy cover (CC), mean solar radiation footprint (SRF), and trees per hectare (TPH) values (Figure 3.7). While this remained relatively consistent overall, differences in variable importance scores existed across TSIA sizes as evidenced by the differences between variable importance scores from TSIA groups within CEI, mean SRF, and mean TPH metrics. Specifically, the greater importance was observed for CEI at the largest spatial scale and the lesser importance of mean SRF and mean TPH at the smallest spatial scale.

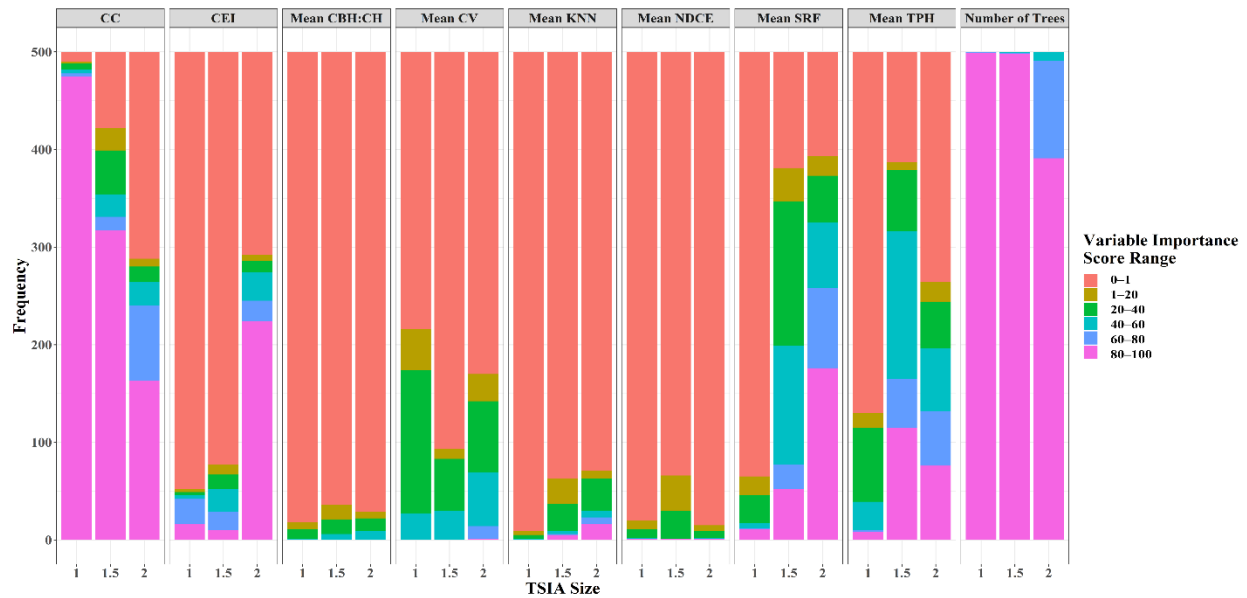


Figure 3.7: Variable importance scores calculated for the forest structure metric predictor variables used in fitting the final MARS model framework. The variable importance score ranges from 0 to 100, with higher scores indicating that the predictor was more influential in model construction ($n = 500$). The chart depicts the frequency with which each forest structure metric was within the respective range of the importance score. The data are partitioned by tree shading influence area (TSIA) size to better illustrate the interaction with forest structure metric. Overall, the most influential forest structure metric predictors are canopy cover (CC), mean solar radiation footprint (SRF) value, and mean trees per hectare (TPH).

The models describing forest structure at TSIA 1.5 performed best overall with a mean prediction accuracy $R^2 = 0.70$ (RMSE = 267 m²) (Figure 3.8), followed by those at TSIA 1.0 and TSIA 2.0 with mean prediction accuracies of $R^2 = 0.66$ (RMSE = 286 m²) and $R^2 = 0.61$ (RMSE = 307 m²), respectively. Of note is the increasing variability in model predictive accuracy on

both ends of the persistent snow patch area, especially on the larger end where wide fanning indicates greater uncertainty.

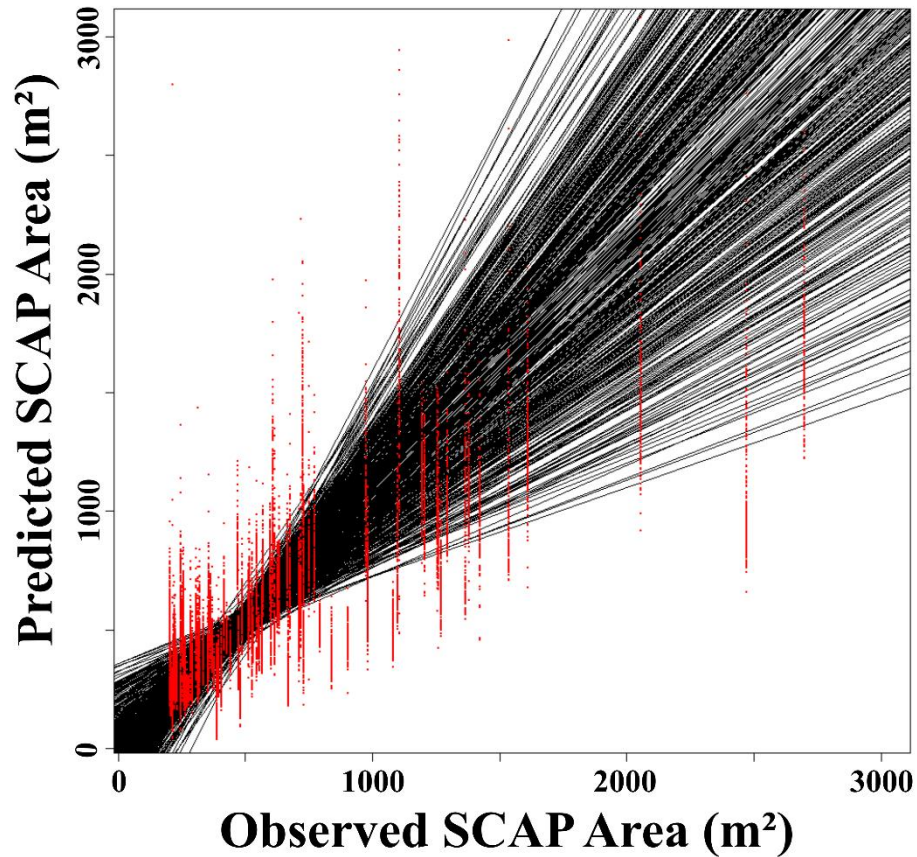


Figure 3.8: A collection of the simple linear relationships reflecting each model’s predictive ability for the TSIA 1.5. Each line represents the prediction accuracy of a single model, and the red points are the value pairs for the predicted vs. observed persistent snow patch sizes (m²). The mean performance statistics for the entire set of prediction models in TSIA 1.5 is $R^2 = 0.70$ and a $RMSE = 267 \text{ m}^2$.

3.5 Discussion

Seasonal snowpack provides vital water resources for both human- and ecosystem-oriented services in semi-arid environments. Quantifying the spatially heterogeneous and often ephemeral nature of this snow at the mid- (10–1000 ha) and landscape-scales (400+ ha) requires accurate spatially extensive and temporally dense datasets (T. Sankey et al., 2015). The structure and arrangement of trees in dry forests are central components influencing snow cover and persistent snowpack. In this study, we demonstrate an accurate method to provide near real-time estimates of mid-scale snow covered area (SCA) and assess how forest structure influences persistent snow patch size in a thinned ponderosa pine forest on the southern edge of the North American continental snow distribution. We found that forest structure metrics emphasizing the spatial arrangement of trees and tree groups were more influential on persistent snow cover (Figure 3.7), and that these effects were most pronounced when considering trees within 1.5 times their height to persistent snow cover (Figure 3.8).

We first quantified snow-covered area (SCA) across the discontinuous forest of our 76-ha study site using UAV snow-series datasets. In forested environments, SCA is often underestimated in remote sensing data propagating from lower resolution satellite and airborne imagery, with trees masking the ground surface and tree shadows being misclassified as ‘non-snow’ (Hall et al., 2001; Huang et al., 2017; Metsämäki et al., 2002; Vikhamar & Solberg, 2003). The overall accuracy of our high-resolution binary snow classification was 90.2%, indicating strategic UAV data acquisition, associated high-resolution imagery, and a relatively straightforward classification process can be used to quantify SCA in forested areas (Eker et al., 2019). Furthermore, by capturing inter-storm reductions in SCA (Figure 3.5), we demonstrate

this approach can effectively delineate regions harboring the most persistent SCA and do so at a fine spatial resolution (Figure 3.6). This level of detail and accuracy provided the foundation for our assessment of forest structure impact on persistent snow cover patches.

Except for crown diameter (CD), we found good overall agreement between the UAV SfM estimates and our validation datasets. Horizontal forest structure metrics were more influential than vertical structure metrics in predicting persistent snow patch size (Figure 3.7). Specifically, tree canopy cover (CC), trees per ha (TPH), and solar radiation footprint (SRF) were the most explanatory variables. This result supports our hypotheses that snow cover and, therefore, subcanopy shortwave radiation, is moderated by the spatial arrangement of trees more than by the vertical structure of individual trees.

While the horizontal metrics of CC, TPH, and SRF were the most influential predictor variables, they were also the metrics with the greatest variability when grouped by persistent snow patch size. These are metrics of foliar cover and tree stem density that directly influence subcanopy shading, which subsequently impacts the relatively shallow, intermittent, and spatially heterogeneous snow cover found at our study site. In addition to the horizontal metrics, we expected the mean CEI and mean KNN distance values to be influential because they describe the location and spacing of trees. However, their lack of influence might indicate a need to adjust the scale and scope at which these metrics are calculated. For example, the spacing of groups of trees might be a more valuable metric than the spacing of individual trees when considering sub-canopy ground shading.

In contrast to the horizontal metrics, variables in the vertical metric group were only slightly or moderately useful predictors of persistent snow patch size (Figure 3.7). We

anticipated that forest patches composed of trees with noticeably different vertical structures would result in differences in the forest canopy shading and ultimately statistically significant impacts on persistent snow patch size. This is illustrated in Figure 3.9, where the amount of shading seemingly provided by trees with higher CBH:CH ratio and lower CV values (Panel A) is noticeably lower compared to the amount of shading provided by trees with overall larger crowns (Panel B). The post-treatment forest structure conditions in Figure 3.9A are more common than those in Figure 3.9B. A potential cause for this could be a combination of the relatively homogenous vertical structure metrics observed across the study site (Figure 1B) and the relatively low agreement ($R^2 = 0.50$; RMSE = 3.23 m) between the TLS and field-measured CBH values.

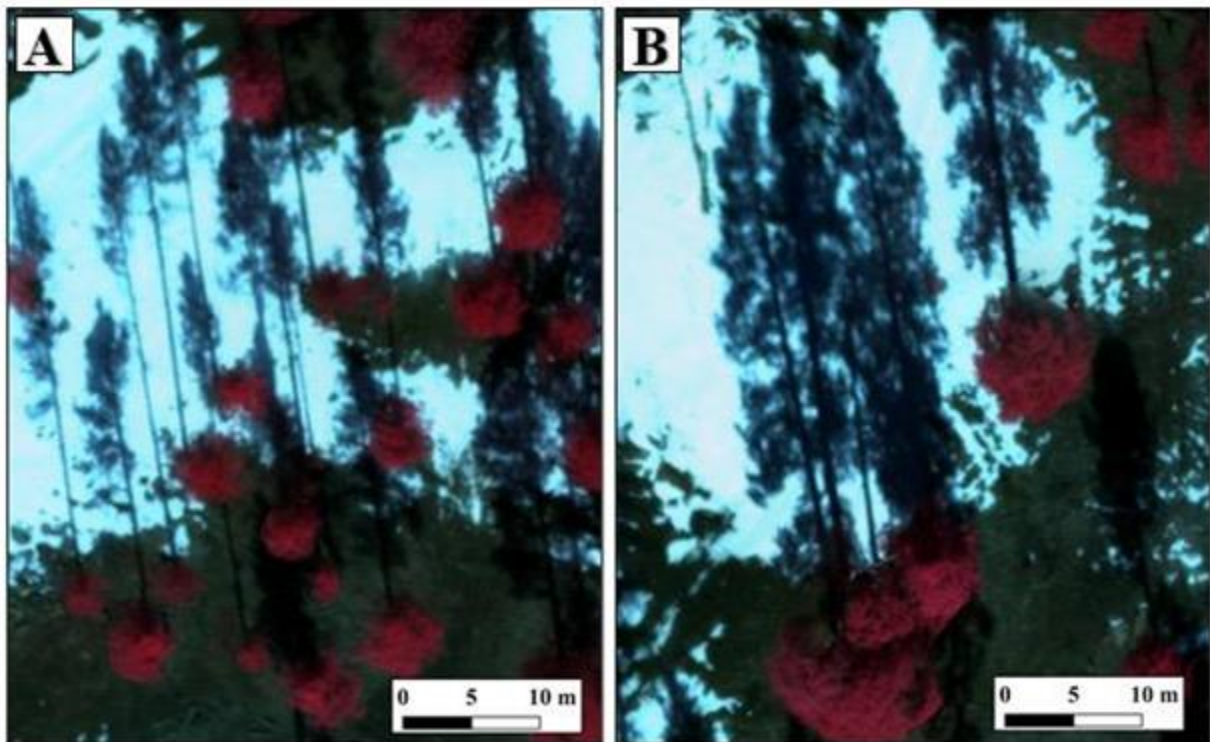


Figure 3.9: A comparison of trees and their shadows with different vertical structure metrics, namely CBH:CH and CV. The perceived difference in forest canopy shading between trees with high CBH:CH and low CV values (Panel A) are compared to those trees with overall larger crowns (Panel B). These canopy shading differences were expected to result in vertical forest structure metrics being significant in the modeling of persistent snow patch size.

Mean canopy height (CH) had strong agreement between both the field-measured and TLS-estimated values and the TLS- and SfM-estimated values, as well as low variability when grouped by persistent snow patch size. Accurate tree height estimates are not surprising given the ability for SfM and TLS to accurately estimate tree height regardless of forest density (Belmonte et al., 2019; Donager et al., 2018; Sankey et al., 2017) and the relatively homogenous post-settlement forest structure conditions present across the study site. Given the low variable importance scores, mean CH appeared unimportant when modeling persistent snow patch area. However, we believe the importance of mean CH is evidenced in the superior predictive ability of the TSIA 1.5 category. More specifically, using tree CH to define the north–south width of forest canopy gaps (in the northern hemisphere), specifically to 1.5 times the average crown height of adjacent trees, provides the most consistent estimates of both snow cover and snow persistence. Early research shows that snow persisted in 'zones of retention' corresponding to 1.5 to 2 times the height of adjacent tree stands in ponderosa pine forests (Ffolliott et al., 1965). While these early studies assumed that persistent snow retention zones were driven by forest structure, mainly tree CH, we use high-resolution UAV-based estimates of CH to confirm the 1.5 CH value as well as to identify horizontal metrics contributing to persistent snow. Our results indicate that mean tree CH and tree patch spacing at 1.5 times CH are important considerations

in forest restoration, in addition to the horizontal metrics described above, for maximizing snow cover retention and water yield.

As thinning-based restoration is expanded throughout dry forests that harbor seasonal snowpack, it is crucial to understand how restoration-driven canopy reduction will impact forest water balance (Sankey et al., 2020) and snowmelt water inputs into shallow groundwater reservoirs. Previous research shows that snow accumulation in discontinuous or disturbed forests can be greater in less dense forests and within large canopy openings (Mazzotti et al., 2019; T. Sankey et al., 2015). The restoration thinning at our study site significantly reduced both canopy cover (from about 40% to 10%) and tree density (from about 212 TPH to 65 TPH), while increasing the number of forest patches (from 39 to 133) and decreasing the mean forest patch area (from 0.68 ha to 0.13 ha) (Belmonte et al., 2019). While this study focused on developing remote sensing techniques to quantify snowpack dynamics, contrasting the treated versus the untreated portions of our study area suggest important treatment impacts that should be confirmed by more replicated comparisons. Specifically, our results show there was more overall persistent snow cover in the thinned portion of the study site compared to the untreated portion (10% and 7%, respectively). Our results generally support and provide further insight into restoration-based reductions in forest density to promote snow cover. For example, the largest persistent snow patches were located adjacent to forest patches with 31–33% canopy cover (CC), while the smallest were located adjacent to patches with 50–52% CC, a trend which is supported by the optimal snow persistence CC value of 24% provided by regional satellite-derived estimates (Belmonte et al., 2019).

Our findings suggest that tailoring future forest restoration treatments to promote persistent snow cover in southwestern U.S. dry forest ecosystems should continue to focus on horizontal forest structure metrics like forest density and canopy cover at the landscape-scale (>1000 ha). Our results also underscore and refine the importance of horizontal forest structure metrics like CC, TPH, and SRF, regardless of spatial scale. However, we propose these criteria be emphasized during the creation of forest patches at relatively fine patch scale (<4 ha). It is critical to regional restoration efforts to continue implementing the commonly accepted standards in southwestern dry forest restoration, like promoting variation in interspace size, tree group size and within-group tree spacing (Eker et al., 2019). In addition, we propose landscape-scale restoration treatment goals should also be implemented at fine spatial scale, operating within and among individual forest patches. For example, assuming a restoration treatment reflects diversity in forest patch size, spacing, and density, an overarching goal may be to achieve 24–33% CC across a 1000-ha treatment area. While this level of CC could be measured across the entire treatment area, having individual forest patches at 24–33% CC and distributed with distances at 1.5 times the average tree height within the patch should also promote localized persistent snow cover.

3.6 Conclusions

This study considered the inclusion of detailed forest structure metrics in quantifying persistent snow cover in a dry southwestern U.S. forest. We found the size (m²) of persistent snow patches can be effectively predicted using targeted forest structure metrics. Specifically, the most effective predictor metrics included tree shadows that are 1.5 times the tree heights, as well as tree density and canopy cover within this shaded area. While our findings underscore the

importance of forest canopy shading on persistent snow cover, they also indicate the relationship between persistent snow cover and fine-scale forest structure is likely more complex, rooted in different variables, or present at different spatial scales. Maximizing persistent snow cover in dry forest environments can be achieved by controlling subcanopy shading at the ground surface through an optimal set of fine-scale forest structure and spacing metrics. Future research and restoration efforts can achieve this by coupling our UAV-based methodology for quantifying persistent snow cover with more descriptive measurements of snow dynamics, such as snow depth and snow water equivalent.

Our results support the utility of thinning-based forest restoration in dry southwestern forests to promote snow cover retention and forest health. We show there is a wide range of persistent snow patch sizes across thinned forest, and that differences in fine-scale forest structure are important for maximizing snow persistence. Adjusting existing restoration thinning prescriptions to reflect landscape-scale goals in fine-scale forest patches will help further this objective while promoting broader ecosystem health and resiliency.

3.7 References

- Allen, C. D., Breshears, D. D., & McDowell, N. G. (2015). On underestimation of global vulnerability to tree mortality and forest die-off from hotter drought in the Anthropocene. *Ecosphere*, 6(8), 1–55. <https://doi.org/10.1890/ES15-00203.1>
- Allen, C. D., Savage, M., Falk, D. A., Suckling, K. F., Swetnam, T. W., Schulke, T., Stacey, P. B., Morgan, P., Hoffman, M., & Klingel, J. T. (2002). Ecological Restoration of Southwestern Ponderosa Pine Ecosystems: A Broad Perspective. *Ecological Applications*, 12(5), 1418–1433. [https://doi.org/10.1890/1051-0761\(2002\)012\[1418:EROSPP\]2.0.CO;2](https://doi.org/10.1890/1051-0761(2002)012[1418:EROSPP]2.0.CO;2)
- Alonzo, M., Andersen, H.-E., Morton, D., Cook, B., Alonzo, M., Andersen, H.-E., Morton, D. C., & Cook, B. D. (2018). Quantifying Boreal Forest Structure and Composition Using UAV Structure from Motion. *Forests*, 9(3), 119. <https://doi.org/10.3390/f9030119>
- Baker, M. B., & Ffolliott, P. F. (2003). Role of Snow Hydrology in Watershed Management. *Journal of the Arizona-Nevada Academy of Science*, 35(1), 42–47. <https://doi.org/10.2307/40056925>
- Bales, R. C., Hopmans, J. W., O'Geen, A. T., Meadows, M., Hartsough, P. C., Kirchner, P., Hunsaker, C. T., & Beaudette, D. (2011). Soil moisture response to snowmelt and rainfall in a sierra nevada mixed-conifer forest. *Vadose Zone Journal*, 10(3), 786–799. <https://doi.org/10.2136/vzj2011.0001>
- Barnett, T. P., Adam, J. C., & Lettenmaier, D. P. (2005). Potential impacts of a warming climate on water availability in snow-dominated regions. In *Nature* (Vol. 438, Issue 7066, pp. 303–309). <https://doi.org/10.1038/nature04141>

- Barnett, T. P., Pierce, D. W., Hidalgo, H. G., Bonfils, C., Santer, B. D., Das, T., Bala, G., Wood, A. W., Nozawa, T., Mirin, A. A., Cayan, D. R., & Dettinger, M. D. (2008). Human-Induced Changes in the Hydrology of the Western United States. In *New Series* (Vol. 319, Issue 5866).
- Bauwens, S., Bartholomeus, H., Calders, K., & Lejeune, P. (2016). Forest Inventory with Terrestrial LiDAR: A Comparison of Static and Hand-Held Mobile Laser Scanning. *Forests*, 7(12), 127. <https://doi.org/10.3390/f7060127>
- Belmonte, A., Sankey, T., Biederman, J. A., Bradford, J., Goetz, S. J., Kolb, T., & Woolley, T. (2019). UAV-derived estimates of forest structure to inform ponderosa pine forest restoration. *Remote Sensing in Ecology and Conservation*, rse2.137. <https://doi.org/10.1002/rse2.137>
- Biederman, J. A., Brooks, P. D., Harpold, A. A., Gochis, D. J., Gutmann, E., Reed, D. E., Pendall, E., & Ewers, B. E. (2014). Multiscale observations of snow accumulation and peak snowpack following widespread, insect-induced lodgepole pine mortality. *Ecohydrology*, 7(1), 150–162. <https://doi.org/10.1002/eco.1342>
- Bottero, A., D'amato, A. W., Palik, B. J., Bradford, J. B., Fraver, S., Battaglia, M. A., & Asherin, L. A. (2017). Density-dependent vulnerability of forest ecosystems to drought. *Journal of Applied Ecology*. <https://doi.org/10.1111/1365-2664.12847>
- Broxton, P. D., Harpold, A. A., Biederman, J. A., Troch, P. A., Molotch, N. P., & Brooks, P. D. (2015). Quantifying the effects of vegetation structure on snow accumulation and ablation in mixed-conifer forests. *Ecohydrology*, 8(6), 1073–1094. <https://doi.org/10.1002/eco.1565>

- Broxton, Patrick D., van Leeuwen, W. J. D., & Biederman, J. A. (2020). Forest cover and topography regulate the thin, ephemeral snowpacks of the semiarid Southwest United States. *Ecohydrology*. <https://doi.org/10.1002/eco.2202>
- Calders, K., Origo, N., Burt, A., Disney, M., Nightingale, J., Raunonen, P., Åkerblom, M., Malhi, Y., & Lewis, P. (2018). Realistic Forest Stand Reconstruction from Terrestrial LiDAR for Radiative Transfer Modelling. *Remote Sensing*, *10*(6), 933. <https://doi.org/10.3390/rs10060933>
- Churchill, D. J., Larson, A. J., Dahlgreen, M. C., Franklin, J. F., Hessburg, P. F., & Lutz, J. A. (2013). Restoring forest resilience: From reference spatial patterns to silvicultural prescriptions and monitoring. *Forest Ecol Manag*, *291*(Canadian Journal of Forest Research 39 2009), 442–457. <https://doi.org/10.1016/j.foreco.2012.11.007>
- Clark, J. S., Iverson, L., Woodall, C. W., Allen, C. D., Bell, D. M., Bragg, D. C., D'Amato, A. W., Davis, F. W., Hersh, M. H., Ibanez, I., Jackson, S. T., Matthews, S., Pederson, N., Peters, M., Schwartz, M. W., Waring, K. M., & Zimmermann, N. E. (2016). The impacts of increasing drought on forest dynamics, structure, and biodiversity in the United States. *Global Change Biology*, *22*(7), 2329–2352. <https://doi.org/10.1111/gcb.13160>
- D'Amato, A. W., Bradford, J. B., Fraver, S., & Palik, B. J. (2011). Forest management for mitigation and adaptation to climate change: Insights from long-term silviculture experiments. *Forest Ecology and Management*, *262*(5), 803–816. <https://doi.org/10.1016/j.foreco.2011.05.014>
- Dandois, J. P., Olano, M., & Ellis, E. C. (2015). Optimal altitude, overlap, and weather

conditions for computer vision uav estimates of forest structure. *Remote Sensing*, 7(10), 13895–13920. <https://doi.org/10.3390/rs71013895>

Dassot, M., Constant, T., & Fournier, M. (2011). The use of terrestrial LiDAR technology in forest science: Application fields, benefits and challenges. *Annals of Forest Science*, 68(5), 959–974. <https://doi.org/10.1007/s13595-011-0102-2>

Davis, R. E., Hardy, J. P., Ni, W., Woodcock, C., McKenzie, J. C., Jordan, R., & Li, X. (1997). Variation of snow cover ablation in the boreal forest: A sensitivity study on the effects of conifer canopy. *Journal of Geophysical Research Atmospheres*, 102(24), 29389–29395. <https://doi.org/10.1029/97jd01335>

Diaz-Varela, R., Gonzalez-Ferreiro, E., Correia, A. C., Nunes, A., Tomé, M., Guerra-Hernandez, J., Silva, J., Sarmiento, A., & Fontes, L. (2016). Using high resolution UAV imagery to estimate tree variables in Pinus pinea plantation in Portugal. *Forest Systems*, 25(2), eSC09. <https://doi.org/10.5424/fs/2016252-08895>

Dickerson-Lange, S. E., Gersonde, R. F., Hubbart, J. A., Link, T. E., Nolin, A. W., Perry, G. H., Roth, T. R., Wayand, N. E., & Lundquist, J. D. (2017). Snow disappearance timing is dominated by forest effects on snow accumulation in warm winter climates of the Pacific Northwest, United States. *Hydrological Processes*, 31(10), 1846–1862. <https://doi.org/10.1002/hyp.11144>

Dickerson-Lange, S. E., Lutz, J. A., Martin, K. A., Raleigh, M. S., Gersonde, R., & Lundquist, J. D. (2015). Evaluating observational methods to quantify snow duration under diverse forest canopies. *Water Resources Research*, 51(2), 1203–1224.

<https://doi.org/10.1002/2014WR015744>

Dieterich, J. H. (1980). Chimney Spring forest fire history. In *Chimney Spring forest fire history*.

<https://doi.org/10.5962/bhl.title.98633>

Donager, J. J., Sankey, T. T., Sankey, J. B., Sanchez Meador, A. J., Springer, A. E., & Bailey, J.

D. 2018. Examining forest structure with terrestrial lidar: Suggestions and novel techniques based on comparisons between scanners and forest treatments. *Earth and Space Science* 5 (11), 753-776

Ehleringer, J. R., & Dawson, T. E. (1992). Water uptake by plants: perspectives from stable isotope composition. *Plant, Cell and Environment*, 15, 1073–1082.

Ehleringer, J. R., Phillips, S. J., Schuster, W. S. F., & Sandquist, D. S. (1991). Differential utilization of summer rains by desert plants. *Oecologia*, 88, 430–434.

Eker, R., Bühler, Y., Schlögl, S., Stoffel, A., & Aydın, A. (2019). Monitoring of Snow Cover Ablation Using Very High Spatial Resolution Remote Sensing Datasets. *Remote Sensing*, 11(6), 699. <https://doi.org/10.3390/rs11060699>

Ellis, C. R., Pomeroy, J. W., Essery, R. L. H., & Link, T. E. (2011). Effects of needleleaf forest cover on radiation and snowmelt dynamics in the Canadian Rocky Mountains. *Canadian Journal of Forest Research*, 41(3), 608–620. <https://doi.org/10.1139/X10-227>

Essery, R., Bunting, P., Hardy, J., Link, T., Marks, D., Melloh, R., Pomeroy, J., Rowlands, A., & Rutter, N. (2008). Radiative transfer modeling of a coniferous canopy characterized by airborne remote sensing. *Journal of Hydrometeorology*, 9(2), 228–241.
<https://doi.org/10.1175/2007JHM870.1>

- Essery, R., Pomeroy, J., Parviainen, J., & Storck, P. (2003). Sublimation of Snow from Coniferous Forests in a Climate Model. *Journal of Climate*, 16(11), 1855–1864.
[https://doi.org/10.1175/1520-0442\(2003\)016<1855:SOSFCF>2.0.CO;2](https://doi.org/10.1175/1520-0442(2003)016<1855:SOSFCF>2.0.CO;2)
- Ffolliott, P.F., Gottfried, G. J. (2003). *Contributions of Snow Research to Forest Watershed Management in the Southwestern United States*. 29–38.
- Ffolliott, P. F. (1993). Snowpack dynamics in mountain areas: Research findings in the southwestern United States. *International Symposium of Mountainous Areas*, 129–139.
- Ffolliott, P. F., Gottfried, G. J., & Baker, M. B. (1989). Water yield from forest snowpack management: Research findings in Arizona and New Mexico. *Water Resources Research*, 25(9), 1999–2007. <https://doi.org/10.1029/WR025i009p01999>
- Ffolliott, P. F., Hansen, E. A., & Zander, A. D. (1965). Snow in natural openings and adjacent ponderosa pine stands on the Beaver Creek watersheds. *USDA Forest Service Research Note No. 53*, 1–8.
- Ffolliott, P. F., & Thorud, D. B. (1974). A Technique to Evaluate Snowpack Profiles in and Adjacent to Forest Openings. *Hydrology and Water Resources in Arizona and the Southwest*. <http://hdl.handle.net/10150/300274>
- Fitch, R. A., Kim, Y. S., Waltz, A. E. M., & Crouse, J. E. (2018). Changes in potential wildland fire suppression costs due to restoration treatments in Northern Arizona Ponderosa pine forests. *Forest Policy and Economics*, 87, 101–114.
<https://doi.org/10.1016/j.forpol.2017.11.006>

- Forzieri, G., Castelli, F., & Vivoni, E. R. (2011). Vegetation Dynamics within the North American Monsoon Region. *American Meteorological Society*, 1763–1783.
<https://doi.org/10.1175/2010JCLI3847.1>
- French, H., & Binley, A. (2004). Snowmelt infiltration: Monitoring temporal and spatial variability using time-lapse electrical resistivity. *Journal of Hydrology*, 297(1–4), 174–186.
<https://doi.org/10.1016/j.jhydrol.2004.04.005>
- Goeking, S. A., & Tarboton, D. G. (2020). Forests and Water Yield: A Synthesis of Disturbance Effects on Streamflow and Snowpack in Western Coniferous Forests. *Journal of Forestry*, 2020, 1–21. <https://doi.org/10.1093/jofore/fvz069>
- Gorelick, N., Hancher, M., Dixon, M., Ilyushchenko, S., Thau, D., & Moore, R. (2017). Planetary-scale geospatial analysis for everyone. *Remote Sensing of Environment*.
- Gottfried, G. J., & Ffolliott, P. F. (1981). Evaluation of the Use of Soil Conservation Service Snow Course Data in Describing Local Snow Conditions in Arizona Forests. *Hydrology and Water Resources in Arizona and the Southwest*. <http://hdl.handle.net/10150/301230>
- Hall, D. K., Foster, J. L., Salomonson, V. V., Klein, A. G., & Chien, Y. L. (2001). Development of a technique to assess snow-cover mapping errors from space. *IEEE Transactions on Geoscience and Remote Sensing*, 39(2).
<https://ieeexplore.ieee.org/stamp/stamp.jsp?arnumber=905251>
- Harder, P., Schirmer, M., Pomeroy, J., & Helgason, W. (2016). Accuracy of snow depth estimation in mountain and prairie environments by an unmanned aerial vehicle. *The Cryosphere*, 10, 2559–2571. <https://doi.org/10.5194/tc-10-2559-2016>

- Harpold, A. A., Biederman, J. A., Condon, K., Merino, M., Korgaonkar, Y., Nan, T., Sloat, L. L., Ross, M., & Brooks, P. D. (2014). Changes in snow accumulation and ablation following the Las Conchas Forest Fire, New Mexico, USA. *Ecohydrology*, 7(2), 440–452. <https://doi.org/10.1002/eco.1363>
- Harpold, A. A., & Brooks, P. D. (2018). Humidity determines snowpack ablation under a warming climate. *Proceedings of the National Academy of Sciences of the United States of America*, 115(6), 1215–1220. <https://doi.org/10.1073/pnas.1716789115>
- Hereford, R. (2014). *Climate Variation at Flagstaff, Arizona's Mountain Town Compiled from National Weather Service Data*.
- Hidalgo, H. G., Das, T., Dettinger, M. D., Cayan, D. R., Pierce, D. W., Barnett, T. P., Bala, G., Mirin, A., Wood, A. W., Bonfils, C., Santer, B. D., & Nozawa, T. (2009). Detection and attribution of streamflow timing changes to climate change in the Western United States. *Journal of Climate*, 22(13), 3838–3855. <https://doi.org/10.1175/2009JCLI2470.1>
- Huang, X., Deng, J., Wang, W., Feng, Q., & Liang, T. (2017). Impact of climate and elevation on snow cover using integrated remote sensing snow products in Tibetan Plateau. *Remote Sensing of Environment*, 190, 274–288. <https://doi.org/10.1016/j.rse.2016.12.028>
- Hudak, A., Smith, A. M., Evans, J. G., & Falkowski, M. J. (2006). Estimating Coniferous Forest Canopy Cover from LiDAR and Multispectral Data. *American Geophysical Union, Fall Meeting 2006*.
- Huete, A. "A Soil-Adjusted Vegetation Index (SAVI)." *Remote Sensing of Environment* 25 (1988): 295-309.

- Iglhaut, J., Cabo, C., Puliti, S., Piermattei, L., O'Connor, J., & Rosette, J. (2019). Structure from Motion Photogrammetry in Forestry: a Review. *Current Forestry Reports*, 5(3), 155–168. <https://doi.org/10.1007/s40725-019-00094-3>
- Iizuka, K., Yonehara, T., Itoh, M., & Kosugi, Y. (2018). Estimating Tree Height and Diameter at Breast Height (DBH) from Digital surface models and orthophotos obtained with an unmanned aerial system for a Japanese Cypress (*Chamaecyparis obtusa*) Forest. *Remote Sensing*, 10(1), 13. <https://doi.org/10.3390/rs10010013>
- James, T., Evans, A., Madly, E., & Kelly, C. (2014). *The Economic Importance of the Colorado River to the Basin Region*. <https://businessforwater.org/wp-content/uploads/2016/12/PTF-Final-121814.pdf>
- Kangas, A., Gobakken, T., Puliti, S., Hauglin, M., & Naesset, E. (2018). Value of airborne laser scanning and digital aerial photogrammetry data in forest decision making. *Silva Fenn*, 52(1). <https://doi.org/10.14214/sf.9923>
- Kerhoulas, L. P., Kolb, T. E., & Koch, G. W. (2013). Tree size, stand density, and the source of water used across seasons by ponderosa pine in northern Arizona. *Forest Ecology and Management*, 289, 425–433. <https://doi.org/10.1016/j.foreco.2012.10.036>
- Kolb, T. E., Fettig, C. J., Ayres, M. P., Bentz, B. J., Hicke, J. A., Mathiasen, R., Stewart, J. E., & Weed, A. S. (2016). Observed and anticipated impacts of drought on forest insects and diseases in the United States. *Forest Ecology and Management*, 380, 321–334. <https://doi.org/10.1016/j.foreco.2016.04.051>
- Kongoli, C., Romanov, P., & Ferraro, R. (2012). Snow cover monitoring from remote-sensing

- satellites: Possibilities for drought assessment. In *Remote Sensing of Drought: Innovative Monitoring Approaches* (pp. 359–386). <https://doi.org/10.1201/b11863>
- Kuhn, M. (2008). Building Predictive Models in R Using the caret Package. *Journal of Statistical Software, Articles*, 28(5), 1–26.
- Larson, A. J., & Churchill, D. (2012). Tree spatial patterns in fire-frequent forests of western North America, including mechanisms of pattern formation and implications for designing fuel reduction and restoration treatments. *Forest Ecology and Management*, 267, 74–92. <https://doi.org/10.1016/j.foreco.2011.11.038>
- Lawler, R. R., & Link, T. E. (2011). Quantification of incoming all-wave radiation in discontinuous forest canopies with application to snowmelt prediction. *Hydrological Processes*, 25(21), 3322–3331. <https://doi.org/10.1002/hyp.8150>
- Lendzioch, T., Langhammer, J., & Jenicek, M. (2019). Estimating Snow Depth and Leaf Area Index Based on UAV Digital Photogrammetry. *Sensors*, 19(5), 1027. <https://doi.org/10.3390/s19051027>
- Liang, X., Hyypä, J., Kaartinen, H., Pyörälä, J., Lehtomäki, M., Holopainen, M., Kankare, V., Luoma, V., Saarinen, N., Chen, L., & Wang, Y. (2019). International benchmarking of terrestrial laser scanning approaches for forest inventories; joint project of eurosdr and isprs; part i: Objective, datasets, evaluation criteria and methods. *Official Publication - EuroSDR*, 2019(71), 1–29. <https://doi.org/10.1016/j.isprsjprs.2016.01.006>
- Malle, J., Rutter, N., Mazzotti, G., & Jonas, T. (2019). Shading by Trees and Fractional Snow Cover Control the Subcanopy Radiation Budget. *Journal of Geophysical Research:*

Atmospheres, 124(6), 3195–3207. <https://doi.org/10.1029/2018JD029908>

Mazzotti, G., Currier, W. R., Deems, J. S., Pflug, J. M., Lundquist, J. D., & Jonas, T. (2019).

Revisiting Snow Cover Variability and Canopy Structure Within Forest Stands: Insights From Airborne Lidar Data. *Water Resources Research*, 55(7), 6198–6216.

<https://doi.org/10.1029/2019wr024898>

McCabe, G. J., Wolock, D. M., Pederson, G. T., Woodhouse, C. A., & McAfee, S. (2017).

Evidence that recent warming is reducing upper Colorado river flows. *Earth Interactions*, 21(10), 1–14. <https://doi.org/10.1175/EI-D-17-0007.1>

Metsämäki, S., Vepsäläinen, J., Pulliainen, J., & Sucksdorff, Y. (2002). Improved linear

interpolation method for the estimation of snow-covered area from optical data. *Remote Sensing of Environment*, 82(1), 64–78. [https://doi.org/10.1016/S0034-4257\(02\)00025-1](https://doi.org/10.1016/S0034-4257(02)00025-1)

Meyer, C. L., & Sisk, T. D. (2001). Butterfly Response to Microclimatic Conditions Following

Ponderosa Pine Restoration. *Restoration Ecology*, 9(4), 453–461.

<https://doi.org/10.1046/j.1526-100X.2001.94014.x>

Miziński, B., & Niedzielski, T. (2017). Fully-automated estimation of snow depth in near real

time with the use of unmanned aerial vehicles without utilizing ground control points. *Cold Regions Science and Technology*, 138, 63–72.

<https://doi.org/10.1016/j.coldregions.2017.03.006>

Mohan, M., Silva, C., Klauberg, C., Jat, P., Catts, G., Cardil, A., Hudak, A., & Dia, M. (2017).

Individual Tree Detection from Unmanned Aerial Vehicle (UAV) Derived Canopy Height Model in an Open Canopy Mixed Conifer Forest. *Forests*, 8(9), 340.

<https://doi.org/10.3390/f8090340>

Molotch, N. P., Blanken, P. D., Williams, M. W., Turnipseed, A. A., Monson, R. K., & Margulis, S. A. (2007). Estimating sublimation of intercepted and sub-canopy snow using eddy covariance systems. *Hydrological Processes*, 21(12), 1567–1575.

<https://doi.org/10.1002/hyp.6719>

Molotch, N. P., Brooks, P. D., Burns, S. P., Litvak, M., Monson, R. K., McConnell, J. R., & Musselman, K. (2009). Ecohydrological controls on snowmelt partitioning in mixed-conifer sub-alpine forests. *Ecohydrology*, 2(2), 129–142. <https://doi.org/10.1002/eco.48>

Molotch, N. P., & Meromy, L. (2014). Physiographic and climatic controls on snow cover persistence in the Sierra Nevada Mountains. *Hydrological Processes*, 28(16), 4573–4586.

<https://doi.org/10.1002/hyp.10254>

Musselman, K. N., Molotch, N. P., & Brooks, P. D. (2008). Effects of vegetation on snow accumulation and ablation in a mid-latitude sub-alpine forest. *Hydrological Processes*, 22(15), 2767–2776. <https://doi.org/10.1002/hyp.7050>

Musselman, Keith N., Molotch, N. P., Margulis, S. A., Lehning, M., & Gustafsson, D. (2012). Improved snowmelt simulations with a canopy model forced with photo-derived direct beam canopy transmissivity. *Water Resources Research*, 48(10).

<https://doi.org/10.1029/2012WR012285>

Næsset, E. (2004). Practical large-scale forest stand inventory using a small-footprint airborne scanning laser. *Scandinavian Journal of Forest Research*, 19(2), 164–179.

<https://doi.org/10.1080/02827580310019257>

- Newman, B. D., Campbell, A. R., & Wilcox, B. P. (1998). Lateral subsurface flow pathways in a semiarid Ponderosa pine hillslope. *Water Resources Research*, 34(12), 3485–3496.
<https://doi.org/10.1029/98WR02684>
- Niedzielski, T., Spallek, W., & Witek-Kasprzak, M. (2018). Automated Snow Extent Mapping Based on Orthophoto Images from Unmanned Aerial Vehicles. *Pure and Applied Geophysics*, 175(9), 3285–3302. <https://doi.org/10.1007/s00024-018-1843-8>
- Nolin, A. W. (2011). Recent advances in remote sensing of seasonal snow. In *Journal of Glaciology* (Vol. 56, Issue 200, pp. 1141–1150).
<https://doi.org/10.3189/002214311796406077>
- Noss, R. F., Beier, P., Wallace Covington, W., Edward Grumbine, R., Lindenmayer, D. B., Prather, J. W., Schmiegelow, F., Sisk, T. D., & Vosick, D. J. (2006). Recommendations for Integrating Restoration Ecology and Conservation Biology in Ponderosa Pine Forests of the Southwestern United States. *Restoration Ecology*, 14(1), 4–10.
<https://doi.org/10.1111/j.1526-100X.2006.00099.x>
- Price, A. G., & Hendrie, L. K. (1983). Water motion in a deciduous forest during snowmelt. *Journal of Hydrology*, 64(1–4), 339–356. [https://doi.org/10.1016/0022-1694\(83\)90076-8](https://doi.org/10.1016/0022-1694(83)90076-8)
- Pugh, E., & Small, E. (2012). The impact of pine beetle infestation on snow accumulation and melt in the headwaters of the Colorado River. *Ecohydrology*, 5(4), 467–477.
<https://doi.org/10.1002/eco.239>
- Puliti, S., Ørka, H. O., Gobakken, T., & Næsset, E. (2015). Inventory of small forest areas using an unmanned aerial system. *Remote Sensing*, 7(8), 9632–9654.

<https://doi.org/10.3390/rs70809632>

- Reutebuch, S. E., Andersen, H.-E., & McGaughey, R. J. (2005). Light Detection and Ranging (LIDAR): An Emerging Tool for Multiple Resource Inventory. *Journal of Forestry*, *103*(6), 286–292. <https://academic.oup.com/jof/article-abstract/103/6/286/4598654>
- Revuelto, J., L pez-Moreno, J. I., Azorin-Molina, C., & Vicente-Serrano, S. M. (2015). Canopy influence on snow depth distribution in a pine stand determined from terrestrial laser data. *Water Resources Research*, *51*(5), 3476–3489. <https://doi.org/10.1002/2014WR016496>
- Reynolds, R. T., Meador, A. J. S., Youtz, J. A., Nicolet, T., Matonis, M. S., Jackson, P. L., DeLorenzo, D. G., & Graves, A. D. (2013). Restoring composition and structure in southwestern frequent-fire forests. *USDA Forest Service, RMRS-GTR-3*.
- Richer, E. E., Kampf, S. K., Fassnacht, S. R., & Moore, C. C. (2013). Spatiotemporal index for analyzing controls on snow climatology: Application in the Colorado Front Range. *Physical Geography*, *34*(2), 85–107. <https://doi.org/10.1080/02723646.2013.787578>
- Roth, T. R., & Nolin, A. W. (2017). Forest impacts on snow accumulation and ablation across an elevation gradient in a temperate montane environment. *Hydrol. Earth Syst. Sci*, *21*, 5427–5442. <https://doi.org/10.5194/hess-21-5427-2017>
- Rouse, J., R. Haas, J. Schell, and D. Deering. *Monitoring Vegetation Systems in the Great Plains with ERTS*. Third ERTS Symposium, NASA (1973): 309-317.
- Roussel, J.-R., Caspersen, J., B land, M., Thomas, S., & Achim, A. (2017). Removing bias from LiDAR-based estimates of canopy height: Accounting for the effects of pulse density and footprint size. *Remote Sensing of Environment*, *198*, 1–16.

<https://doi.org/10.1016/J.RSE.2017.05.032>

Runge, V., Hocking, T. D., Romano, G., Afghah, F., Fearnhead, P., & Rigai, G. (2020). *gfpop: an R Package for Univariate Graph-Constrained Change-point Detection*.

<http://arxiv.org/abs/2002.03646>

Sackett, S. S. (1980). Reducing natural ponderosa pine fuels using prescribed fire: two case studies. In *USDA Forest Service Research Note: Vol. RM-392*.

Safeeq, M., Shukla, S., Arismendi, I., Grant, G. E., Lewis, S. L., & Nolin, A. (2016). Influence of winter season climate variability on snow-precipitation ratio in the western United States. *International Journal of Climatology*, *36*(9), 3175–3190. <https://doi.org/10.1002/joc.4545>

Sankey, T., Donager, J., McVay, J., & Sankey, J. B. (2017). UAV lidar and hyperspectral fusion for forest monitoring in the southwestern USA. *Remote Sensing of Environment*, *195*, 30–43. <https://doi.org/10.1016/j.rse.2017.04.007>

Sankey, T., Donald, J., McVay, J., Ashley, M., O'Donnell, F., Lopez, S. M., & Springer, A. (2015). Multi-scale analysis of snow dynamics at the southern margin of the North American continental snow distribution. *Remote Sensing of Environment*, *169*, 307–319. <https://doi.org/10.1016/j.rse.2015.08.028>

Sankey, T. T., Leonard, J. M., & Moore, M. M. (2019). Unmanned Aerial Vehicle – Based Rangeland Monitoring: Examining a Century of Vegetation Changes. *Rangeland Ecology and Management*. <https://doi.org/10.1016/j.rama.2019.04.002>

Schultz, C. A., Jedd, T., & Beam, R. D. (2012). The Collaborative Forest Landscape Restoration

- Program: A History and Overview of the First Projects. *Journal of Forestry*, 110(7), 381–391. <https://doi.org/10.5849/jof.11-082>
- Syednasrollah, B., & Kumar, M. (2014). Net radiation in a snow-covered discontinuous forest gap for a range of gap sizes and topographic configurations. *Journal of Geophysical Research*, 119(17), 10,323-10,342. <https://doi.org/10.1002/2014JD021809>
- Shin, P., Sankey, T., Moore, M. M., & Thode, A. E. (2018). Evaluating Unmanned Aerial Vehicle Images for Estimating Forest Canopy Fuels in a Ponderosa Pine Stand. *Remote Sensing*, 10(8), 1266. <https://doi.org/10.3390/rs10081266>
- Sicart, J. E., Pomeroy, J. W., Essery, R. L. H., Hardy, J., Link, T., & Marks, D. (2004). A sensitivity study of daytime net radiation during snowmelt to forest canopy and atmospheric conditions. *Journal of Hydrometeorology*, 5(5), 774–784. [https://doi.org/10.1175/1525-7541\(2004\)005<0774:ASSODN>2.0.CO;2](https://doi.org/10.1175/1525-7541(2004)005<0774:ASSODN>2.0.CO;2)
- Simonin, K., Kolb, T. E., Montes-Helu, M., & Koch, G. W. (2007). The influence of thinning on components of stand water balance in a ponderosa pine forest stand during and after extreme drought. *Agricultural and Forest Meteorology*, 143(3–4), 266–276. <https://doi.org/10.1016/j.agrformet.2007.01.003>
- Sturm, M., Goldstein, M. A., & Parr, C. (2017). Water and life from snow: A trillion dollar science question. *Water Resources Research*, 53(5), 3534–3544. <https://doi.org/10.1002/2017WR020840>
- Udall, B., & Overpeck, J. (2017). The twenty-first century Colorado River hot drought and implications for the future. *Water Resources Research*, 53(3), 2404–2418.

<https://doi.org/10.1002/2016WR019638>

Varhola, A., Coops, N. C., Bater, C. W., Teti, P., Boon, S., & Weiler, M. (2010). The influence of ground- and lidar-derived forest structure metrics on snow accumulation and ablation in disturbed forests. *Canadian Journal of Forest Research*, 40(4), 812–821.

<https://doi.org/10.1139/X10-008>

Varhola, A., Coops, N. C., Weiler, M., & Moore, R. D. (2010). Forest canopy effects on snow accumulation and ablation: An integrative review of empirical results. In *Journal of Hydrology* (Vol. 392, Issues 3–4, pp. 219–233). Elsevier.

<https://doi.org/10.1016/j.jhydrol.2010.08.009>

Veatch, W., Brooks, P. D., Gustafson, J. R., & Molotch, N. P. (2009). “Quantifying the effects of forest canopy cover on net snow accumulation at a continental, mid-latitude site.”

Ecohydrology, 2(2), 115–128. <https://doi.org/10.1002/eco.45>

Vikhamar, D., & Solberg, R. (2003). Snow-cover mapping in forests by constrained linear spectral unmixing of MODIS data. *Remote Sensing of Environment*, 88(3), 309–323.

<https://doi.org/10.1016/j.rse.2003.06.004>

Wang, W., Huang, X., Deng, J., Xie, H., & Liang, T. (2014). Spatio-Temporal Change of Snow Cover and Its Response to Climate over the Tibetan Plateau Based on an Improved Daily Cloud-Free Snow Cover Product. *Remote Sensing*, 7(1), 169–194.

<https://doi.org/10.3390/rs70100169>

Webster, C., & Jonas, T. (2018). Influence of canopy shading and snow coverage on effective albedo in a snow-dominated evergreen needleleaf forest. *Remote Sensing of Environment*,

214, 48–58. <https://doi.org/10.1016/j.rse.2018.05.023>

White, J. C., Wulder, M. A., Vastaranta, M., Coops, N. C., Pitt, D., & Woods, M. (2013). The utility of image-based point clouds for forest inventory: A comparison with airborne laser scanning. *Forests*, 4(3), 518–536. <https://doi.org/10.3390/f4030518>

Wilcox, B. P., Newman, B. D., Brandes, D., Davenport, D. W., & Reid, K. (1997). Runoff from a semiarid Ponderosa pine hillslope in New Mexico. *Water Resources Research*, 33(10), 2301–2314. <https://doi.org/10.1029/97WR01691>

Winkler, R. D. (2011). Streamline Watershed Management Bulletin, Volume 14, Number 2. *Water Management Bulletin*, 14(2). <http://www.forrex.org/streamline>

Woodhouse, C. A., Pederson, G. T., Morino, K., McAfee, S. A., & McCabe, G. J. (2016). Increasing influence of air temperature on upper Colorado River streamflow. *Geophysical Research Letters*, 43(5), 2174–2181. <https://doi.org/10.1002/2015GL067613>

Woods, S. W., Ahl, R., Sappington, J., & McCaughey, W. (2006). Snow accumulation in thinned lodgepole pine stands, Montana, USA. *Forest Ecology and Management*, 235(1–3), 202–211. <https://doi.org/10.1016/j.foreco.2006.08.013>

Ziegler, J. P., Hoffman, C., Battaglia, M., & Mell, W. (2017). Spatially explicit measurements of forest structure and fire behavior following restoration treatments in dry forests. *Forest Ecology and Management*, 386, 1–12. <https://doi.org/10.1016/j.foreco.2016.12.002>

CHAPTER 4: Soil moisture response to seasonal drought conditions and forest structure in a thinned semi-arid forest

4.1 Abstract

Prolonged drought conditions in semi-arid forests can lead to widespread vegetation stress and mortality. However, the distribution of these effects is not spatially uniform. In this study, we use high spatial temporal resolution soil water potential time-series data to assess the effects of fore-summer drought period on the timing, magnitude, and extent of drying throughout the top 100 cm of the soil profile. Additionally, we use high-resolution terrestrial lidar measurements of forest structure to develop relationships between soil drying and fine-scale forest structure. We found that at all depths (25, 50, and 100 cm) soil drying onset occurs significantly earlier in dry years and significantly more days are observed below a critical drying threshold for ponderosa pine trees. These results were observed during two abnormally dry years. Additionally, we show that significantly drier soils are found in areas with higher stand-level basal area, canopy cover, and tree density conditions. We also show that overall drier soils were found in areas with shorter trees. Overall, our results suggest that prolonged and seasonal drought conditions can compound to create significant soil moisture deficits, and that tailored restoration thinning can be used to increase and prolong the availability of deep soil water to trees during drought using specific tree density and size parameters.

4.2 Introduction

Persistent water stress in vegetation can degrade the health and functioning of water-limited forest ecosystems (Allen et al., 2010; Porporato et al., 2001). While drought conditions are not

abnormal in water-limited forest ecosystems, climate change-driven increases in air temperature and variability in vapor pressure deficit are likely contributing to hotter and more frequent droughts as well as shifts in the average regional conditions leading to ecological drought (Bradford et al., 2020a; Breshears et al., 2005; Vicente-Serrano et al., 2010, 2013; Zhang et al., 2021). When consistent soil moisture deficits occur in the vegetation root zone, especially during the growing season, the physiological processes controlling vegetation functioning, structure, and overall health are negatively impacted (Chapin, 1991; Chapin et al., 1987; Maherali & DeLucia, 2001; Williams et al., 2001). Adverse impacts to plants can accumulate during prolonged drought conditions (Adams et al., 2009; Palmer, 1965), and are exacerbated when low soil moisture occurs simultaneously with high air temperatures (Breshears et al 2018).

Consequently, drought conditions can promote unsustainable levels of tree water stress and eventually coincide with or contribute to widespread growth declines and eventual mortality, especially in the semi-arid forests of the American Southwest (Allen et al., 2015; Clark et al., 2016; Ganey & Vojta, 2011; Koepke & Kolb, 2013; Mueller et al., 2005; Williams et al., 2010).

Spatio-temporal feedbacks drive differences in the movement and partitioning of water along the soil-vegetation-atmosphere continuum, helping determine the availability of soil moisture to vegetation across a landscape (Entekhabi et al., 1996; Guswa et al., 2002; Koster et al., 2004; Seyfried et al., 2005; Thornthwaite, 1952; van der Schrier & Barkmeijer, 2007; Wilcox et al., 2003). This high spatial and temporal variability in water cycling is enhanced in semi-arid ecosystems where high atmospheric moisture demand and infrequent, seasonally restricted precipitation contribute to lower baseline soil water levels and large fluctuations in soil moisture availability (Corradini, 2014; Loik et al., 2004). In some semi-arid ecosystems, up to 95% of annual precipitation inputs are used for vegetation transpiration and soil evaporation, with up to

one third from the top ~10 cm of the soil profile (Allen et al., 1998; Oki & Kanae, 2006; Stoy et al., 2019; Wang et al., 2014; Wei et al., 2017; Raz-Yaseef et al., 2009, 2012). In turn, these ecosystem-wide soil moisture dynamics promote variation in the spatial distribution of vegetation across the landscape (D'Odorico et al., 2007a; Quevedo Tejada Cetaqua et al., 2008; Sandvig & Phillips, 2006; Snyder & Tartowski, 2006). Additionally, spatially variable soil moisture levels can translate into patterns in vegetation water stress and mortality at the landscape-scale (400+ ha) (Andrews et al., 2020; Bales et al., 2011; Goulden & Bales, 2019).

Landscape-scale spatial variability in vegetation water stress and mortality is enhanced at the fine-scale (< 4 ha) by the distribution and orientation of forest patches, which also determines the amount of ground shading by forest canopy cover (Andrews et al., 2020; N. Raz-Yaseef et al., 2010; Teuling, 2005). In areas shaded by dense forest canopy, lower rates of soil evaporation are observed with water yield increases also found based on location-specific climatological and topographical conditions (D'Odorico et al., 2007; Duff et al., 1997; Goeking & Tarboton, 2020; Qubaja et al., 2020; Sahin & Hall, 1996; Tyagi et al., 2013). At the fine-scale and within individual forest patches, these effects are more nuanced and differences in soil moisture levels can be driven by the structure and distribution of individual trees (Breshears et al., 1997; Gray et al., 2002; Teng-Chiu Lin et al., 1992). For example, within denser forest patches with higher canopy cover, increased canopy interception and tree water uptake result in lower overall soil moisture levels. In contrast, higher soil moisture levels are often observed in less dense forest patches with lower canopy cover as well as within gaps directly adjacent to their north side (Gray et al., 2002; Raz-Yaseef, et al., 2010).

In semi-arid ponderosa pine forests of the southwestern U.S., melt water from seasonal snowpack is a primary input to soil moisture levels throughout the soil profile. As with soil moisture, the spatial distribution of seasonal snowpack is governed by the size, shape, spacing, and structure of trees and tree groups (Davis et al., 1997; Dickerson-Lange et al., 2015; Essery et al., 2003, 2008; Lawler & Link, 2011; Molotch et al., 2009; Roth & Nolin, 2017; Veatch et al., 2009; Belmonte et al., 2021). Forest stands with low or discontinuous canopy cover as well as interspaces adjacent to the north side of tree groups tend to have higher rates of snow accumulation, ablation, and persistence (Dickerson-Lange et al., 2017; Gottfried & Ffolliott, 1981; Revuelto et al., 2015). Differences in the spatial distribution of persistent snowpack are reflected in non-uniform soil water inputs during spring snowmelt (Newman et al., 2004). This effect is exacerbated by the high evapotranspiration rates during the fore-summer drought period, which significantly reduces the soil moisture levels in the upper soil horizon (< 40 cm) (Brandes & Wilcox, 2000). While the main source of water for southwestern pine forests originates from deeper in the soil profile, continued reductions in near-surface soil water inputs could interrupt recharge rates (Eggemeyer et al., 2009; Kerhoulas et al., 2013; Stahle et al., 2009). This has prompted forest managers to seriously consider the effects of landscape-scale soil water limitation and prioritize water management in forest ecosystems to reduce water stress and preserve productivity and resilience (Grant et al., 2013; Goeking & Tarboton, 2020). Quantifying the fine-scale patterns in forest-structure driven soil moisture variability can provide forest managers with actionable insight into the ecohydrological implications of thinning-based restoration practices.

Many forest ecosystems across the western United States have become overly dense and in turn increasingly vulnerable to widespread mortality from disease, drought, and catastrophic

wildfire (Fulé et al., 2004; Kolb et al., 1994; Larson & Churchill, 2012; Moore et al., 2004; Reynolds et al., 2013; Swetnam & Allen, 1999; Swetnam & Betancourt, 2010). This has prompted the scientific community, government officials, and the public to increase funding for landscape-scale forest restoration (Allen et al., 2002; Covington & Moore, 2006; Fitch et al., 2018; Fulé, 2008; Schultz et al., 2012). A central component of forest restoration includes the selective thinning of overly dense stands to help reduce the risk of catastrophic wildfire, enhance wildlife habitat, promote vegetation health, and stabilize the water balance in treated forests. While the overarching goals of restoration treatments allude to promoting ecohydrological health and resiliency, they do not specifically address how selective thinning can be used to achieve this. As more forest is designated for restoration and the effects of climate warming continue to stress these ecosystems, a better understanding of the forest structure-soil moisture variability relationship is imperative for promoting landscape-scale ecohydrological health (Bradford et al., 2020b).

Thinning treatments applied to southwestern ponderosa pine forests have been shown to increase soil water availability and in turn reducing water stress and increasing carbon uptake of the remaining forest (Dore et al., 2012; Feeney et al., 2011; Zausen et al., 2005). These results are important for assessing the effects of specific thinning treatments on landscape-scale forest vulnerability to drought-induced growth declines and mortality, however they did not directly infer soil moisture response to fine-scale forest structure differences and how this differs along the soil profile (Gleason et al., 2017). Distinguishing such nuance will help tailor future restoration efforts to ensure that thinning utilizes specific tree structure and spatial patterns, potentially benefiting ecosystem water balance and promoting resilience to climate change effects (Kerhoulas et al., 2013; Simonin et al., 2007).

Using a total of 112 soil water potential sensors, this study provides a detailed, quantitative measurement of soil moisture availability and its persistence in response to drought and forest structure conditions in a post-restoration environment. Specifically, we quantify soil moisture in the top 100 cm of the profile across a range of forest density conditions at a previously thinned restoration site over two consecutive years of 2019 and 2020, both of which experienced at or below average precipitation, providing an opportunity to evaluate critical differences in soil moisture during high-stress years (Figure 4.1).

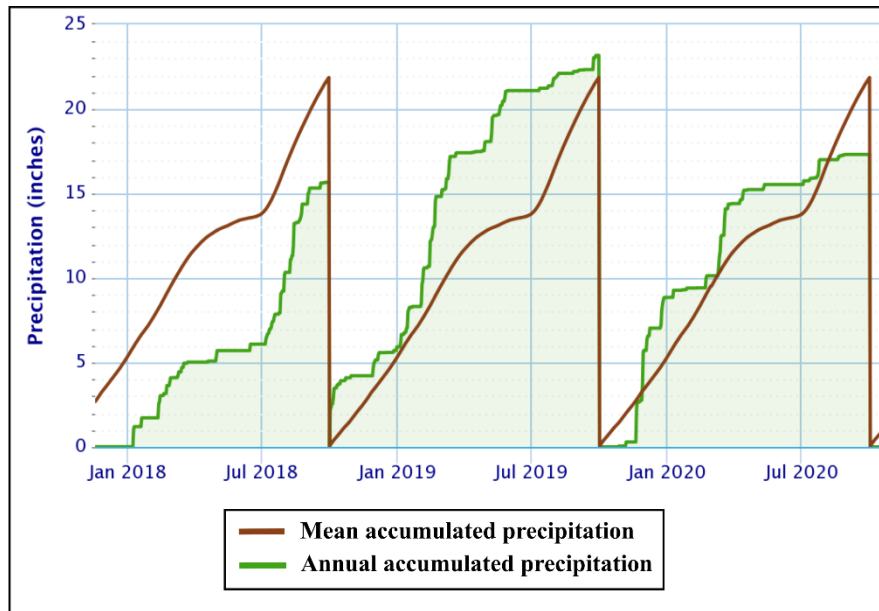


Figure 4.1: Total accumulated precipitation for Flagstaff, AZ area beginning at the start of the water year (October 1). The mean accumulated precipitation values are summarized beginning for the water year of 2000 and ending for values recorded in early 2021 (Source: NOAA).

Additionally, we assess how fine-scale forest structure components drive differences in the timing, magnitude, and amount of soil drying across soil depths during the critical drying period following spring snowmelt. In this study, this critical time of the year is termed the fore-

summer drought period and starts on April 1, ending at the onset of the North American Monsoon which usually arrives in late July. Soil moisture deficits experienced during the fore-summer drought period are believed to contribute to prolonged vegetation stress and eventual mortality (Andrews et al., 2020; Allen et al., 2015); so minimizing the magnitude of moisture deficit during this critical period will help promote broader ecosystem health and resiliency.

4.3 Materials and methods

4.3.1 Study site description

The study area is located in the Coconino National Forest about 6.5 km from the City of Flagstaff in northern Arizona, USA (12S 438346 N., 3901732 E. UTM). It includes 76 ha of forested land with flat topography (0-10% slopes) and ranges in elevation between 2,200-2,275 m above sea level with an ephemeral watercourse running towards the southwest through the site (Figure 4.2). The region has a sub-humid climate with an average of 560 mm of precipitation and is characterized by strong seasonal trends including a winter snow, early summer drought, and late-summer monsoonal seasons (<http://www.wrcc.dri.edu>). Ponderosa pine (*Pinus ponderosa*) dominates both the region's and study area's vegetation, while the study area is punctuated by occasional Gambel oak (*Quercus gambelii*) and Rocky Mountain juniper (*Juniperus scopulorum*). Arizona fescue (*Festuca arizonica*), mountain muhly (*Muhlenbergia montana*), mutton bluegrass (*Poa fendleriana*), bottlebrush squirreltail (*Sitanion hystrix*), and Buckbush (*Ceanothus fendleri*) comprise the understory vegetation, which is typical of the region's ponderosa forest. The last naturally occurring wildfire was recorded in the study area in 1876, however a prescribed fire was performed in 1976 that eliminated 63% of the smaller surface

fuels and 69% of the larger woody surface fuels (up to 8 cm in diameter) (Dieterich, 1980; Sackett, 1980).

As a part of ongoing forest restoration efforts, a mechanical thinning treatment was implemented across the study area during 2017-2018. This provided our study site with a 53-ha treated area of thinned forest adjoining a 23-ha untreated portion. The overarching goal of the restoration treatment was to reduce the risk of catastrophic wildfire by re-creating the less dense pre-settlement forest conditions and promote healthy overstory vegetation and the regeneration of understory vegetation (Allen et al., 2002). More specific treatment objectives included creating a wide size range of tree groups and interspaces, while promoting diversity in tree group shapes and their spatial arrangement across the treatment unit (Belmonte et al., 2019; Larson & Churchill, 2012; Reynolds et al., 2013). The restoration treatment for the study site prescribed creating irregular tree groups, increasing overall interspace, retaining all non-ponderosa pine species, and significantly reducing the number of smaller ponderosa pine trees site wide.

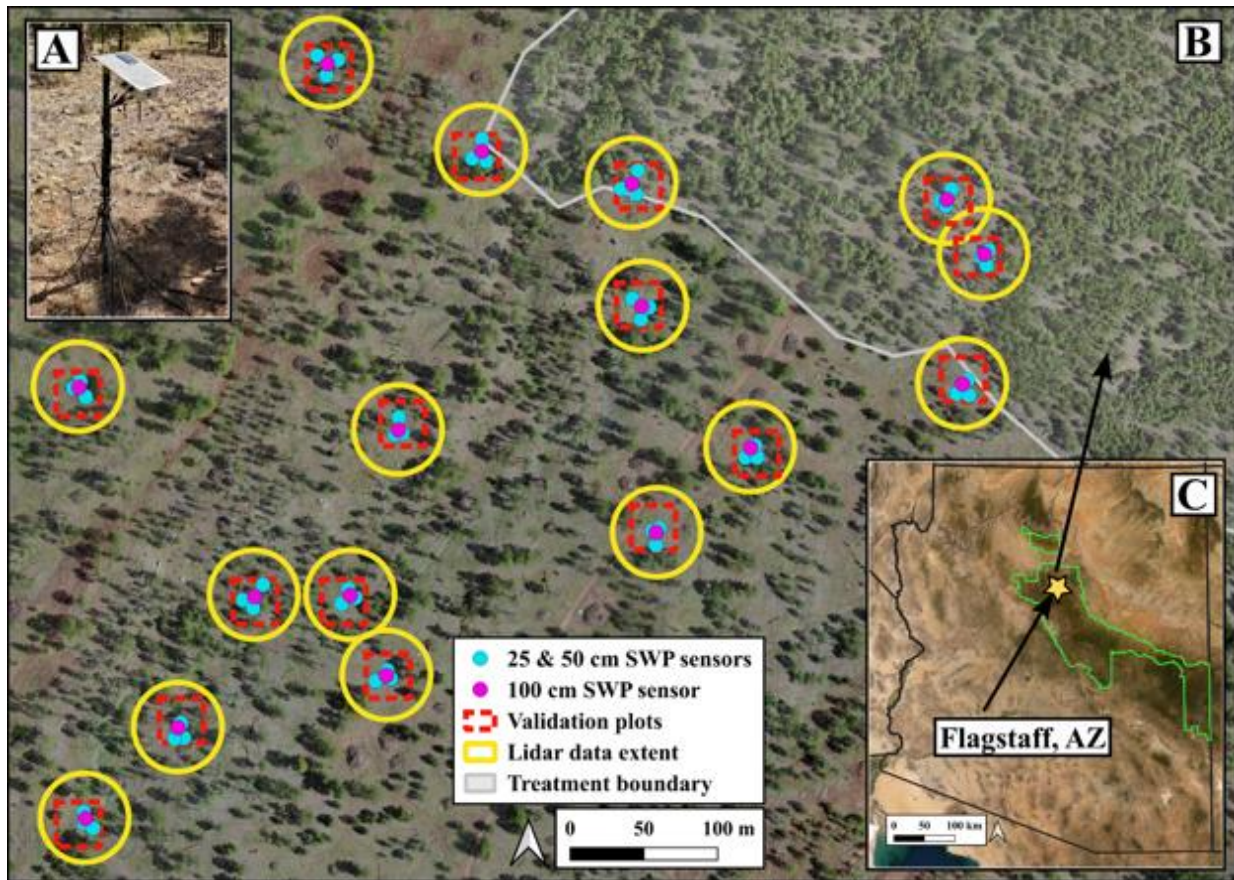


Figure 4.2: Study site map showing the location and extent of soil moisture and forest structure field data collection across the study site (Panel B), which is within the larger 4FRI forest restoration area near Flagstaff, AZ, USA (Panel C). All soil water potential sensors are connected to data loggers ($n = 16$) (Panel A) located in areas with varying forest density. Forest structure data collection was centered on each data logger, with lidar and validation datasets overlapping to facilitate accuracy assessment.

4.3.2 Soil water potential data

Soil water potential (SWP) and soil temperature (ST) were measured using an array of dielectric water potential sensors ($n = 112$) installed at the center of the forest structure data plots ($n = 16$) during the spring of 2018 (Figure 4.1). Each Meter Terros 21 (formerly Decagon MPS-6) sensor

measures soil water potential (SWP) in kilopascals (kPa) with an accuracy of 0.1 kPa and soil temperature (ST) in degrees Celsius (°C) with an accuracy of 0.1 °C (Decagon Devices, 2017). SWP values indicate the amount of pressure required to remove water from the soil. The more negative a SWP value, the more energy is required for plant roots to move water from the soil. Each plot has two co-located sensors at depths of 25 cm and 50 cm at three different locations ($n = 6$), and one additional sensor installed at depth of 100 cm (Figure 4.1). As a result, each plot has a total of seven sensors. Each sensor was programmed to record hourly measurements of both SWP and ST on a data logger located within each plot. The data from each plot was then wirelessly transmitted to a main data logger located at the center of the study site, which compiled and transmitted the data over the cellular network to an offsite database (Yamamoto et al., 2010).

The full SWP dataset consists of hourly measurements throughout the year when sensors were operational (Figure 4.3). Here, we focus on the period lasting from April 1 through the end of the fore-summer drought in each year, since this is known to be a critical time for tree water availability. In this study, the fore-summer drought is defined as the period beginning when the spring snowmelt ceases and the soil is typically near full saturation (April 1), and lasts until the onset of the North American Monsoon season, which typically occurs in the mid-late summer. At our study site, the end of the fore-summer drought period was detected in SWP data by monsoonal precipitation that ranged between 5-10 mm. This estimate is based on precipitation data from the nearest weather station, located 5.6 km to the west. Sporadic equipment malfunction during the course of data collection resulted in slightly different numbers of sensors functioning each year. To mediate this issue, each sensor was characterized by its depth and a combination of localized forest structure metrics (described in section 4.3). Each sensor's data

was analyzed to control for quality and quantity, and unrealistic values or large data gaps were thrown out entirely. The final time-series dataset consists of the average daily SWP value for each sensor throughout the fore-summer drought season (Figure 4.3).

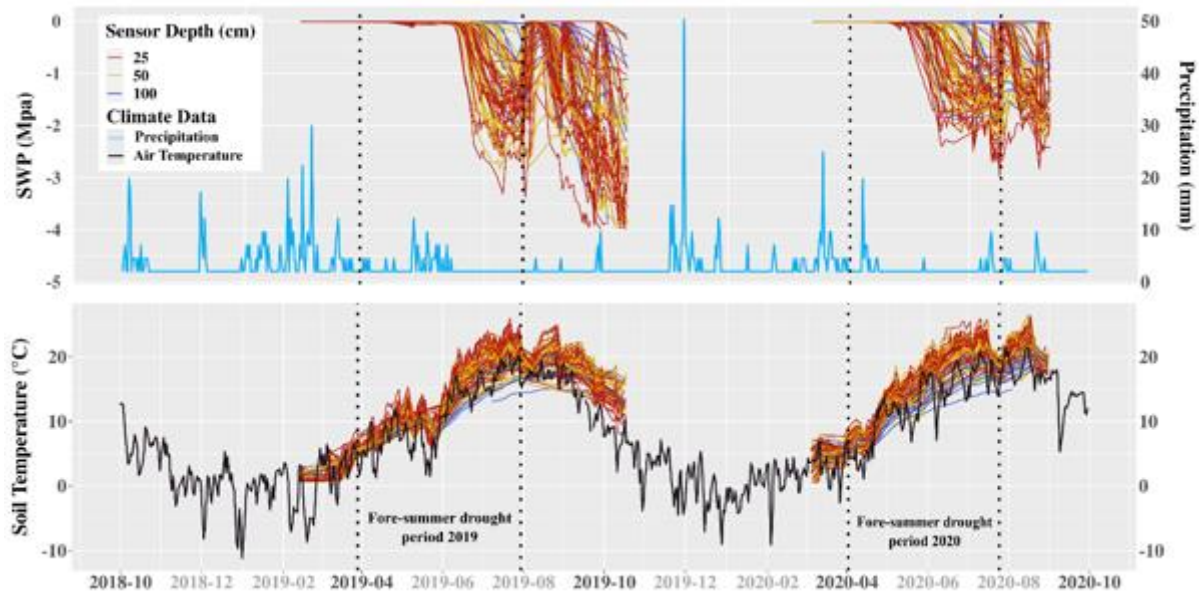


Figure 4.3: The complete soil moisture (SWP) and temperature (ST) time-series datasets for 2019 and 2020, with the respective fore-summer drought seasons depicted with dashed lines. Precipitation and air temperature data from the nearest (5.6 km away) National Oceanic and Atmospheric Administration (NOAA) climate data station (GHCND:USS0011P02S) is also shown for the full time frame. Since precipitation data are often localized during monsoonal storms, the soil moisture response recorded at the study site varies from the precipitation recorded at the NOAA station. However, it provides insight consistent with soil moisture responses as well as context for inter-annual trends. Importantly, both 2019 and 2020 precipitation totals were among the lowest on record, 77% and 59% of normal in 2019 and 2020 respectively, likely exacerbating the underlying drought conditions at the study site.

The final time-series dataset was then used to generate three different metrics, as our key response variables, that quantify: 1) the timing of soil drying, 2) magnitude of soil drying, and 3) overall moisture level at each sensor location. The first metric is termed Onset, and it is a measure of when soil moisture drying occurred after April 1. Onset corresponds to the number of days it took a sensor to begin a downward trajectory and fall below a threshold value of -0.1 MPa into a drying trend (more negative MPa values). This value is not significant to a physical property of soil drying rather it is used as a proxy for the inflection point which marks a sensor's downward path towards drying. The second metric measures the number of days below -1.0 MPa, which is a critical drying threshold (CDT) causing vegetation stress in ponderosa pine forests (Breshears et al., 1997; Feeney et al., 1998; Gaylord et al., 2007; Gyenge et al., 2002; Sala et al., 2005). The final metric is the average soil moisture or SWP value (MPa), termed meanSWP, experienced by a sensor starting from the day it crosses the Onset threshold and stopping at the end of the fore-summer drought period.

4.3.3 Forest structure metrics

Forest structure was estimated for each plot using terrestrial laser scanner (TLS) point cloud data collected from 0.28 ha plots ($n = 16$; 4.48 ha) centered on each SWP data logger (Figure 4.4). The TLS data were collected during the summer of 2019 using a Leica Geosystems BLK360 Imaging Laser Scanner (Leica Geosystems AG, 2020). Each TLS plot included three or more scans that were merged together to ensure full coverage and georeferenced with fixed reference targets on adjustable tripods at 1 m above ground. Targets were four 50 x 50 cm reflective reference panels strategically located within each plot for optimal scan-to-scan visibility (Donager et al., 2019). The location of each reference target was recorded at its center point (1 m

AGL) and corrected using the Trimble GeoXH handheld GPS unit and GPS Pathfinder Office software. TLS data post-processing was performed using CloudCompare and consisted of creating a single georeferenced point cloud for each plot. Each scan was aligned with another using the four ground target center points as common points, until all scans were merged into a single point cloud. Then, each point cloud was georeferenced using the GPS coordinates of the target; the overall X, Y, and Z positional accuracy of the point clouds ($n = 16$) is 0.46 m. Finally, the average point spacing of all point clouds was 0.03 m (ranging 0.025 – 0.046 m), and they were subsampled to 0.01 m to ensure consistent point spacing across scans.

To estimate forest structure metrics, the TLS point clouds were first post-processed and classified into ground/non-ground points, then an individual tree segmentation was performed using the Li et al. (2012) algorithm in the lidR package (Roussel et al., 2017) in RStudio (R-Studio Team, 2015). The resulting segmented point clouds were then used to estimate each tree's location (X, Y in UTM 12N m), crown height (m), and average of its widest and narrowest crown diameters (m) using the rLiDAR package in R-Studio (Mohan et al., 2017). Finally, the diameter at breast height (DBH in cm) was estimated at 1.37 m above the ground level for each segmented tree using the TreeLS package in RStudio (Conto et al., 2017). The TLS point cloud data were validated using field-based measurements taken from 137 trees located within 30x30m validation plots ($n = 16$; 1.44 ha) and were also centered at SWP data logger locations. Using the Trimble GeoXH handheld GPS unit with an attached laser range finder module, each tree's geographic position (X,Y,Z coordinates), crown height, and diameter were measured and differentially corrected in GPS Pathfinder Office. Additionally, each tree's diameter at breast height in cm was measured using a diameter tape at a height of 1.37 m above the ground level.

To assess the differences in sensor-level soil moisture related to forest structure, a set of forest structure summaries were calculated specific to each sensor's location (Figure 4.4). To accomplish this, trees were selected from each TLS point cloud within a 10m radius footprint unique to each sensor. Once the trees were selected, their crown height, diameter at breast height, and crown volume were averaged. Next, the stand basal area (m^2/ha), trees per hectare, and percent canopy cover were calculated across the 10m radius footprint. Separately, the total incoming ground-surface solar radiation (w/m^2) was calculated for the dates comprising the fore-summer drought period to quantify the effects of forest canopy shading. This was accomplished using a ray-tracing algorithm relying on the TLS point cloud data to calculate the accumulated hourly solar radiation based on the high-resolution structure of each tree (Seyednasrollah & Kumar, 2014; Seyednasrollah et al., 2013). Additionally, the total area (m^2) of persistent snow cover was calculated across the plot to quantify the potentially lingering effects of forest-structure-driven snow persistence from the winter season (Belmonte et al., 2021). This was accomplished using data from a previous UAV-image-derived time-series analysis of snow cover at the same study site (Belmonte et. al., 2021). Finally, after each sensor's forest structure metrics were calculated, each metric was categorized into three groups based on the statistical distribution of its values.

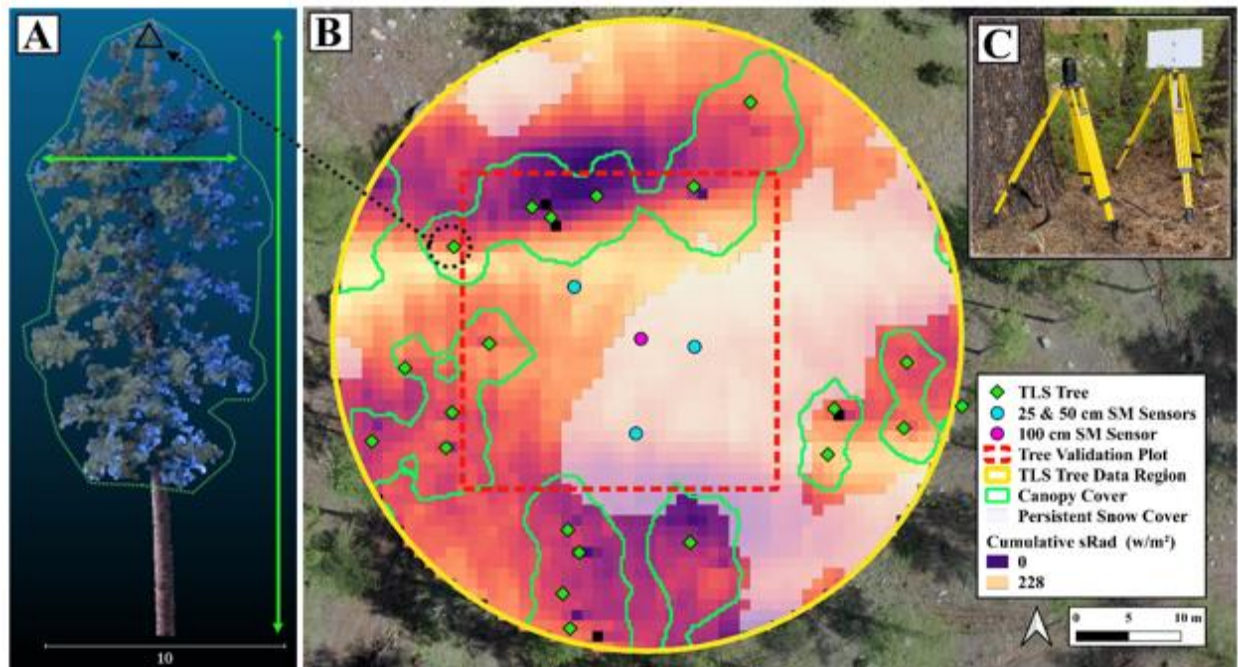


Figure 4.4: Forest structure metrics were calculated using plot-level lidar data collected at each soil moisture data logger location ($n = 16$). Additionally, validation measurements were collected in 30x30 m plots to assess the accuracy of lidar-derived forest structure estimates. Panel A depicts a segmented tree from the lidar point cloud data, while Panel B provides an illustration of all the lidar-derived forest structure metrics estimated at a single plot. Panel C shows the terrestrial laser scanner (TLS) instrument and one of the ground targets used during data collection.

4.3.4 Data analysis

Differences in the soil moisture metrics (Onset, critical drying threshold, and meanSWP) for each year (2019 and 2020), soil depth (25cm, 50cm, 100cm), and forest structure metrics (crown height, DBH, crown volume, basal area, trees per hectare, canopy cover, solar radiation, and snow cover) were assessed using a series of one-way ANOVA tests. First, differences in soil

moisture response were compared between the 2019 and 2020 fore-summer drought seasons using data from sensors across all depths. Secondly, data from both years was used to test for soil moisture differences among soil depths. Finally, data from both years was used to test for significant differences in soil moisture in response, parsed by depth, to forest structure metrics, which were grouped according to low, medium, and high conditions. Assumptions of equality in depth, year, and forest structure group-level variances and normality in residuals were tested using Bartlett's and Shapiro-Wilk tests, respectively. Additionally, inspection of group-level histograms and boxplots were used to identify any indications of non-normality. In the case of significant differences among soil depth groups, Tukey's HSD post-hoc test was performed to assess group-level differences.

4.4 Results

4.4.1 Soil moisture data summary

After April 1, the two consecutive fore-summer drought seasons spanned 120 days and 115 days in 2019 and 2020, respectively. The 2019 fore-summer drought season ended on July 30, 2019, while in 2020 it ended on July 25, 2020, with the first soil-wetting rainstorm aligning with increased SWP levels and decreases in both soil and air temperatures (Figure 4.3). The SWP measurements from the 2019 fore-summer drought season consisted of time-series data from 66 total sensors: 31 sensors at 25 cm, 26 sensors at 50 cm, and 9 sensors at 100 cm. The 2020 fore-summer drought data set included 66 total sensors: 30 sensors at 25 cm, 24 sensors at 50 cm, and 12 sensors at 100cm. Figure 4.5 illustrates the mean SWP values summarized by year and depth and includes both the onset and critical drying thresholds to illustrate the differences in these metrics by year and depth.

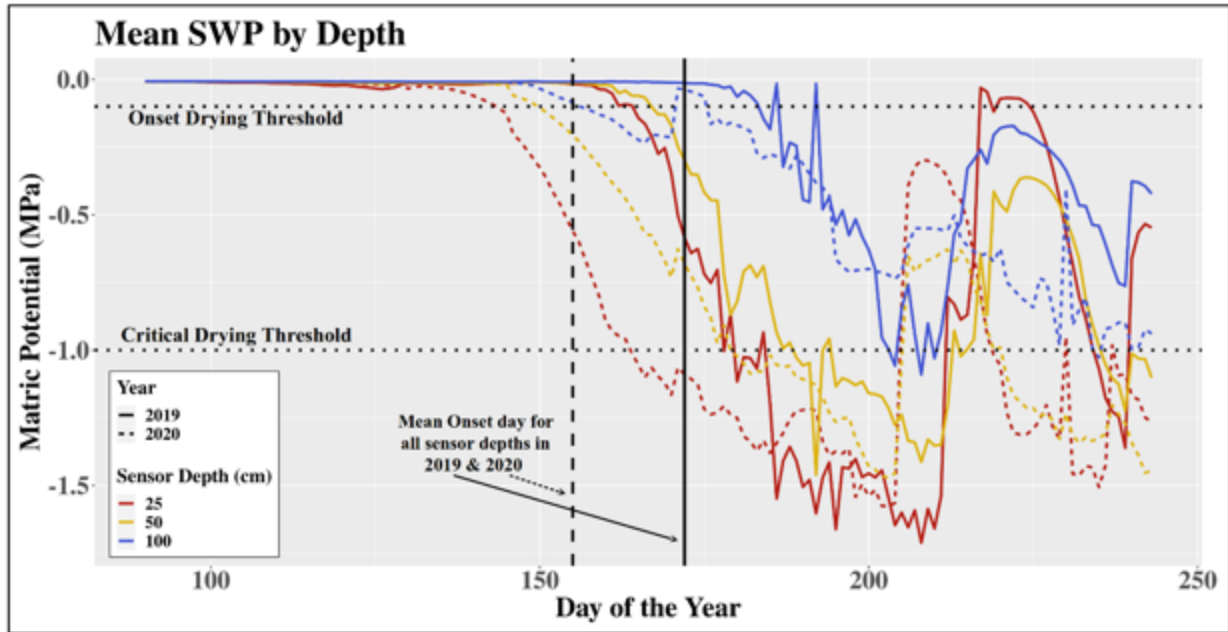


Figure 4.5: Soil moisture time-series data from 2019 and 2020 fore-summer drought seasons, with the x-axis day of year for the start of the fore-summer drought period (April 1) being day 91 and day 92 for 2019 and 2020 respectively. Each line shows the mean daily soil water potential (SWP) measurement (colored by depth) and illustrates the soil ‘drying down’ between spring snow melt (April 1) and late summer monsoon. Rain events can be observed when a curve sharply turns upward toward 0 MPa, which indicates soil becoming more saturated. The critical drying threshold (CDT) depicted at -1.0 MPa is the point at which ponderosa pine trees begin to experience moisture-related stress.

4.4.1.1 Soil moisture differences between years

Combining data from all sensors, we observed a significant difference in Onset between the 2019 (M=177.1, SD=17.8) and 2020 (M=158.2, SD=19.1) fore-summer drought seasons ($F(1,130) = 78.8, p = 4.6e^{-15}$). On average, Onset started 18.8 days ($p = 0.00$) earlier in 2020 than in 2019.

There was also a significant difference in CDT between the 2019 (M=19.6, SD=13.5) and 2020 (M=27.3, SD=19.1) fore-summer drought seasons ($F(1,130) = 10.5, p = 0.001$). On average, there were 7.7 additional days in 2020 ($p = 0.003$) spent below the CDT than in 2019. There were no significant differences in mean SWP between the 2019 and 2020 seasons.

4.4.1.2 Soil moisture differences among depths

When considering data by soil depth, there were significant differences in the Onset between sensors at 25 cm (M=157.9, SD=14.4), 50 cm (M=168.3, SD=13.8), and 100 cm (M = 194.2, SD=26.4) (Figure 4.6). Sensors at 25 cm had an Onset 10.1 days ($p = 0.0002$) and 37.7 days ($p = 0.00$) earlier than sensors at 50 and 100 cm, respectively. Sensors at 50 cm had an Onset 27.5 days ($p = 0.00$) earlier than those at 100 cm. There were significant differences in the number of days spent below the CDT between sensors at 25 cm (M=29.9, SD=15.8), 50 cm (M= 21.4, SD=15.9), and 100 cm (M=9.6, SD=12.7) (Figure 4.6). Sensors at 25 cm spent an additional 8.5 days ($p = 0.008$) and 20.9 days ($p = 0.0005$) under the critical drying threshold than sensors at 50 cm and 100 cm, respectively. Sensors at 50 cm spent an additional 12.5 days ($p = 0.004$) below the critical drying threshold than those at 100 cm. Additionally, there were significant differences in the mean SWP values between sensors at 25 cm (M= -1.1, SD= 0.37), 50 cm (M=-0.95, SD=0.44), and 100 cm (M=-0.59, SD=0.56), with sensors at 100 cm being 0.54 and 0.36 MPa wetter than those at 25 and 50 cm, respectively (Figure 4.6).

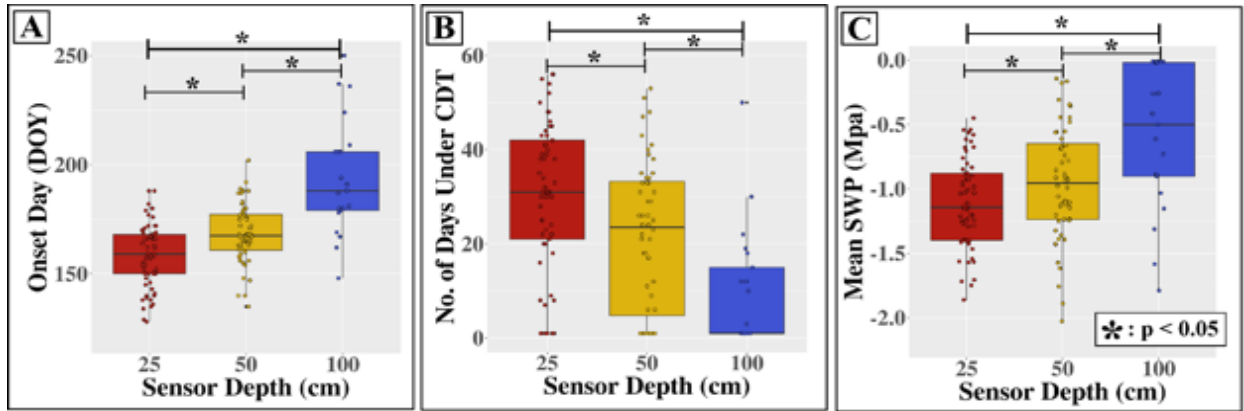


Figure 4.6: Mean differences in each soil moisture metric by depth, with Panel A showing differences for Onset Day (DOY), Panel B showing differences for the number of days spent under the CDT, and Panel C showing differences in the mean SWP (MPa). Significant were found for each depth-level comparison.

4.4.2 Forest structure - soil moisture differences

Forest structure metrics were derived using trees segmented from the lidar point cloud, which correctly identified 98% ($n = 1280$) of the trees from within the field-measured validation plots ($n = 16$ validation plots, totaling 5.17 ha). An accuracy assessment compared a subset of tree metrics between the lidar-derived and field-measured trees including tree crown height (m), crown diameter (m), DBH (cm), and geographic location (X,Y in UTM 12N m). Relationships between the lidar-derived and field-measured trees were generally strong, with a $R^2 = 0.95$ for tree crown height. A full summary of the accuracy assessment process and forest structure metric relationships are reported in Belmonte et al., 2021. Forest structure summaries were then calculated specific to each SWP sensor location. Figure 4.7 illustrates how forest structure was distributed throughout the entire sensor collection.

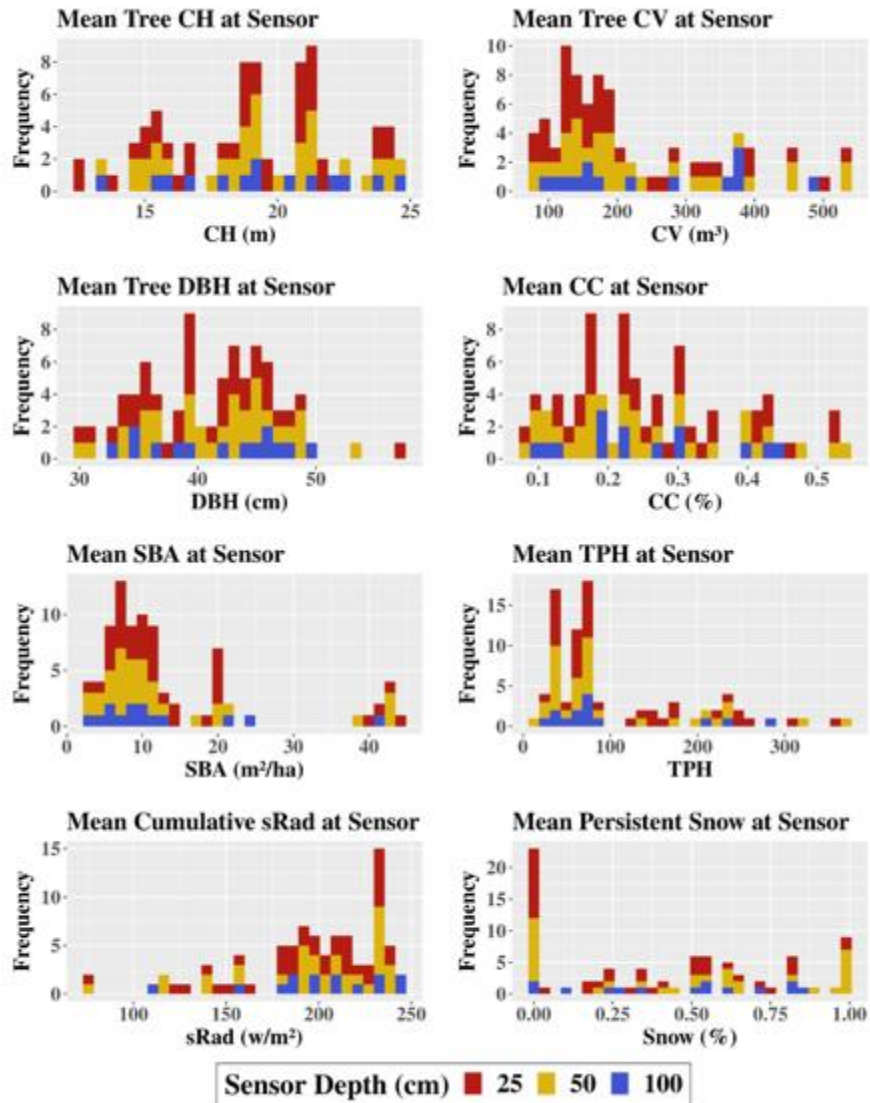


Figure 4.7: Histograms of the forest structure metric summaries calculated at each sensor location ($n = 84$), with sensor depths differentiated by color. Key indicators of the post-treatment forest structure are apparent in the distributions of mean canopy cover (CC), basal area (SBA), and trees per hectare (TPH), all of which reflect the overall lower forest density conditions across the study site compared to the conditions observed prior to the restoration thinning project (Belmonte et al., 2019).

When considering the Onset day for sensors at 25 cm, there were significant differences related to tree crown height ($F(2,57) = 6.8, p = 0.002$), diameter at breast height ($F(2,57) = 2.9, p = 0.05$), solar radiation ($F(2,57) = 7.8, p = 0.0009$), basal area ($F(2,57) = 11.6, p = 0.0006$), trees per hectare ($F(2,57) = 11.5, p = 0.0008$), and canopy cover ($F(2,57) = 22.1, p = 9.77e-06$), with significant group-level differences present for crown height, basal area, trees per hectare, and canopy cover (Table 4.1). For sensors at 50 cm, there were significant differences in Onset day related to tree crown height ($F(2,48) = 15.8, p = 5.89e-06$), basal area ($F(2,48) = 23.1, p = 4.72e-05$), trees per hectare ($F(2,48) = 13.8, p = 0.0005$), snow cover ($F(2,48) = 4.7, p = 0.01$), and canopy cover ($F(2,46) = 7.3, p = 0.001$), with significant group-level differences in tree crown height, basal area, trees per hectare, and canopy cover (Table 4.1). There were no significant differences in Onset day for sensors at 100 cm due to forest structure.

When considering the number of critical drying threshold for sensors at 25 cm, there were significant differences related to tree crown height ($F(2,57) = 9.6, p = 0.002$), diameter at breast height ($F(2,57) = 5.4, p = 0.006$), and canopy cover ($F(2,57) = 7.5, p = 0.0013$), with significant differences among groups within tree crown height and diameter at breast height (Table R1). For sensors at 50 cm, there were significant differences related to tree crown height ($F(2,46) = 17.9, p = 1.5e-06$), snow cover ($F(2,46) = 10.4, p = 0.0001$), and basal area ($F(2,46) = 14.9, p = 8.7e-06$), with significant differences among tree crown height and snow cover groups (Table 4.1). Again, there were no significant differences in the number of CDT days related to FS in sensors at 100 cm.

Finally, when considering the mean SWP values, sensors at 25 cm had significant differences related to tree crown height ($F(2,57) = 3.9, p = 0.001$) and diameter at breast height

($F(2,57) = 4.5, p = 0.01$) (Table 4.1). For sensors at 50 cm, the significant differences in mean SWP values were related to tree crown height ($F(2,46) = 7.3, p = 0.001$) and basal area ($F(2,46) = 4.5, p = 0.01$), with significant differences among groups for tree crown height and basal area (Table 4.1). For sensors at 100 cm there were no significant differences in mean SWP values.

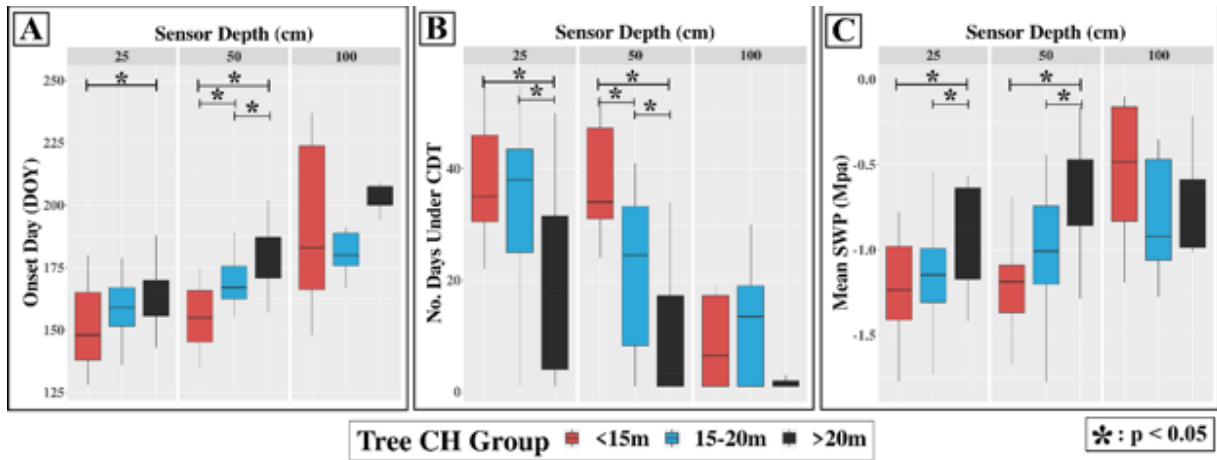


Figure 4.8: Differences in Onset day (Panel A), number of critical drying threshold days (Panel B), and mean SWP (Panel C) related to tree crown height (CH). Significant Tukey’s pairwise comparisons are shown by the starred bars. Mean tree crown height was the most prevalent predictor of soil moisture metric differences across all sensor depths.

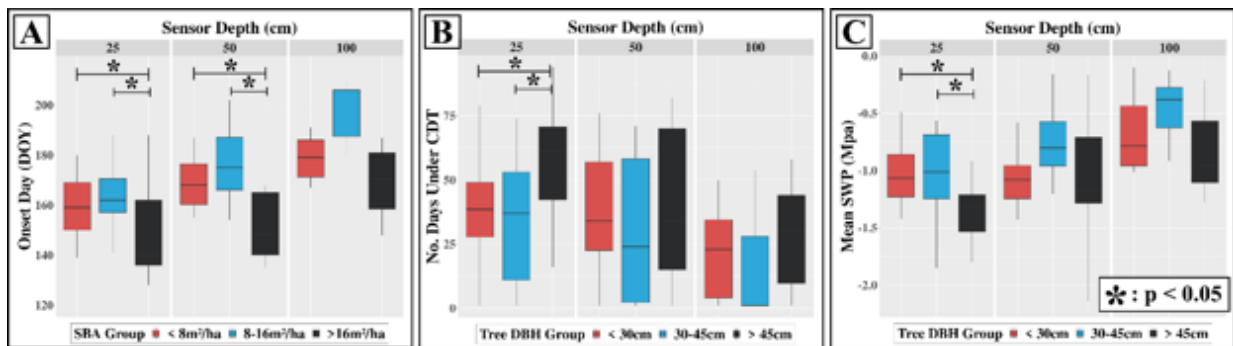


Figure 4.9: Notable forest structure-driven differences in each soil moisture metric. For Onset day (Panel A), basal area (BA) had significant pairwise differences for sensors at 25 & 50 cm,

with higher BA translating to significantly earlier drying Onset day. Additionally, there were significant pairwise differences in tree diameter at breast height related to the number of critical drying threshold days (Panel B) and mean SWP (Panel C) for sensors at 25 cm. Here, trees with larger diameter at breast height contributed to more days spent under the threshold and lower (drier) overall SWP values.

Table 4.1: Summary of the significant Tukey’s post-hoc group-level comparisons for the combinations of SM and FS metrics parsed by sensor depth. Forest metric group value ranges are as follows: tree crown height (CH), short (< 15 m), medium (15—20 m), tall (> 20 m); diameter at breast height (DBH) small (< 30 cm), medium (30—45 cm), large (> 45cm); basal area (BA) low (< 8 m²/ha), medium (8—16 m²/ha), high (> 16 m²/ha); trees per hectare (TPH) low (< 60), medium (60—130), high (> 130); canopy cover (CC) low (< 15%), medium (15—30%), high (> 30%), solar radiation (sRad) low (< 180 w/m²), medium (180—220 w/m²), high (> 220 w/m²); snow cover (SC) low (< 25%), medium (25—60%), high (> 60%).

SM Metric	Sensor Depth	FS Metric	Tukeys Post-hoc Comparisons	Mean Difference (p < 0.05)
Onset Day	25 cm	CH	tall vs. short trees	+13.2 days
		BA	high vs. low density	-10.5 days
			high vs. medium density	-14.9 days
		TPH	high vs. medium density	-12.2 days
		CC	high vs. medium cover	-15.5 days
	50 cm	CH	medium vs. short trees	+13.6 days
			tall trees vs. short trees	+23.6 days
			tall trees vs. medium trees	+10.1 days

		BA	high vs. low density	-12.6 days	
			high vs. medium density	-18.6 days	
		TPH	high vs. low density	-14.5 days	
			high vs. medium density	-13.8 days	
		CC	high vs. medium cover	-12.7 days	
CDT Days	25 cm	CH	tall vs. short trees	-19.2 days	
			tall vs. medium trees	-14.6 days	
		DBH	large vs. small trees	+11.3 days	
			large vs. medium trees	+15.8 days	
		50 cm	CH	tall vs. short trees	-28.7 days
	tall vs. medium trees			-11.7 days	
	medium vs. short trees			-17.1 days	
	BA		high vs. low density	+12.9 days	
			high vs. medium density	+26.3 days	
	TPH	high vs. low density	+18.1 days		
high vs. medium density		+17.7 days			
		CC	high vs. medium cover	+16.9 days	
		SC	medium vs. low snow	+19.8 days	
			high vs. low snow	+15.1 days	
Mean SWP	25 cm	CH	tall trees vs. short trees	+0.33 Mpa	
			tall trees vs. medium trees	+0.29 Mpa	
		DBH	large vs. small trees	-0.29 Mpa	
			large vs. medium trees	-0.28 Mpa	
		sRad	high vs. low exposure	-0.28 Mpa	
	high vs. med exposure		-0.44 Mpa		
			CC	medium vs. low cover	+0.36 Mpa
	50 cm	CH	tall vs. short trees	+0.59 Mpa	
			tall vs. medium trees	+0.41 Mpa	

BA	medium vs. low density	+0.41 Mpa
SC	medium vs. low snow	-0.52 Mpa
	high vs. low snow	-0.69 Mpa

4.5 Discussion

In this study, we assess soil drying during two consecutive fore-summer drought periods in the midst of regional multi-year drought (Chikamoto et al., 2017). We also examine relationships between soil moisture and forest structure to improve our understanding of local-scale soil moisture variability. Our results show three important relationships between fine-scale patterns in soil drying and post-thinning forest structure: significant differences in drying trends between two fore-summer drought seasons, significant differences in soil drying trends across soil depths, and significant differences in soil drying based on forest structure conditions (section 4.4.2). The timing, magnitude, and amount of soil drying are critical to assessing the severity of seasonal drought and provide context for the impacts of multi-year drought. We measured soil water potential (SWP) across 53 ha of thinned and 23 ha of unthinned forest with a network of SWP sensors installed along the top 100 cm of the soil profile. Our results highlight important trends in soil moisture response to fore-summer drought conditions, which we discuss below. In doing so, our findings provide insight into the potential impacts that landscape-scale restoration can have on soil moisture persistence during the region’s driest period of the year.

4.5.1 Multi-year drought impact

There was below average precipitation (77% and 59% of normal, in 2019 and 2020 respectively) in both water years preceding each fore-summer drought period, although the length of the fore-

summer drought periods was roughly equal in 2019 and 2020 (120 vs. 115 days, respectively). These notably dry conditions provided an excellent opportunity to study both the general response of SWP to limited water resources as well as to forest structure because it provided a clear overall drying signal. We first show that soil drying behavior was significantly different between the fore-summer drought seasons of 2019 and 2020 despite no significant differences in overall measured SWP levels and length of fore-summer drought period. This is reflected in both the timing of soil drying Onset, which occurred ~19 days earlier in 2020 than in 2019, as well as ~8 more days spent below the critical drying threshold (CDT) in 2020 than in 2019. The below average precipitation in 2019 and its continued trend likely set the stage for the significantly lower soil moisture observed in 2020. Additionally, after the 2019 fore-summer drought period, a further soil drying trend was observed with many sensors recording SWP values below the critical drying threshold of -1.0 MPa (Figure 4.3). Interestingly, the non-significant difference in overall mean SWP values between the fore-summer drought periods in the two years hints at an underlying and consistently low soil moisture availability when considering the entire soil profile. Continued multi-year meteorological drought conditions can exacerbate soil drying in the deeper and more stable portions of the soil profile, increasing the likelihood for tree mortality from prolonged soil moisture deficits (Breshears et al., 2018; Fettig et al., 2019; Goulden & Bales, 2019).

Next, we show that differences in soil moisture metrics among soil depths occur regardless of year and forest density conditions (Figure 4.5). More specifically and consistent with previous studies (Breshears et al., 1997; Goulden & Bales, 2019), soil moisture measurements from shallower sensors exhibited significantly earlier soil drying Onset, more days spent below the CDT, and lower mean SWP values compared to the deeper sensors (Figure

4.6). Our results underscore overall wetter conditions and greater resistance to drying occurred at increasing soil depth and this was consistent despite the ongoing meteorological drought conditions and differences in forest structure. This is shown in the overall significantly wetter conditions in sensors at 100 cm; some of those sensors never entered a drying phase or spent time under the CDT. Consistently, previous research showed that soil drying occurs more rapidly and completely at and near the surface due to increased exposure to solar radiation and the greater density of roots (Capehart & Carlson, 1997; Huang et al., 2018; Martinez et al., 2008). This was observed in nearly all of the sensors at 25 cm having an early Onset drying date, spending more time below the CDT, and exhibiting more complete drying overall (Figure 4.3). Importantly, we show that the sensors at 50 cm can reflect both the extreme drying trends observed in sensors at 25 cm as well as the underlying stability characteristic in sensors at 100 cm. Given the multi-year drought conditions experienced during both fore-summer drought periods, these effects were likely exacerbated by the range in forest structure and density conditions present across the study site from the previously implemented restoration thinning project (Belmonte et al., 2020).

4.5.2 Forest structure effects

Our results show soil moisture at a local scale was significantly and consistently impacted by five specific forest structure metrics: mean tree crown height, mean tree diameter at breast height, basal area, canopy cover, and trees per hectare. Importantly, all the effects of forest structure on soil moisture metrics were observed at 25 and 50 cm, with no significant effects related to soil moisture flux at 100 cm. At both 25 and 50 cm, the forest structure metrics related to density conditions (basal area, canopy cover, and trees per hectare) appeared most frequently

as significant variables influencing soil moisture flux (Table 4.1). Higher levels of basal area, canopy cover, and trees per hectare all translated to an earlier onset of soil drying and more days spent below the CDT at 25 and 50 cm, while the effects on mean SWP values were more nuanced. Interestingly, higher basal area and canopy cover values translated to wetter mean SWP levels at shallow sensors. However, these significant differences were related to only ‘medium’ and ‘low’ categories and can possibly be explained by conditions in the medium basal area and canopy cover groups providing just enough shading to harbor shallower soil moisture content. While the soil moisture response at 100 cm did not show significant effects related to forest structure metrics, there were clear trends similar to those at 25 and 50 cm. However, these trends were observed towards the most extreme ends of the forest density gradient, where less dense forest exhibited wetter overall soil conditions than denser forest (Figure 4.10). Additionally, the higher average tree crown height values also translated to overall wetter soil moisture conditions at 100 cm. This hints at the potential for managing deeper soil moisture via restoration thinning practices.

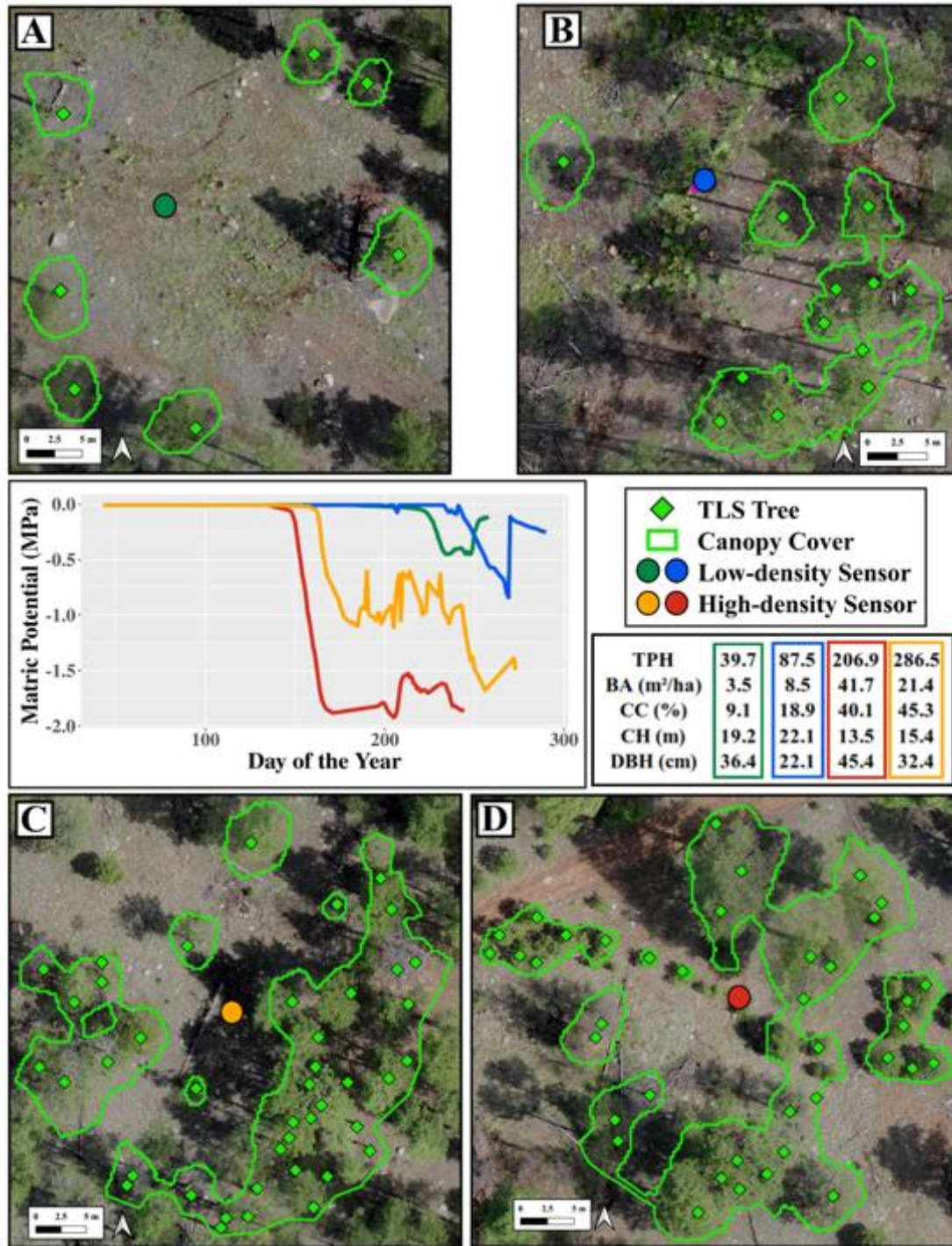


Figure 4.10: Illustration of four different 100 cm soil matrix potential (MPa) time-series data, two from the plots with the lowest forest density conditions (panels A and B) and two from the highest forest density conditions (panels B and C). Soil matrix potential data (middle panel) was

averaged across both fore-summer drought seasons for each sensor to illustrate the soil moisture response at that location. Trees per hectare (TPH), basal area (BA), canopy cover (CC), average tree crown height (CH), and average diameter at breast height (DBH) were summarized across the 20 m radius area centered on each sensor.

Tree crown height is the one metric related to individual tree structure that consistently influenced soil moisture response. Specifically, sensors near taller trees had a later onset of soil drying, spent less days below the CDT, and had wetter overall soil moisture levels (Table 4.1). Taller trees have larger shadow footprints, and thus provide more ground shading during the fore-summer drought period. This suggests an important benefit to soil moisture persistence from ‘strategic’ ground shading. This not only reinforces the complex relationships between soil moisture and forest / tree structure, but also the potential in tailoring restoration thinning to promote soil moisture persistence.

Persistent snow cover levels also had a significant effect on soil moisture response at 50 cm, with more days below the CDT and overall lower mean SWP levels at locations with higher amounts of persistent snow cover throughout the winter season. Counter intuitively, this points to overall drier soil conditions in locations with greater amounts of persistent snow. Our previous observations at this study site show that the primary drivers of persistent snow cover during the winter months were associated with moderate levels of forest density (Belmonte et al., 2021). While this overlaps with our current findings related to soil moisture levels, we found no direct linkages between persistent snow cover and soil moisture via specific forest structure conditions. Instead, our results point to a disconnection between forest-structure-driven trends observed in persistent snow cover during the winter months and those observed in soil drying during the

fore-summer drought period. This underscores an important knowledge gap related to the temporal scale of ecosystem moisture inputs as well as the larger ecohydrological impacts felt by forest structure. Addressing this gap will be vital to enable forest management for moisture regardless of the season.

4.5.3 Management implications

Forest managers will increasingly need to address the nexus of ecosystem water inputs and forest structure as restoration thinning projects continue to be implemented across the dry forests of the western United States and regional climates trend toward hotter and drier conditions. Our results suggest that managers can target soil moisture levels at 50 cm to most effectively impact and monitor forest ecohydrological cycles. Soil drying at 25 cm was rapid and highly variable in response to weather and forest structure conditions, ultimately shedding little insight into the soil moisture trends deeper in the profile. However, soil moisture in sensors at 50 cm reflected both more stability yet also significant responsiveness to forest structure conditions. Our results indicate that forest managers can continue to implement restoration prescriptions focused on density reductions and anticipate less severe soil drying at 50 cm after restoration treatments (Table 4.1). Continued monitoring of soil moisture levels at 50 cm can also shed light on the effects of multi-year drought conditions as well as the anticipated effects on soil drying deeper into the soil profile.

The lack of significant forest structure effects in sensors at 100 cm underscores our finding that wetter and more stable conditions occur deeper into the soil profile. However, further assessment into the forest structure-driven soil moisture differences in 100 cm sensors reveals nuanced but similar forest density-related patterns as were observed in the shallow 25

and 50 cm sensors. Subsetting soil moisture data from sensors in the highest forest density ($n = 2$) and the lowest forest density ($n = 2$) conditions, we show that there are notable differences in soil drying patterns (Figure 4.10). Specifically, sensors at 100 cm in the highest density forest conditions have an earlier soil drying onset, spend more time under the CDT, and appear drier overall than sensors in the lowest density conditions. Similar to shallower sensors, we assume that the factors contributing to the drier conditions in denser forest include greater rates of snow interception by canopy as well as increased water usage and transpiration rates from the greater number of trees. Importantly, these patterns are observed at opposing ends of the forest-density gradient present at our study site, which reflect heavily thinned and overly-dense unthinned forest. While we did not find statistically significant differences among these 100 cm sensors given the limited sample size ($n = 2$ for each end), our results clearly indicate that there is an optimum forest structure that land managers can target to achieve. Our results suggest that this optimum might be found at approximately 30% canopy cover and < 100 trees per hectare. Together, these observed trends emphasize the potential benefits of thinning-based restoration on moderating soil drying deep into the soil profile while also pointing to critical unknowns as multi-year drought conditions persist and significant soil drying pushes deeper into the profile.

4.6 Conclusions

We assessed soil moisture response to seasonal drought conditions as well as the impacts of forest structure changes across a thinned semi-arid forest. Using dense soil water potential time-series data from the top 100 cm of the soil profile, we found significant differences in the timing, magnitude, and overall soil moisture levels across different seasonal drought periods among soil depths and resulting from forest structure conditions. We observed nearly complete drying at all

25 cm locations, a mixture of drying conditions at 50 cm, and a general resistance to drying at 100 cm. Additionally, we found that lower forest density and taller trees were associated with overall wetter soil moisture conditions in soils up to 50 cm deep. Taken together, this reinforces the notion of resilience to deep soil drying in semi-arid forests while also suggesting that this resilience can be fostered with substantial reductions in forest density. Therefore, we recommend that forest restoration practitioners interested in promoting soil moisture stability focus on continued density reductions and monitoring soil moisture response at 50 cm. A better understanding of these relationships is important given that the continued multi-year drought conditions are likely and the prospect of drying trends translating deeper into the soil profile is strong as drought persists. Future research should untangle the complex relationships between deeper soil moisture and fine-scale forest density and structure. In particular, it should focus on the soil moisture response to the spatial and directional arrangement of trees as well as the size and structural composition of their canopies. This information can help to inform highly effective forest thinning plans that aim to both reduce density and maximize the positive impacts of tree canopy shading and size on soil moisture.

4.7 References

- Adams, H. D., Guardiola-Claramonte, M., Barron-Gafford, G. A., Villegas, J. C., Breshears, D. D., Zou, C. B., Troch, P. A., & Huxman, T. E. (2009). Temperature sensitivity of drought-induced tree mortality portends increased regional die-off under global-change-type drought. *Proceedings of the National Academy of Sciences of the United States of America*, *106*(17), 7063–7066. <https://doi.org/10.1073/pnas.0901438106>
- Allen, C. D., Breshears, D. D., & McDowell, N. G. (2015). On underestimation of global vulnerability to tree mortality and forest die-off from hotter drought in the Anthropocene. *Ecosphere*, *6*(8), 1–55. <https://doi.org/10.1890/ES15-00203.1>
- Allen, C. D., Savage, M., Falk, D. A., Suckling, K. F., Swetnam, T. W., Schulke, T., Stacey, P. B., Morgan, P., Hoffman, M., & Klingel, J. T. (2002). Ecological Restoration of Southwestern Ponderosa Pine Ecosystems: A Broad Perspective. *Ecological Applications*, *12*(5), 1418–1433. [https://doi.org/10.1890/1051-0761\(2002\)012\[1418:EROSPP\]2.0.CO;2](https://doi.org/10.1890/1051-0761(2002)012[1418:EROSPP]2.0.CO;2)
- Allen, R. G., Pereira, L. S., Raes, D., & Smith, M. (1998). *Crop evapotranspiration-Guidelines for computing crop water requirements-FAO irrigation and drainage paper 56*. [https://doi.org/ISBN 92-5-104219-5](https://doi.org/ISBN%2092-5-104219-5)
- Anderegg, W. R. L., Schwalm, C., Biondi, F., Camarero, J. J., Koch, G., Litvak, M., Ogle, K., Shaw, J. D., Shevliakova, E., Williams, A. P., Wolf, A., Ziacco, E., & Pacala, S. (2015). Pervasive drought legacies in forest ecosystems and their implications for carbon cycle models. *Science*, *349*(6247), 528–532. <https://doi.org/10.1126/science.aab1833>
- Andrews, C. M., D'Amato, A. W., Fraver, S., Palik, B., Battaglia, M. A., & Bradford, J. B.

- (2020). Low stand density moderates growth declines during hot-droughts in semi-arid forests. *Journal of Applied Ecology*, September 2019, 1–14. <https://doi.org/10.1111/1365-2664.13615>
- Belmonte, A., Sankey, T., Biederman, J. A., Bradford, J., Goetz, S. J., Kolb, T., & Woolley, T. (2019). UAV-derived estimates of forest structure to inform ponderosa pine forest restoration. *Remote Sensing in Ecology and Conservation*, rse2.137. <https://doi.org/10.1002/rse2.137>
- Belmonte, A., Sankey, T., Biederman, J., Bradford, J., Goetz, S., & Kolb, T. (2021). UAV-Based Estimate of Snow Cover Dynamics: Optimizing Semi-Arid Forest Structure for Snow Persistence. *Remote Sensing*, 13(5). <https://doi.org/10.3390/rs13051036>
- Bradford, J. B., Andrews, C. M., Robles, M. D., McCauley, L. A., Woolley, T. J., & Marshall, R. M. (2021). Landscape-scale restoration minimizes tree growth vulnerability to 21st century drought in a dry forest. *Ecological Applications*, 31(2), e2238. <https://doi.org/https://doi.org/10.1002/eap.2238>
- Bradford, J. B., Schlaepfer, D. R., Lauenroth, W. K., & Palmquist, K. A. (2020). Robust ecological drought projections for drylands in the 21st century. *Global Change Biology*, 26(7), 3906–3919. <https://doi.org/https://doi.org/10.1111/gcb.15075>
- Brandes, D., & Wilcox, B. P. (2000). Evapotranspiration and soil moisture dynamics on a semiarid ponderosa pine hillslope. *Journal of the American Water Resources Association*, 36(5), 965–974. <https://doi.org/10.1111/j.1752-1688.2000.tb05702.x>

- Breshears, D. D., Carroll, C. J. W., Redmond, M. D., Wion, A. P., Allen, C. D., Cobb, N. S., Meneses, N., Field, J. P., Wilson, L. A., Law, D. J., McCabe, L. M., & Newell-Bauer, O. (2018). A Dirty Dozen Ways to Die: Metrics and Modifiers of Mortality Driven by Drought and Warming for a Tree Species. *Frontiers in Forests and Global Change*, 1, 4. <https://doi.org/10.3389/ffgc.2018.00004>
- Breshears, D. D., Cobb, N. S., Rich, P. M., Price, K. P., Allen, C. D., Balice, R. G., Romme, W. H., Kastens, J. H., Floyd, M. L., Belnap, J., Anderson, J. J., Myers, O. B., & Meyer, C. W. (2005). Regional vegetation die-off in response to global-change-type drought. *Proceedings of the National Academy of Sciences of the United States of America*, 102(42), 15144–15148. <https://doi.org/10.1073/pnas.0505734102>
- Breshears, D. D., Rich, P. M., Barnes, F. J., & Campbell, K. (1997). Overstory-imposed heterogeneity in solar radiation and soil moisture in a semiarid woodland. *Ecological Applications*, 7(4), 1201–1215. [https://doi.org/10.1890/1051-0761\(1997\)007\[1201:OIHISR\]2.0.CO;2](https://doi.org/10.1890/1051-0761(1997)007[1201:OIHISR]2.0.CO;2)
- Capehart, W. J., & Carlson, T. N. (1997). Decoupling of surface and near-surface soil water content: A remote sensing perspective. *Water Resources Research*, 33(6), 1383–1395. <https://doi.org/https://doi.org/10.1029/97WR00617>
- Chapin, F. S. (1991). Integrated Responses of Plants to Stress. *BioScience*, 41(1), 29–36. <https://doi.org/10.2307/1311538>
- Chapin, F. S., Bloom, A. J., Field, C. B., & Waring, R. H. (1987). Plant Responses to Multiple Environmental Factors. *BioScience*, 37(1), 49–57. <https://doi.org/10.2307/1310177>

- Chikamoto, Y., Timmermann, A., Widlansky, M. J., Balmaseda, M. A., & Stott, L. (2017). Multi-year predictability of climate, drought, and wildfire in southwestern North America. *Scientific Reports*, 7(1), 6568. <https://doi.org/10.1038/s41598-017-06869-7>
- Clark, J. S., Iverson, L., Woodall, C. W., Allen, C. D., Bell, D. M., Bragg, D. C., D'Amato, A. W., Davis, F. W., Hersh, M. H., Ibanez, I., Jackson, S. T., Matthews, S., Pederson, N., Peters, M., Schwartz, M. W., Waring, K. M., & Zimmermann, N. E. (2016). The impacts of increasing drought on forest dynamics, structure, and biodiversity in the United States. *Global Change Biology*, 22(7), 2329–2352. <https://doi.org/10.1111/gcb.13160>
- Corradini, C. (2014). Soil moisture in the development of hydrological processes and its determination at different spatial scales. In *Journal of Hydrology* (Vol. 516, pp. 1–5). Elsevier. <https://doi.org/10.1016/j.jhydrol.2014.02.051>
- Covington, W. W., & Moore, M. M. (2006). Postsettlement Changes in Natural Fire Regimes and Forest Structure. *Journal of Sustainable Forestry*, 2(1–2), 153–181. https://doi.org/10.1300/j091v02n01_07
- D'Odorico, P., Caylor, K., Okin, G. S., & Scanlon, T. M. (2007). On soil moisture-vegetation feedbacks and their possible effects on the dynamics of dryland ecosystems. *Journal of Geophysical Research: Biogeosciences*, 112(4), n/a-n/a. <https://doi.org/10.1029/2006JG000379>
- Davis, R. E., Hardy, J. P., Ni, W., Woodcock, C., McKenzie, J. C., Jordan, R., & Li, X. (1997). Variation of snow cover ablation in the boreal forest: A sensitivity study on the effects of conifer canopy. *Journal of Geophysical Research Atmospheres*, 102(24), 29389–29395.

<https://doi.org/10.1029/97jd01335>

de Conto, T., Olofsson, K., Görgens, E. B., Rodriguez, L. C. E., & Almeida, G. (2017).

Performance of stem denoising and stem modelling algorithms on single tree point clouds from terrestrial laser scanning. *Computers and Electronics in Agriculture*, *143*, 165–176.

<https://doi.org/10.1016/j.compag.2017.10.019>

Dickerson-Lange, S. E., Gersonde, R. F., Hubbart, J. A., Link, T. E., Nolin, A. W., Perry, G. H.,

Roth, T. R., Wayand, N. E., & Lundquist, J. D. (2017). Snow disappearance timing is dominated by forest effects on snow accumulation in warm winter climates of the Pacific Northwest, United States. *Hydrological Processes*, *31*(10), 1846–1862.

<https://doi.org/10.1002/hyp.11144>

Dickerson-Lange, S. E., Lutz, J. A., Martin, K. A., Raleigh, M. S., Gersonde, R., & Lundquist, J.

D. (2015). Evaluating observational methods to quantify snow duration under diverse forest canopies. *Water Resources Research*, *51*(2), 1203–1224.

<https://doi.org/10.1002/2014WR015744>

Dieterich, J. H. (1980). Chimney Spring forest fire history. In *Chimney Spring forest fire history*.

<https://doi.org/10.5962/bhl.title.98633>

Dore, S., Montes-Helu, M., Hart, S. C., Hungate, B. A., Koch, G. W., Moon, J. B., Finkral, A. J.,

& Kolb, T. E. (2012). Recovery of ponderosa pine ecosystem carbon and water fluxes from thinning and stand-replacing fire. *Global Change Biology*, *18*(10), 3171–3185.

<https://doi.org/10.1111/j.1365-2486.2012.02775.x>

Duff, G. A., Myers, B. A., Williams, R. J., Eamus, D., O’Grady, A., & Fordyce, I. R. (1997).

- Seasonal patterns in soil moisture, vapour pressure deficit, tree canopy cover and pre-dawn water potential in a Northern Australian savanna. *Australian Journal of Botany*, 45(2), 211–224. <https://doi.org/10.1071/BT96018>
- Eggemeyer, K. D., Awada, T., Harvey, F. E., Wedin, D. A., Zhou, X., & Zanner, C. W. (2009). Seasonal changes in depth of water uptake for encroaching trees *Juniperus virginiana* and *Pinus ponderosa* and two dominant C4 grasses in a semiarid grassland. *Tree Physiology*, 29(2), 157–169. <https://doi.org/10.1093/TREEPHYS/TPN019>
- Entekhabi, D., Rodriguez-Iturbe, I., & Castelli, F. (1996). Mutual interaction of soil moisture state and atmospheric processes. *Journal of Hydrology*, 184(1–2), 3–17. [https://doi.org/10.1016/0022-1694\(95\)02965-6](https://doi.org/10.1016/0022-1694(95)02965-6)
- Essery, R., Bunting, P., Hardy, J., Link, T., Marks, D., Melloh, R., Pomeroy, J., Rowlands, A., & Rutter, N. (2008). Radiative transfer modeling of a coniferous canopy characterized by airborne remote sensing. *Journal of Hydrometeorology*, 9(2), 228–241. <https://doi.org/10.1175/2007JHM870.1>
- Essery, R., Pomeroy, J., Parviainen, J., & Storck, P. (2003). Sublimation of snow from coniferous forests in a climate model. *Journal of Climate*, 16(11), 1855–1864. [https://doi.org/10.1175/1520-0442\(2003\)016<1855:SOSFCF>2.0.CO;2](https://doi.org/10.1175/1520-0442(2003)016<1855:SOSFCF>2.0.CO;2)
- Feeney, S. R., Kolb, T. E., Covington, W. W., & Wagner, M. R. (2011). Influence of thinning and burning restoration treatments on presettlement ponderosa pines at the Gus Pearson Natural Area. *Canadian Journal of Forest Research*, 28(9), 1295–1306. <https://doi.org/10.1139/x98-103>

- Fettig, C. J., Mortenson, L. A., Bulaon, B. M., & Foulk, P. B. (2019). Tree mortality following drought in the central and southern Sierra Nevada, California, U.S. *Forest Ecology and Management*, 432(August 2018), 164–178. <https://doi.org/10.1016/j.foreco.2018.09.006>
- Fitch, R. A., Kim, Y. S., Waltz, A. E. M., & Crouse, J. E. (2018). Changes in potential wildland fire suppression costs due to restoration treatments in Northern Arizona Ponderosa pine forests. *Forest Policy and Economics*, 87, 101–114. <https://doi.org/10.1016/j.forpol.2017.11.006>
- Fulé, P. Z. (2008). Does it make sense to restore wildland fire in changing climate? *Restoration Ecology*, 16(4), 526–532. <https://doi.org/10.1111/j.1526-100X.2008.00489.x>
- Ganey, J. L., & Vojta, S. C. (2011). Tree mortality in drought-stressed mixed-conifer and ponderosa pine forests, Arizona, USA. *Forest Ecology and Management*, 261, 162–168. <https://doi.org/10.1016/j.foreco.2010.09.048>
- Gaylord, M. L., Kolb, T. E., Wallin, K. F., & Wagner, M. R. (2007). Seasonal dynamics of tree growth, physiology, and resin defenses in a northern Arizona ponderosa pine forest. *Canadian Journal of Forest Research*, 37(7), 1173–1183. <https://doi.org/10.1139/X06-309>
- Gleason, K. E., Bradford, J. B., Bottero, A., D'amato, A. W., Fraver, S., Palik, B. J., Battaglia, M. A., Iverson, L., Kenefic, L., Kern, C. C., Gleason, C. :, Bradford, J. B., Bottero, A., D'amato, A. W., Fraver, S., Palik, B. J., Battaglia, M. A., Iverson, L., Kenefic, L., & Kern, C. C. (2017). Competition amplifies drought stress in forests across broad climatic and compositional gradients. *Ecosphere*, 8(7), e01849. <https://doi.org/https://doi.org/10.1002/ecs2.1849>

- Goeking, S. A., & Tarboton, D. G. (2020). Forests and Water Yield: A Synthesis of Disturbance Effects on Streamflow and Snowpack in Western Coniferous Forests. *Journal of Forestry*, 2020(2), 1–21. <https://doi.org/10.1093/jofore/fvz069>
- Gottfried, G. J., & Ffolliott, P. F. (1981). Evaluation of the Use of Soil Conservation Service Snow Course Data in Describing Local Snow Conditions in Arizona Forests. *Hydrology and Water Resources in Arizona and the Southwest*. <http://hdl.handle.net/10150/301230>
- Goulden, M. L., & Bales, R. C. (2019). California forest die-off linked to multi-year deep soil drying in 2012–2015 drought. *Nature Geoscience*, 12(8), 632–637. <https://doi.org/10.1038/s41561-019-0388-5>
- Grant, G. E., Tague, C. L., & Allen, C. D. (2013). Watering the forest for the trees: An emerging priority for managing water in forest landscapes. *Frontiers in Ecology and the Environment*, 11(6), 314–321. <https://doi.org/10.1890/120209>
- Gray, A. N., Spies, T. A., & Easter, M. J. (2002). Microclimatic and soil moisture responses to gap formation in coastal Douglas-fir forests. *Canadian Journal of Forest Research*, 32(2), 332–343. <https://doi.org/10.1139/x01-200>
- Guswa, A. J., Celia, M. A., & Rodriguez-Iturbe, I. (2002). Models of soil moisture dynamics in ecohydrology: A comparative study. *Water Resources Research*, 38(9), 5-1-5–15. <https://doi.org/10.1029/2001wr000826>
- Gyenge, J. E., Fernández, M. E., Dalla Salda, G., & Schlichter, T. M. (2002). *Silvopastoral systems in Northwestern Patagonia II: water balance and water potential in a stand of Pinus ponderosa and native grassland*.

- Huang, K., Yi, C., Wu, D., Zhou, T., Zhao, X., Blanford, W. J., Wei, S., Wu, H., Ling, D., & Li, Z. (2015). Tipping point of a conifer forest ecosystem under severe drought. *Environmental Research Letters*, *10*(2), 024011. <https://doi.org/10.1088/1748-9326/10/2/024011>
- Huang, M., Wang, X., Keenan, T. F., & Piao, S. (2018). Drought timing influences the legacy of tree growth recovery. *Global Change Biology*, *24*(8), 3546–3559. <https://doi.org/https://doi.org/10.1111/gcb.14294>
- Kannenbergh, S. A., Schwalm, C. R., & Anderegg, W. R. L. (2020). Ghosts of the past: how drought legacy effects shape forest functioning and carbon cycling. *Ecology Letters*, *23*(5), 891–901. <https://doi.org/10.1111/ele.13485>
- Kerhoulas, L. P., Kolb, T. E., & Koch, G. W. (2013). Tree size, stand density, and the source of water used across seasons by ponderosa pine in northern Arizona. *Forest Ecology and Management*, *289*, 425–433. <https://doi.org/10.1016/j.foreco.2012.10.036>
- Koepke, D. F., & Kolb, T. E. (2013). Species variation in water relations and xylem vulnerability to cavitation at a forest-woodland ecotone. *Forest Science*, *59*(5), 524–535. <https://doi.org/10.5849/forsci.12-053>
- Kolb, T. E., Wagner, M. R., & Covington, W. W. (1994). Concepts of forest health: utilitarian and ecosystem perspectives. *Journal of Forestry*, *92*(2), 10–15. <http://scholarsarchive.library.oregonstate.edu/xmlui/handle/1957/17277>
- Koster, R. D., Dirmeyer, P. A., Guo, Z., Bonan, G., Chan, E., Cox, P., Gordon, C. T., Kanae, S., Kowalczyk, E., Lawrence, D., Liu, P., Lu, C. H., Malyshev, S., McAvaney, B., Mitchell, K., Mocko, D., Oki, T., Oleson, K., Pitman, A., ... Yamada, T. (2004). Regions of strong

coupling between soil moisture and precipitation. *Science*, 305(5687), 1138–1140.

<https://doi.org/10.1126/science.1100217>

Larson, A. J., & Churchill, D. (2012). Tree spatial patterns in fire-frequent forests of western North America, including mechanisms of pattern formation and implications for designing fuel reduction and restoration treatments. *Forest Ecology and Management*, 267, 74–92.

<https://doi.org/10.1016/j.foreco.2011.11.038>

Lawler, R. R., & Link, T. E. (2011). Quantification of incoming all-wave radiation in discontinuous forest canopies with application to snowmelt prediction. *Hydrological Processes*, 25(21), 3322–3331. <https://doi.org/10.1002/hyp.8150>

Li, W., Guo, Q., Jakubowski, M. K., & Kelly, M. (2012). A New Method for Segmenting Individual Trees from the Lidar Point Cloud. *Photogrammetric Eng Amp Remote Sens*, 78(1), 75–84. <https://doi.org/10.14358/pers.78.1.75>

Loik, M. E., Breshears, D. D., Lauenroth, W. K., & Belnap, J. (2004). A multi-scale perspective of water pulses in dryland ecosystems: Climatology and ecohydrology of the western USA. In *Oecologia* (Vol. 141, Issue 2, pp. 269–281). <https://doi.org/10.1007/s00442-004-1570-y>

Maherali, H., & DeLucia, E. H. (2001). Influence of climate-driven shifts in biomass allocation on water transport and storage in ponderosa pine. *Oecologia*, 129, 481–491.

Martinez, C., Hancock, G. R., Kalma, J. D., & Wells, T. (2008). Spatio-temporal distribution of near-surface and root zone soil moisture at the catchment scale. *Hydrological Processes*, 22(14), 2699–2714. <https://doi.org/https://doi.org/10.1002/hyp.6869>

Mohan, M., Silva, C., Klauberg, C., Jat, P., Catts, G., Cardil, A., Hudak, A., & Dia, M. (2017).

Individual Tree Detection from Unmanned Aerial Vehicle (UAV) Derived Canopy Height Model in an Open Canopy Mixed Conifer Forest. *Forests*, 8(9), 340.

<https://doi.org/10.3390/f8090340>

Molotch, N. P., Brooks, P. D., Burns, S. P., Litvak, M., Monson, R. K., McConnell, J. R., & Musselman, K. (2009). Ecohydrological controls on snowmelt partitioning in mixed-conifer sub-alpine forests. *Ecohydrology*, 2(2), 129–142. <https://doi.org/10.1002/eco.48>

Moore, M. M., Huffman, D. W., Fulé, P. Z., Wallace Covington, W., & Crouse, J. E. (2004). Comparison of Historical and Contemporary Forest Structure and Southwestern Ponderosa Pine Forests. *Forest Science*, 50(2), 162–176.

Mueller, R. C., Scudder, C. M., Porter, M. E., Talbot Trotter, R., Gehring, C. A., & Whitham, T. G. (2005). Differential tree mortality in response to severe drought: Evidence for long-term vegetation shifts. *Journal of Ecology*, 93(6), 1085–1093. <https://doi.org/10.1111/j.1365-2745.2005.01042.x>

Newman, B. D., Wilcox, B. P., & Graham, R. C. (2004). Snowmelt-driven macropore flow and soil saturation in a semiarid forest. *Hydrological Processes*, 18(5), 1035–1042. <https://doi.org/10.1002/hyp.5521>

Oki, T., & Kanae, S. (2006). Global hydrological cycles and world water resources. In *Science* (Vol. 313, Issue 5790, pp. 1068–1072). <https://doi.org/10.1126/science.1128845>

Palmer, W. C. (1965). Meteorological Drought. In *U.S. Weather Bureau, Res. Pap. No. 45* (p. 58). <https://www.ncdc.noaa.gov/temp-and-precip/drought/docs/palmer.pdf>

- Porporato, A., Laio, F., Ridolfi, L., & Rodriguez-Iturbe, I. (2001). Plants in water-controlled ecosystems: Active role in hydrologic processes and response to water stress III. Vegetation water stress. *Advances in Water Resources*, 24(7), 725–744. [https://doi.org/10.1016/S0309-1708\(01\)00006-9](https://doi.org/10.1016/S0309-1708(01)00006-9)
- Qubaja, R., Amer, M., Tatarinov, F., Rotenberg, E., Preisler, Y., Sprintsin, M., & Yakir, D. (2020). Partitioning evapotranspiration and its long-term evolution in a dry pine forest using measurement-based estimates of soil evaporation. *Agricultural and Forest Meteorology*, 281, 107831. <https://doi.org/10.1016/j.agrformet.2019.107831>
- Quevedo Tejada Cetaqua, D., Quevedo, D. I., & Francés, F. (2008). A conceptual dynamic vegetation-soil model for arid and semiarid zones COST Action on Environmental Monitoring with UAS-HARMONIOUS View project Ecohydrology-based forest management for water provision, carbon sequestration and enhanced climate resilience. In *Hydrol. Earth Syst. Sci* (Vol. 12). www.hydrol-earth-syst-sci.net/12/1175/2008/
- Raz-Yaseef, N., Rotenberg, E., & Yakir, D. (2010). Effects of spatial variations in soil evaporation caused by tree shading on water flux partitioning in a semi-arid pine forest. *Agricultural and Forest Meteorology*, 150(3), 454–462. <https://doi.org/10.1016/j.agrformet.2010.01.010>
- Raz-Yaseef, Naama, Yakir, D., Rotenberg, E., Schiller, G., & Cohen, S. (2010). Ecohydrology of a semi-arid forest: Partitioning among water balance components and its implications for predicted precipitation changes. *Ecohydrology*, 3(2), 143–154. <https://doi.org/10.1002/eco.65>

- Raz-Yaseef, Naama, Yakir, D., Schiller, G., & Cohen, S. (2012). Dynamics of evapotranspiration partitioning in a semi-arid forest as affected by temporal rainfall patterns. *Agricultural and Forest Meteorology*, *157*, 77–85.
<https://doi.org/10.1016/j.agrformet.2012.01.015>
- Revuelto, J., López-Moreno, J. I., Azorin-Molina, C., & Vicente-Serrano, S. M. (2015). Canopy influence on snow depth distribution in a pine stand determined from terrestrial laser data. *Water Resources Research*, *51*(5), 3476–3489. <https://doi.org/10.1002/2014WR016496>
- Reynolds, R. T., Meador, A. J. S., Youtz, J. A., Nicolet, T., Matonis, M. S., Jackson, P. L., DeLorenzo, D. G., & Graves, A. D. (2013). Restoring composition and structure in southwestern frequent-fire forests. *USDA Forest Service, RMRS-GTR-3*.
- Roth, T. R., & Nolin, A. W. (2017). Forest impacts on snow accumulation and ablation across an elevation gradient in a temperate montane environment. *Hydrol. Earth Syst. Sci*, *21*, 5427–5442. <https://doi.org/10.5194/hess-21-5427-2017>
- Roussel, J.-R., Caspersen, J., Béland, M., Thomas, S., & Achim, A. (2017). Removing bias from LiDAR-based estimates of canopy height: Accounting for the effects of pulse density and footprint size. *Remote Sensing of Environment*, *198*, 1–16.
<https://doi.org/10.1016/J.RSE.2017.05.032>
- Sackett, S. S. (1980). Reducing natural ponderosa pine fuels using prescribed fire: two case studies. In *USDA Forest Service Research Note: Vol. RM-392*.
- Sahin, V., & Hall, M. J. (1996). The effects of afforestation and deforestation on water yields. In *Journal of Hydrology ELSEVIER Journal of Hydrology* (Vol. 178).

- Sala, A., Peters, G. D., McIntyre, L. R., & Harrington, M. G. (2005). Physiological responses of ponderosa pine in western Montana to thinning, prescribed fire and burning season. In *Tree Physiology* (Vol. 25, Issue 3). Oxford Academic. <http://heronpublishing.com>
- Sandvig, R. M., & Phillips, F. M. (2006). Ecohydrological controls on soil moisture fluxes in arid to semiarid vadose zones. *Water Resources Research*, 42(8).
<https://doi.org/10.1029/2005WR004644>
- Schultz, C. A., Jedd, T., & Beam, R. D. (2012). The Collaborative Forest Landscape Restoration Program: A History and Overview of the First Projects. *Journal of Forestry*, 110(7), 381–391. <https://doi.org/10.5849/jof.11-082>
- Syednasrollah, B., & Kumar, M. (2014). Net radiation in a snow-covered discontinuous forest gap for a range of gap sizes and topographic configurations. *Journal of Geophysical Research*, 119(17), 10,323-10,342. <https://doi.org/10.1002/2014JD021809>
- Syednasrollah, B., Kumar, M., & Link, T. E. (2013). On the role of vegetation density on net snow cover radiation at the forest floor. *Journal of Geophysical Research Atmospheres*, 118(15), 8359–8374. <https://doi.org/10.1002/jgrd.50575>
- Seyfried, M. S., Schwinning, S., Walvoord, M. A., Pockman, W. T., Newman, B. D., Jackson, R. B., & Phillips, F. M. (2005). ECOHYDROLOGICAL CONTROL OF DEEP DRAINAGE IN ARID AND SEMIARID REGIONS. *Ecology*, 86(2), 277–287.
<https://doi.org/10.1890/03-0568>
- Simonin, K., Kolb, T. E., Montes-Helu, M., & Koch, G. W. (2007). The influence of thinning on components of stand water balance in a ponderosa pine forest stand during and after

extreme drought. *Agricultural and Forest Meteorology*, 143(3–4), 266–276.

<https://doi.org/10.1016/j.agrformet.2007.01.003>

Snyder, K. A., & Tartowski, S. L. (2006). Multi-scale temporal variation in water availability: Implications for vegetation dynamics in arid and semi-arid ecosystems. *Journal of Arid Environments*, 65(2), 219–234. <https://doi.org/10.1016/j.jaridenv.2005.06.023>

Stahle, D. W., Cleaveland, M. K., Grissino-Mayer, H. D., Griffin, R. D., Fye, F. K., Therrell, M. D., Burnette, D. J., Meko, D. M., & Villanueva Diaz, J. (2009). Cool- and warm-season precipitation reconstructions over western New Mexico. *Journal of Climate*, 22(13), 3729–3750. <https://doi.org/10.1175/2008JCLI2752.1>

Stoy, P. C., El-Madany, T. S., Fisher, J. B., Gentine, P., Gerken, T., Good, S. P., Klosterhalfen, A., Liu, S., Miralles, D. G., Perez-Priego, O., Rigden, A. J., Skaggs, T. H., Wohlfahrt, G., Anderson, R. G., Coenders-Gerrits, A. M. J., Jung, M., Maes, W. H., Mammarella, I., Mauder, M., ... Wolf, S. (2019). Reviews and syntheses: Turning the challenges of partitioning ecosystem evaporation and transpiration into opportunities. *Biogeosciences*, 16(19), 3747–3775. <https://doi.org/10.5194/bg-16-3747-2019>

Swetnam, T. W., Allen, C. D., & Betancourt, J. L. (1999). Applied historical ecology: Using the past to manage for the future. *Ecological Applications*, 9(4), 1189–1206. [https://doi.org/10.1890/1051-0761\(1999\)009\[1189:AHEUTP\]2.0.CO;2](https://doi.org/10.1890/1051-0761(1999)009[1189:AHEUTP]2.0.CO;2)

Swetnam, T. W., & Betancourt, J. L. (2010). Mesoscale Disturbance and Ecological Response to Decadal Climatic Variability in the American Southwest. In *Advances in Global Change Research* (Vol. 41, pp. 329–359). Springer International Publishing.

https://doi.org/10.1007/978-90-481-8736-2_32

Teng-Chiu Lin, by, Rich, P. M., Heisler, D. A., & Barnes, F. J. (1992). *Influences of Canopy Geometry on Near-Ground Solar Radiation and Water Balances of Pinyon-Juniper and Ponderosa Pine Woodlands*. American Society for Photogrammetry and Remote Sensing 1992 Annual Meeting. Albuquerque, NM, pp. 285-294.

Teuling, A. J. (2005). Improved understanding of soil moisture variability dynamics. *Geophysical Research Letters*, 32(5), L05404. <https://doi.org/10.1029/2004GL021935>

Thornthwaite, C. W. (1952). Evaporation in the Hydrologic Cycle. In *The Physical and Economic Foundation of Natural Resources: The Physical Basis of Water Supply and Its Principal Uses* (pp. 25–35). Interior and Insular Affairs Committee House of Representatives, United States Congress.

Tyagi, J. V, Qazi, N., Rai, • S P, Singh, • M P, & Rai, S. P. (2013). Analysis of soil moisture variation by forest cover structure in lower western Himalayas, India. *Journal of Forestry Research*, 24(2), 317–324. <https://doi.org/10.1007/s11676-013-0355-8>

van der Schrier, G., & Barkmeijer, J. (2007). North American 1818-1824 drought and 1825-1840 pluvial and their possible relation to the atmospheric circulation. *Journal of Geophysical Research: Atmospheres*, 112(D13), n/a-n/a. <https://doi.org/10.1029/2007JD008429>

Veatch, W., Brooks, P. D., Gustafson, J. R., & Molotch, N. P. (2009). ‘Quantifying the effects of forest canopy cover on net snow accumulation at a continental, mid-latitude site.’ *Ecohydrology*, 2(2), 115–128. <https://doi.org/10.1002/eco.45>

- Vicente-Serrano, S. M., Beguería, S., & López-Moreno, J. I. (2010). A multiscalar drought index sensitive to global warming: The standardized precipitation evapotranspiration index. *Journal of Climate*, *23*(7), 1696–1718. <https://doi.org/10.1175/2009JCLI2909.1>
- Vicente-Serrano, S. M., Gouveia, C., Camarero, J. J., Beguería, S., Trigo, R., López-Moreno, J. I., Azorín-Molina, C., Pasho, E., Lorenzo-Lacruz, J., Revuelto, J., Morán-Tejeda, E., & Sanchez-Lorenzo, A. (2013). Response of vegetation to drought time-scales across global land biomes. *Proceedings of the National Academy of Sciences of the United States of America*, *110*(1), 52–57. <https://doi.org/10.1073/pnas.1207068110>
- Wang, L., Good, S. P., & Caylor, K. K. (2014). Global synthesis of vegetation control on evapotranspiration partitioning. *Geophysical Research Letters*, *41*(19), 6753–6757. <https://doi.org/10.1002/2014GL061439>
- Wei, Z., Yoshimura, K., Wang, L., Miralles, D. G., Jasechko, S., & Lee, X. (2017). Revisiting the contribution of transpiration to global terrestrial evapotranspiration. *Geophysical Research Letters*, *44*(6), 2792–2801. <https://doi.org/10.1002/2016GL072235>
- Wilcox, B. P., Breshears, D. D., & Allen, C. D. (2003). Ecohydrology of a resource-conserving semiarid woodland: Effects of scale and disturbance. *Ecological Monographs*, *73*(2), 223–239. [https://doi.org/10.1890/0012-9615\(2003\)073\[0223:EOARSW\]2.0.CO;2](https://doi.org/10.1890/0012-9615(2003)073[0223:EOARSW]2.0.CO;2)
- Williams, M., Law, B. E., Anthoni, P. M., & Unsworth, M. H. (2001). Use of simulation model and ecosystem flux data to examine carbon-water interactions in ponderosa pine. *Tree Physiology*, *21*, 287–298.
- Williams, P. A., Allen, C., Millar, C. I., Swetnam, T. W., Michaelsen, J., Still, C. J., & Leavitt, S.

- W. (2010). Forest responses to increasing aridity and warmth in the southwestern United States. *Proceedings of the National Academy of Sciences of the United States of America*, *107*(50), 21289–21294. <https://doi.org/10.1073/pnas.0914211107>
- Yamamoto, K., He, Y., Heinrich, P. L., Orange, A., Ruggeri, B., Wilberger, H., & Flikkema, P. G. (2010). WiSARDNet field-to-desktop: building a wireless cyberinfrastructure for environmental monitoring. In C. van Riper III, B. F. Wakeling, & T. D. Sisk (Eds.), *The Colorado Plateau IV: Shaping Conservation Through Science and Management: Vol. IV* (Issue IV, pp. 101–108). The University of Arizona Press.
- Zausen, G. L., Kolb, T. E., Bailey, J. D., & Wagner, M. R. (2005). Long-term impacts of stand management on ponderosa pine physiology and bark beetle abundance in northern Arizona: A replicated landscape study. *Forest Ecology and Management*, *218*(1–3), 291–305. <https://doi.org/10.1016/j.foreco.2005.08.023>
- Zhang, F., Biederman, J. A., Dannenberg, M. P., Yan, D., Reed, S. C., & Smith, W. K. (2021). Five Decades of Observed Daily Precipitation Reveal Longer and More Variable Drought Events Across Much of the Western United States. *Geophysical Research Letters*, *48*(7), e2020GL092293. <https://doi.org/https://doi.org/10.1029/2020GL092293>

CHAPTER 5: DISCUSSION

The three chapters in this dissertation each address a specific aspect of an applied remote sensing framework aimed at improving forest monitoring, management for water resources, and overall ecosystem health. The first study in this dissertation uses high-resolution UAV-borne multispectral imagery and SfM models to quantify fine- and mid-scale forest structure changes resulting from a thinning restoration project in a ponderosa pine forest in northern Arizona. Regarding fine-scale forest structure metrics, I find that UAV images and derived data products are effective at identifying the location (Table 2.2) and estimating the height of individual trees (Figure 2.3), but not effective for quantifying tree crown width (Table 2.3). I show that increased forest density degraded the accuracy of all fine-scale forest structure metric estimates, and that estimates from the highest-density conditions (up to 778 TPH) are subject to a variety of data quality-related deficiencies. More specifically, I show that UAV images are effective at estimating forest structure in conditions where tree stem density is below 500 TPH. I find similar density-related limitations in my assessment of UAV image-derived mid-scale forest structure metrics, specifically in the under-estimation of percent canopy cover in high-density conditions (Figure 2.4). When these results are considered in the context of assessing the effectiveness of a forest restoration treatment, I show that despite deficiencies in high-density conditions, this methodology can be used to efficiently and effectively monitor forest structure changes resulting from thinning-based restoration. Specifically, pre- and post-treatment forest density, patch and interspace conditions can be assessed rapidly and accurately with the UAV image-derived methodology proposed here. Land managers such as the Nature Conservancy and the US Forest Service can effectively deploy UAV platforms to rapidly and accurately estimate the variables I

evaluate in this chapter. This can save time and funding in evaluating thinning treatment progress and prescription guidelines.

My chapter 3 uses high-resolution remote sensing datasets to begin the examination of forest ecohydrological variables in response to thinning-based restoration practices. In this study, I develop and demonstrate a methodology that uses UAV image-derived data to quantify mid-scale snow covered area (SCA) and identify specific regions of persistent SCA. I illustrate that at our 76-ha forested study site, snow can be classified from high-resolution UAV imagery with up to 90.2% accuracy and that persistent snow patches can be identified using multi-day ‘snow-series’ imagery datasets (Figure 3.6). Modeling results show that percent canopy cover, trees per hectare, and cumulative solar radiation were the most important predictors of persistent snow patch size. Also, model predictions were most accurate when considering forest structure metrics from trees within a distance of 1.5 times their height to the persistent snow patch. Finally, my results show that the largest persistent snow patches were located adjacent to forest patches with 31-33% canopy cover and that there was more overall persistent snow cover in thinned versus unthinned forest (10% and 7%, respectively). This underscores that restoration thinning can promote snow cover and that future restoration efforts can use fine-scale forest structure assessments to tailor prescriptions to maximize persistent snow cover. Specifically, in such efforts and prescriptions, land managers can seek to establish forest patches with a mean canopy cover of 31-33% and tree density of <500 trees/ha. Furthermore, forest patches can be optimally created with distances 1.5 times their height between patches to maximize snow accumulation and persistence on the ground. These methods and findings can be employed by restoration practitioners interested in adding a snow cover component to their prescription planning and adaptive management frameworks. Additionally, these methods can be used to assess snow cover

changes in key sub-watersheds to help inform larger watershed runoff forecasting throughout the snow melt season.

The final study in this dissertation extends the examination of forest thinning and ecohydrological variables into soil moisture response during the critical seasonal drought period following snowmelt. I assessed soil drying in the top 100 cm of the soil profile during two consecutive fore-summer drought periods, and how forest structure influences the local-scale soil moisture variability. Dense soil water potential (SWP) time-series measurements characterized the timing, magnitude, and overall soil moisture levels across a gradient of forest structure conditions, providing insight into soil moisture persistence in a thinned forest throughout the driest time of the water year. I show that soil drying occurs earlier and more completely in the fore-summer drought period preceding a water year with existing meteorological drought conditions. This trend is also evident within the soil profile, with shallower sensors showing significantly drier soil conditions regardless of year and forest density conditions. When considering forest structure-related differences, I show that for sensors at 25 and 50 cm, higher stand basal area, percent canopy cover, and trees per hectare values all translate into significantly earlier soil drying onset and more days spent below a critical drying threshold. Importantly, these trends were also observed in sensors at 100 cm, but they were not statistically significant (Figure 4.10). Sensors at 25 cm showed rapid and highly variable response to meteorological and forest structure conditions, while sensors at and below 50 cm showed a clearer and more stable signal. Overall, my results show that forest managers can use fine-scale forest structure metrics, specifically density-related metrics, to promote soil moisture levels at and below 50 cm (Table 4.2). In addition to serving as the foundation for future long-term analyses of seasonal and multi-

year drought impacts to restored forests, these data and results can immediately help inform restoration planning efforts of the soil moisture benefits of strategic forest density reduction.

Taken together, these studies use cutting-edge remote sensing techniques and unprecedented high density soil moisture measurements to assess forest structure changes from thinning-based restoration as well as assess the impacts of forest structure on specific ecohydrological feedbacks. These studies provide explicit methodological frameworks to quantify forest structure, and importantly, how forests can be managed to optimize water resources through snow and soil moisture persistence in the winter and spring seasons.

5.1 Management Implications

This research focused on using applied remote sensing techniques and methodologies to improve forest management practices in the dry forests of the Southwestern U.S., and assess how water resource availability can be influenced by restoration thinning practices. Before gauging the effects of thinned forests on water resource availability, a reliable method for quantifying forest structure is needed. In Chapter 2, I first demonstrate a methodology for quantifying the forest structure changes from restoration thinning and for assessing the effectiveness of a treatment. This methodology provides forest managers an accurate and cost-effective tool for measuring and comparing restoration thinning outcomes at different scales. Managers can acquire data at the fine-scale (< 4ha) to inform adaptive management benchmarks specific to a thinning project, allowing for adjustments to thinning guidelines for other successive projects to meet broader landscape-scale (400+ ha) goals. Importantly, with minor changes based on forest density conditions and desired data product resolution, the methodology developed here can be adapted and enhanced to provide mid- and landscape-scale estimates of forest structure. This is important

to inform restoration planning as the scale and scope change in response to management directives.

Next, the quantification of forest structure is extended into the development of a remote sensing methodology for quantifying persistent snow cover. First, this methodology can be an important tool for forest managers to use when assessing persistent snow resulting from different intensities and patterns of restoration thinning. This could allow for an optimal set of parameters to be established for regional thinning projects and tailored as site-specific conditions change. Second and more generally, my results show that snow cover can be promoted through strategic thinning-based forest density reductions in Southwestern dry forests. Importantly, these results show that forest structure metrics often used for structuring mid- and landscape-scale thinning outcomes, like canopy cover and stand-level tree density, can be used to create fine-scale forest patches that maximize persistent snow cover.

Finally, to extend the understanding of forest structure effects on water resource availability, the final chapter provides insight into soil moisture dynamics throughout the driest time of the year and in response to thinned forest conditions. While the specific remote sensing methods and analyses developed here can be readily applied to gauging soil drying patterns in other restored forests, the key outcomes of this study can provide forest managers with soil moisture-related benchmarks for restoration planning. Results indicate that managers can use thinning to target soil moisture response at 50 cm, and that monitoring is also best achieved at 50 cm. The benefits to targeting and monitoring soil moisture response at 50 cm were due to both a responsiveness to forest structure differences as well as stability reflected at points deeper in the soil profile. Importantly, this study showed that overall reductions in forest density are consistent

with wetter soil conditions, and that strategic ground shading corresponding with approximately 30% canopy cover and < 100 trees per hectare can moderate soil drying at the fine-scale. This can provide forest managers with an additional tool to achieve a broad range of ecosystem benefits from restoration thinning and guard against the effects of anticipated multi-year drought conditions.

While the methodologies and analyses developed in this research reflect conditions in a typical Southwestern ponderosa pine forest and restoration thinning project, minor changes to data collection and analytical structure can widen the geographical scope. More specifically, increasing the spatial resolution both UAV and lidar-based forest structure measurements can extend these methods to denser forest conditions and areas with greater diversity in overstory trees. Considering quantifying the effects of forest structure on snow, the addition of snow depth and snow water equivalence measurements could greatly enhance the understanding of snow dynamics in regions with greater and more consistent snowpack. The forest structure effects on persistent snow and soil moisture drying are likely intensified in the Southwestern dry forest ecosystems by a combination of high solar angles, high vapor pressure deficits, and an overall drier climate. However, both restoration and drying trends emerging in other forested ecosystems can provide an opportunity to further refine the methods and management recommendations presented in this research.

CHAPTER 6: CONCLUSIONS

The work summarized in this dissertation reflects the accomplishment of several goals critical to the continued development of forest management practices in the Southwest as well as the ecohydrological processes governing regional water resource availability. First, I have developed a novel method for assessing the outcomes of thinning-based restoration practices in Southwestern ponderosa pine forests. This methodology uses commercially available equipment and software, can be readily applied to ongoing mid-scale forest restoration projects, and customized according to site- and prescription-specific considerations. Additionally, this method can be easily improved upon and added to with updates to the remote sensing technology available, providing restoration managers an evolving toolset for adaptive management. Second, I have developed a novel method for measuring and assessing persistent snowpack at fine- and mid-scales. Importantly, I used data produced from this novel method to assess the fine-scale relationship between forest structure and persistent snowpack. While I took an important step towards understanding the forest structure drivers of snow persistence, more work is needed to better understand these complex relationships before they can be considered at the landscape scale.

Finally, I conducted a crucial investigation of the soil moisture response to seasonal drought and its relationship with forest structure conditions. Core to this investigation is my launching of the instrument network that has generated an unprecedented soil matric potential dataset, including data from over 100 individual sensors spread across 76 ha of thinned and unthinned forest. This dataset and subsequent analyses showed that the timing, magnitude, and overall level of soil drying was significantly lower in the year following continued

meteorological drought conditions and showed that soil drying significantly decreases with depth. Importantly, this study also confirmed that less-dense forest structure conditions translate to wetter soil moisture levels. More work is needed to continue soil water potential data collection, make assessments across multiple years, and better understand the complex relationships to forest structure.

Together, these studies provide a detailed look into the applications of high-resolution remote sensing to quantifying forest biophysical variables and how future forest management can be tailored to maximize water resources throughout the semi-arid forests of the Southwestern U.S. As climate change effects continue to threaten our natural systems, resource managers can leverage advances in applied remote sensing and sensor networks to more effectively promote broader ecosystem resiliency.